ACCURATE CALCULATIONS OF NONLINEAR OPTICAL PROPERTIES USING FINITE FIELD METHODS

ACCURATE CALCULATIONS OF NONLINEAR OPTICAL PROPERTIES USING FINITE FIELD METHODS

By

AHMED MOHAMMED

B.Sc. (Chemistry)

M.Sc. (Physical Chemistry)

A Thesis

Submitted to the School of Graduate Studies

In Partial Fulfillment of the Requirements for the Degree

Doctor of Philosophy

McMaster University

DOCTOR OF PHILOSOPHY (2017) McMaster University

(Chemistry & Chemical Biology) Hamilton, Ontario, Canada

TITLE: Accurate Calculations of Nonlinear Optical Properties Using Finite Field Methods

AUTHOR: Ahmed Mohammed M.Sc. Physical Chemistry, McMaster University

M.Sc. Physical Chemistry, Inha University

B.Sc. Chemistry, Assiut University

SUPERVISOR: Professor Paul W. Ayers

NUMBER OF PAGES: xvi, 212

ABSTRACT

Molecular nonlinear optical (NLO) properties are extensively studied using both theory and experiment because of their use in myriad applications. Experimental measurements of the most interesting molecules' NLO properties are difficult, so experimental data for molecules with desirable NLO properties is scarce. Theoretical tools don't suffer from the same limitations and can provide significant insights into the physico-chemical phenomena underlying the nonlinear responses, can help in interpreting response behaviour of molecules, and can guide design the materials with desirable response properties. Here, I present my work on developing methods for accurately calculating the NLO properties of molecules using the finite field (FF) approach.

The first chapter provides a background for the finite field and electronic structure methods used in this dissertation. Chapter two is a thorough investigation of the finite field method. The limitations of the method are highlighted and the optimal conditions for overcoming its drawbacks and obtaining meaningful and accurate results are described. Chapter three presents the first systematic study of the dependence of optimal field strengths on molecular descriptors. The first protocol for predicting the optimal field for the second hyperpolarizability is presented and successfully tested, and the dependence of the optimal field strength for the first hyperpolarizability on the molecular structure is investigated. Chapter four is an assessment of various DFT functionals in calculating the second hyperpolarizabilities of organic molecules and oligomers. This study shows the limitations of conventional DFT methods and the importance of electron

correlation to response properties. In chapter five we present a new method of calculating NLO properties using a rational function model that is shown to be more robust and have lower computational cost than the traditional Taylor expansion. Finally, chapter six includes a summary of the thesis and an overview of future work.

ACKNOWLEDGEMENTS

First I would like to express my deepest gratitude for my supervisor, Professor Paul W. Ayers for giving me the opportunity to work in his group and introducing me to the field of nonlinear optics. I appreciate the interesting scientific discussions we had over the years.

I would like to thank Dr. Bain, Dr. Dumont, and Dr. Moran-Mirabal who were my committee. Thanks to their help, encouragement, and constructive suggestions.

I'm very grateful to Dr. Peter Limacher for his immense help and guidance. I appreciate the numerous discussions I had with him. Many thanks to Anand Patel for his help with calculations and writing.

I would also like to thank all the previous and current members of the Ayers group for their help and support: Cristina González, Mathew Chan, David Kim, Fanwang Meng, Derrick Yang, Yilin Zhao, Kumru Dikmenli, Sophie Kervazo, Michael Richer, Dr. Ramón Alain Miranda Quintana, Dr. Stijn Fias, Dr. Rogelio Cuevas-Saavedra, Dr. Debajit Chakraborty, Dr. Paul Johnson, Dr. Farnaz Heidarzadeh, Dr. Alfredo Guevara, Dr. James Anderson, Dr. Sandra Rabi, Dr. Pawel Tecmer, Dr. Katharina Boguslawski, Dr. Marco Franco Perez, Dr. Carlos Cardenas, Dr. Yuli (Annie) Liu, Dr. Lourdes Romero, Dr. Steven Burger, Dr. Eleonora Echegaray, Dr. Chunying Rong, Ivan Vinogradov, Caitlin Lanssens, and Pavel Kulikov. Thanks to all of them for being such good friends.

Thanks to the Natural Sciences and Engineering Research Council (NSERC), the department of chemistry and chemical biology, and McMaster University for financial support.

Last but not least, I would like to express my deepest gratitude for my family. Thank you for your love and support.

Table of Contents

List of Figures

List of Tables

Preface

This thesis contains published and unpublished material. The coauthors of the published content have been listed in the footnotes of each chapter. This section is to clarify my contribution to each chapter.

This thesis is consisted of an introduction, four journal articles, and a summary. The introduction outlines the key concepts and methods used in the thesis. Chapters 2, 3, and 5 are reprints of published articles. Chapter 4 is a manuscript in preparation for publication. The first section of each chapter is a motivation linking it to the previous one and clarifying its relevance to the subject of the thesis. Chapter 6 is a summary of the thesis and an outline of directions for future research.

Chapter 2 is reprint of the article "Finding Optimal Finite Field Strengths Allowing for a Maximum of Precision in the Calculation of Polarizabilities and Hyperpolarizabilities," published in the Journal of Computational Chemistry. I'm the first author of this article; Dr. Peter Limacher and Prof. Benoit Champagne are coauthors. I constructed and did all the electronic structure and finite field calculations for the (120 molecules of the) data set, along with the analysis of the results. Dr. Peter Limacher derived the equations and did the rest of the calculations. Dr. Limacher wrote the first draft of this chapter and Prof. Champagne and I revised it. Prof. Paul W. Ayers participated in the discussions.

Chapter 3 is a reprint of the manuscript "Predicting Optimal Finite Field Strengths for Calculating the First and Second Hyperpolarizabilities Using Simple Molecular Descriptors," published in Chemical Physics Letters. I'm the first author; Dr. Peter Limacher and Prof. Paul W. Ayers are coauthors. I did all computational work. I wrote the first draft, Dr. Limacher edited it, and Prof. Paul W. Ayers revised the final version.

Chapter 4 is a reprint of the manuscript "Benchmarking Density Functionals for the Second Hyperpolarizability of Organic Molecules," which is in preparation for publication. I did all the computational work in this chapter. I wrote the first draft of the manuscript; Dr. Limacher and Prof. Paul W. Ayers revised it.

Chapter 5 is reprint of the article "Finite Field Method for Nonlinear Optical Property Prediction Using Rational Function Approximants," published in the Journal of Physical Chemistry A. I'm the second author of this article, Anand Patel is the first author, and Dr. Peter Limacher and Prof. Paul W. Ayers are coauthors. I did all electronic structure calculations in this article. I programmed and did the calculations for the polynomial model; Anand Patel programmed and calculated the response properties for the rational functions. Anand Patel wrote the first draft and I revised it. Prof. Ayers and Dr. Limacher revised the final version.

For the three studies mentioned at the end of chapter 1 but not included in the thesis, I did all the computational work and wrote the first draft, which then was revised by the coauthors.

The author of this thesis performed most of the programming, computations, and writing for the content of this thesis. The coauthors helped with discussion, some calculations and writing, and revised the final version of the manuscripts. Chapter 2 was guided by Dr. Peter Limacher. Chapters 3 and 4 were guided by Prof. Paul W. Ayers and Dr. Peter Limacher. Chapter 5 was principally guided by Prof. Paul W. Ayers.

Chapter 1

Introduction

1.1 Motivation

Nonlinear optics describes the behaviour of light in nonlinear materials and media.[1-4] While all molecules and materials are nonlinear to some extent, in most cases the optical properties of a substance are not significantly affected by light. However, for sufficiently intense light (typically from strong lasers), one can observe nonlinear optical phenomena: phenomena related to the way intense light alters the optical properties of material systems.

Mathematically, nonlinear materials have a response that depends on the strength of the applied field in a nonlinear manner. For example, in conventional or linear optics, the dipole moment per unit volume of a substance, the dielectric polarization *P*, depends on the strength of the applied optical field *F* through the relation

$$P(t) = \chi^{(1)} F(t) \tag{1.1}$$

where $\chi^{(1)}$ is the linear susceptibility. In nonlinear optics, however, the response is described by the power series

$$P(t) = \chi^{(1)}F(t) + \chi^{(2)}F^2(t) + \chi^{(3)}F^3(t) + ... \quad (1.2)$$

where $\chi^{(2)}$ and $\chi^{(3)}$ are the second- and third-order nonlinear susceptibilities, respectively. Clearly Eq. (1.1) is always valid for sufficiently small fields; nonlinear optical materials are those where the nonlinear terms in Eq. (1.2) are practically significant. The nonlinear response of materials leads to many optical phenomena including changes in the optical properties of the material, generation of new light frequencies, and/or changes in the phase or the amplitude of the emergent light.

Nonlinear optical effects were postulated in the 1930s, but these effects were considered unimportant and nonlinear terms were largely ignored for the next three decades. Focussed research on nonlinear optics started with the discovery of second-harmonic generation by Franken and coworkers[5] in 1961, soon after building the first laser in 1960.[6,7] The high intensity of laser light made the nonlinear effects nonnegligible, and the field of nonlinear optics grew rapidly thereafter. The improved performance of nonlinear materials in some applications sustains current research in this area. This thesis develops new methods for computing the nonlinear response of molecules to external electric fields.

The dependence of the energy of a molecule, *E*, on an external static homogenous electric field *F*, can be written as a Taylor expansion of the form

$$E\left(F\right)=E\left(0\right)+\left.\frac{\partial E}{\partial F}\right|_0 F+\frac{1}{2!}\left.\frac{\partial^2 E}{\partial F^2}\right|_0 F^2+\frac{1}{3!}\left.\frac{\partial^3 E}{\partial F^3}\right|_0 F^3+\frac{1}{4!}\left.\frac{\partial^4 E}{\partial F^4}\right|_0 F^4+\ldots \qquad (1.3)$$

$$E\left(F\right)=E\left(0\right)-\mu F-\frac{1}{2}\alpha F^2-\frac{1}{6}\beta F^3-\frac{1}{24}\gamma F^4+\ldots \qquad (1.4)$$

Here, μ is the permanent dipole moment of the molecule. The dipole polarizability, α, is the response of the electron cloud of an atom or a molecule to the effect of external electric field. The dipole polarizability is a linear response property; it can be defined from the second derivative of the electronic energy of a molecule with respect to the external electric field, or as the first-order (linear) derivative of the dipole moment with respect to an electric field. The third derivative of the energy is called the first hyperpolarizability β, and the fourth derivative is called the second hyperpolarizability γ. Both β and γ are nonlinear response properties. For example, γ measures the cubic response of a molecular property (the dipole moment) to an applied electric field.

Predicting nonlinear optical (NLO) properties (β and γ) using quantum chemical methods is still challenging, and developing new methods and improving existing methods is an active area of research in computational chemistry.[8-19] In contrast with other methods used to calculate NLO properties, such as response theory, coupled-perturbed Hartree-Fock, or the sum-over-states method, the finite field (FF) method is a

straightforward and easy-to-implement technique that is easily applied for any quantum chemistry method. In FF approaches, properties of interest are determined directly from the molecular energy calculated at different external fields, without requiring any additional information about excited states or analytical derivatives of the energy. These advantages make the FF approach applicable to all levels of theory; one simply adds a term for the external field to the molecular Hamiltonian.

In this thesis I present my work on using the finite field methods to calculate accurate nonlinear optical properties of molecules. These properties are of great interest to both chemistry and materials sciences, and thus have received great interest from both theory and experiment alike. The remaining sections of this chapter highlight nonlinear optical properties, methods of calculating response properties, electronic structure methods, and explain the key concepts used in the thesis.

1.2 Nonlinear Optical Properties

1.2.1 Importance

Nonlinear optical (NLO) properties of molecules and polymers are of particular interest in organic chemistry and materials science, where new molecules/materials with desirable properties for engineering applications are sought.[20-26] NLO materials play a main role in nonlinear optics and have applications in information technology and data storage, optical communication, optical computing, dynamic holography, harmonic

generation, optical switching, and frequency mixing.[27-34] These response properties play an important role in studying other phenomena as well: weakly interacting systems, scattering processes, atom cooling and trapping, core-polarization and core-valence correlation, interactions between molecules and solvents and ionic reagents, and dielectric and refractive properties of rare gases. In the past few decades, optical devices have started to replace electronic devices in many areas of application.

The dipole polarizability α gives rise to refractive index and phenomena such as birefringence, materials with a refractive index dependent on the polarization and propagation direction of applied light. The first hyperpolarizability β is linked to the second-harmonic generation (SHG), a nonlinear optical process that doubles the frequency of the input optical wave and is one of the most investigated nonlinear optical phenomena. It also gives rise to parametric generation and frequency mixing. The second hyperpolarizability γ is connected to phenomena such as optical bistability and conjugation, stimulated Raman scattering, third-harmonic generation, and optical switching and computing.

1.2.2 Materials

Nonlinear optical (NLO) materials utilized in photonic devices possess high chromophore densities and display large optical nonlinearity, ultrafast response time, high damage threshold, and low optical losses. Nonlinear optics emerged from solid-state physics, and early experimental and theoretical investigations were mainly focused on

materials of interest to solid-state physics including crystals, inorganic semiconductors, and insulators. Inorganic materials have excellent chemical and mechanical properties, but most of them suffer from low nonlinear efficiency. These limitations led to the search for new materials with good NLO properties.

Organic nonlinear optical materials have been widely investigated because of their potentially high nonlinear properties and rapid response compared to inorganic ones. Organic molecules show extremely large NLO responses including two-photon absorption (TPA) and second-harmonic generation (SHG). Compared to inorganic materials, organic molecules exhibit superior optical properties such as ultrafast response time, high damage threshold, lower dielectric constants, and flexible designs that can be systematically improved. A large number of organic dyes, charge transfer complexes, fullerenes, π-conjugated polymers, nano-composites, liquid crystals, and organometallic compounds have been extensively investigated for nonlinear optics.

Conjugated molecules that lead to charge transfer systems have been widely studied for their NLO properties.[35-38] Many theoretical simulations and experiments have been conducted to understand the origin of nonlinearity in these molecules.[39,40] The conjugated π-electron systems allow charge transfer within the molecule as a response to the external electric field. Factors that contribute to nonlinear response in these systems are the electron-richness of the π-conjugated center, planarity of the molecule, molecular symmetry, and dimensionality of charge transfer networks. The instantaneous NLO

responses of these systems mainly arise from electron delocalization. Typical systems of interest here are the π-conjugated polyene and polyyne chains.

Adding an electron donating group at one end of a π-conjugated chain and an electron withdrawing one on the other end gives Donor–Acceptor (D–A) π-conjugated systems, sometimes referred to as push-pull molecules. The magnitude of NLO properties for these molecules increases superlinearly with the length of conjugated backbone, which is the distance between the donor and the acceptor. These systems, in their asymmetrical D–π–A or symmetrical D–π–A–π–D or A–π–D–π–A type have attracted much interest[40-46] because of their strong nonlinear response properties and application in three-dimensional optical data storage,[47,48] photodynamic therapy,[49] two-photon fluorescence microscopy,[50] etc. NLO properties of these molecules depend on donor-acceptor strength, conjugation length, molecular structure, and intramolecular charge transfer (ICT). The response of these systems can be easily tuned by changing the donor and acceptor moieties.

1.2.3 Experimental NLO Properties

Nonlinear optics is an active area of research in experimental chemistry.[51] The goal of the chemist is to understand NLO properties of materials and to be able to design molecules with fine-tuned magnitude and time of response.

Several experimental methods are available for measuring NLO properties of molecules in the gas phase and in solution. Experimental techniques for measuring α in the gas phase include the determination of the refractive index (RI) $n(\omega)$,[52] the measurement of the relative dielectric permittivity (DP) $\varepsilon(\omega)$,[53] molecular beam deflection techniques (MBD),[54] matter-wave interferometry (MWI),[55] and electron-molecule scattering (EMS).[56] The hyper-Rayleigh scattering technique can be used to measure the first hyperpolarizability β.[57,58] The second hyperpolarizability γ can be measured by the femtosecond Degenerate Four Wave Mixing (DFWM) technique.[59] However, there are many challenges to experimental measurement of response properties. The measured value depends on the method of measurement, and different references report different values for the same method.[51] Some measurements have high uncertainty or lead to different results and the reported value is an average. Experimental response properties are the tensor average of an ensemble of interacting molecules with different conformations and orientations measured at different frequencies. There are also vibronic contribution, local field factors, and solvent effects. It is difficult to isolate vibronic contributions in experimental measurements. Moreover, experimental data are scarce or unavailable for molecules with strong NLO properties.

These factors make comparisons between theoretical and experimental values of response properties difficult. To reproduce experimental dipole polarizabilities, an average of the tensor elements of α needs to be calculated as

$$\langle \alpha \rangle = \frac{1}{3}\left(\alpha_{xx} + \alpha_{yy} + \alpha_{zz} \right) \tag{1.5}$$

where α_{xx}, α_{yy}, and α_{zz} are tensor elements that can be calculated theoretically.

The average first hyperpolarizability, $\langle \beta \rangle$, for a molecule with a dipole moment oriented along the *x* axis is

$$\langle \beta \rangle = \frac{1}{5}\sum_i \left(\beta_{xii} + \beta_{ixi} + \beta_{iix} \right) = \frac{3}{5}\sum_i \beta_{iix} \tag{1.6}$$

and the average second hyperpolarizability, $\langle \gamma \rangle$, is

$$\langle \gamma \rangle = \frac{1}{5}\left(\gamma_{xxxx} + \gamma_{yyyy} + \gamma_{zzzz} + 2\gamma_{xxyy} + 2\gamma_{xxzz} + 2\gamma_{yyzz} \right) \tag{1.7}$$

The complication of intermolecular interactions makes understanding the structure-property relationship challenging. Experimentally measured nonlinear responses include not only local factors within the molecule, but also solute-solvent and solute-solute aggregates, interactions with solvents that can lead to conformational changes, and in some cases even chemical reactions with the solvent. These problems make uncovering the contribution of local factors to NLO properties challenging for experimentalists.

These challenges give theory a key role in understanding NLO properties. Theoretical tools can identify the compounds with the most interesting NLO responses and interpret the underlying physicochemical phenomena, thereby guiding the design of

new molecules with targeted NLO properties. Discovering new materials with superior optical properties may lead to new optical devices that replace electronic circuits with optical ones. Progress in photonic technology relies on discovering new materials with superior nonlinear performance, which require understanding the contribution of local factors to optical properties and structure-property relationships.

1.3 Calculation of Optical Response Properties

Accurate calculations of the interactions of electromagnetic fields with molecules are important for the development of various optical devices. Several methods are available for calculating NLO properties that include: response theory (RT), coupled-perturbed Hartree-Fock (CPHF), coupled-perturbed Kohn-Sham (CPKS), sum-over-states (SOS), and the finite field (FF) methods. These methods are outlined in the next sections.

1.3.1 Response Theory

Response theory is one of the most accurate methods for calculating NLO properties.[60,61] The method is based on time-dependent perturbation theory. As can be inferred from the name, response functions show how a property responds to an external perturbation. The key advantage of this method is that it replaces a computationally demanding explicit summation over excited states with a set of coupled response equations that must be solved.

When an external electrostatic potential is applied to a molecule, the perturbed Hamiltonian becomes

$$\hat{H}(x) = \hat{H}_0 + \hat{V}(x) \tag{1.8}$$

where $H(x)$ is the perturbed Hamiltonian, H_0 is the isolated molecular Hamiltonian, and $V(x)$ is the perturbation potential. The total energy of the system can be expanded with respect to x as

$$E(x) = \frac{\langle \Psi(x) | H(x) | \Psi(x) \rangle}{\langle \Psi(x) | \Psi(x) \rangle} = E^{(0)} + E^{(1)}x + \frac{1}{2}E^{(2)}x^2 + ... \tag{1.9}$$

where $E^{(0)} = E(0)$ is the unperturbed zeroth-order energy associated with the unperturbed Hamiltonian H_0. The energy derivatives are defined as

$$E^{(1)} = \left.\frac{dE}{dx}\right|_{x=0} ; \; E^{(2)} = \left.\frac{d^2E}{dx^2}\right|_{x=0} ; \; etc. \tag{1.10}$$

These energy derivatives are molecular properties and contain information about the response of the system to external fields.

The dipole moment can be decomposed into permanent and field-induced contributions

$$\mu_i(F) = \mu_i(0) + \sum_j \alpha_{i,j} F_j + ... \tag{1.11}$$

Response properties are obtained by the analytical differentiation of the energy expression with respect to the field. Specifically, the permanent dipole moment is written as

$$\mu_i = -\left.\frac{\partial E}{\partial F_i}\right|_{F=0} \tag{1.12}$$

Similarly, the electric dipole polarizability, the first hyperpolarizability, and the second hyperpolarizability are defined by the following expressions, respectively,

$$\alpha_{i,j} = -\left.\frac{\partial^2 E}{\partial F_i \partial F_j}\right|_{F=0} \tag{1.13}$$

$$\beta_{i,j,k} = -\left.\frac{\partial^3 E}{\partial F_i \partial F_j \partial F_k}\right|_{F=0} \tag{1.14}$$

$$\gamma_{i,j,k,l} = -\left.\frac{\partial^4 E}{\partial F_i \partial F_j \partial F_k \partial F_l}\right|_{F=0} \tag{1.15}$$

The third and higher-order hyperpolarizabilities are defined in the same manner.

1.3.2 Coupled-Perturbed Schemes

When a molecule is subjected to an external static homogenous electric field, *F*, the interaction between the external field and the charges in the molecule produces an induced dipole moment, $\Delta\mu$, that can be written as a Taylor expansion with the form

$$\Delta\mu(F) = \alpha F + \frac{1}{2}\beta F^2 + \frac{1}{6}\gamma F^3 + \ldots \quad (1.16)$$

The dipole polarizability, α, can be calculated through coupled-perturbed iterative procedures that compute the first-order response of the density matrix, $D^{(1)}$, to the applied electric field. In these methods, α is written as

$$\alpha = 2\sum_{p,q} M_{pq} D_{pq}^{(1)} \quad (1.17)$$

where M_{pq} is an element of the dipole moment matrix. At the HF level, evaluating $D^{(1)}$ is done through the coupled-perturbed Hartree-Fock (CPHF) method,[62-65] while the coupled-perturbed Kohn-Sham (CPKS) procedure is used when DFT functionals are used.[66-70] Calculating higher derivatives of energy, β and γ, can be done in a similar fashion, within a coupled-perturbed scheme, by including higher-orders responses of the density matrix, which can be calculated iteratively.

1.3.3 Sum-Over-States Method

The sum-over-states method[71-73] provides accurate calculated response properties. The advantage of this approach over response-theory approaches is that it reveals which excited states contribute most to a given response property. Moreover, the frequency dependence of responses is easily included. However, the method is computationally demanding because it requires explicit calculation of the contributions of all possible excited states to the property, and the numerical evaluation of a sum over many terms is

subject to roundoff errors. The difficulty of generating the higher excited states needed for the method can limit its applicability too.

In the sum-over-states method, the polarizability α can be calculated from perturbation theory as

$$\alpha = \sum_{i \neq f} \frac{\left| \langle f \mid V \mid i \rangle \right|^2}{E_f - E_i} \tag{1.18}$$

where *i* represents the state of interest, *f* is all the other states, and *V* is the transition moment between states (e.g., the dipole operator for the dipole polarizability). Expressions for higher-order derivatives are more complicated and computationally demanding.

These three schemes of calculating response properties are analytical and they don't suffer from any intrinsic numerical ill-conditioning. However, these approaches are computationally demanding, which limits the system size to which they can be applied. The difficulty of implementing these methods (especially response theory calculations) makes them unavailable for many existing software programs and new methods, especially for higher-order derivatives. Due to the difficulty in deriving and implementing the mathematical expressions, these three methods cannot be easily tested for new computational methods, and therefore it is rare to use nonlinear optical properties to assess the quality of new computational methods. Similarly, it is rare to use the best

new methods to compute the nonlinear optical responses of experimentally interesting molecules.

1.3.4 Finite Field Methods

The finite field (FF) method is widely used for calculating NLO properties of molecules and oligomers because of its low computational cost and ease of implementation.[69,74,75] The method only requires calculating the energy of the molecule in external fields. Unlike the previous schemes, it doesn't require analytical derivatives with respect to the field components or any information about excited states. This makes it applicable to all levels of theory and easy programmable into new codes. It is an ideal technique to test new electronic structure methods.

The finite field expressions for calculating the response properties are obtained by arranging Eq. (1.4) as

$$\mu = -\frac{E(F) - E(-F)}{2F} \tag{1.19}$$

$$\alpha = -\frac{E(F) + E(-F) - 2\mathrm{E}(0)}{F^2} \tag{1.20}$$

$$\beta = -\frac{E(2F) - E(-2F) - 2\big(\mathrm{E}(F) - E(-\mathrm{F})\big)}{2F^3} \tag{1.21}$$

$$\gamma = -\frac{E(2F) + E(-2F) - 4\big(\mathrm{E}(F) + E(-\mathrm{F})\big) + 6E(0)}{F^4} \tag{1.22}$$

The finite field (FF) method has some limits and drawbacks. It is limited to the calculation of static response properties, because time-dependent fields are too complicated to be handled in a straightforward manner. But the most crucial downside is the dependence of the calculated response properties on the choice of the initial field strength for doing the calculation. This is a well-known problem of the FF method. Evaluation of response properties at too small fields leads to noise due to the finite convergence thresholds for the energy and wave function optimization. Choosing a too strong field strength also leads to inaccuracies that stem from two factors. First, the higher order terms in the Taylor expansion in Eq. (1.4) are not negligible anymore and contribute to the energy of the molecule. The second, and more problematic, effect is the change in the electron configuration of the molecule at a certain field strength. For fields that are sufficiently strong, an excited state at a zero field will become lower in energy than the former ground state. Hence, all properties evaluated at such field strengths reflect the behaviour of this excited state. Moreover, strong enough field strengths can lead to the ionization of the molecule. Therefore, obtaining meaningful molecular response properties by the FF method depends on doing the calculation in a window of feasible field strengths that have a lower bound of noise and an upper bound of results corresponding to the excited or ionized states of the system. Although this is a serious problem of the FF method, there is no systematic way of estimating the optimal field strength for evaluating these properties and avoiding nonmeaningful results.

Another problem of the FF method is that calculated FF properties need further refinements to eliminate contributions from the higher derivative terms in the Taylor expansion. A well-known scheme to improve the accuracy of the evaluated properties is based on Richardson extrapolation.[76] Contamination from higher-order terms in the Taylor series is eliminated by applying Richardson extrapolation iteratively to values calculated at different initial field strengths. This scheme is known to improve the precision of the FF properties in the first few iterations.[15,69] However, there are no thorough investigations of the number of iterations that lead to the most precise results.

1.4 Electronic Structure Methods

1.4.1 Introduction

The main goal of computational chemistry is understanding, quantifying, and predicting chemical phenomena based on the fundamental equations and principles of theoretical chemistry. Computational chemists use efficient software to simulate atoms, molecules, and solids. Sometimes computational approaches are complementary to experiment: for example, computational approaches can reveal chemical phenomena in atomistic detail. Assessing and improving some of the current computational approaches is one of the main goals of this thesis.

The past few decades have witnessed a rapid increase in the types, size, and complexity of systems that can be approached with computational chemistry methods.

This progress has allowed theoretical chemists to enter new areas of application and provide new perspectives to other research fields, including biological chemistry and materials science. The increased scope of computational chemistry is attributed to two main factors: the exponential growth in computing power and the development of improved theoretical methods (mathematical methods and computer algorithms). The current scope of computational chemistry includes predicting molecular structures, electronic and thermal properties of materials, drug binding affinities, correlations between molecular structures and properties, vibrational frequencies, molecular spectra, electronic charge distributions, dipole and higher multipole moments, and (of primary relevance for this thesis) nonlinear optical properties of molecules and oligomers.[77-79]

1.4.2 The Schrödinger Equation

The shape of the potential energy surface (PES)[80] determines the structure, function, and the dynamics of molecules and can be determined by solving the Schrödinger equation. Solving the Schrödinger equation gives a description of the position and motion of nuclei and electrons. The time-independent Schrödinger equation for a molecule can be written as

$$\hat{H}\,\Psi(\mathbf{R}_1,\mathbf{R}_2,....,\mathbf{R}_N,\mathbf{r}_1,\mathbf{r}_2,....,\mathbf{r}_n) = E\,\Psi(\mathbf{R}_1,\mathbf{R}_2,....,\mathbf{R}_N,\mathbf{r}_1,\mathbf{r}_2,....,\mathbf{r}_n) \qquad (1.23)$$

where $\hat{H}$ is the Hamiltonian operator (the sum of kinetic energy and potential energy operators for the system), Ψ is the wave function for nuclei and electrons in the molecule,

$\mathbf{R}_I$ is the position of nucleus I and $\mathbf{r}_i$ is the position of electron i, and E is the molecular energy associated with the wave function. The molecular Hamiltonian in atomic units for a molecule with n electrons and N nuclei can be written as

$$\hat{H} = -\frac{1}{2}\sum_{I}^{N}\frac{\nabla_I^2}{m_I} - \frac{1}{2}\sum_{i}^{n}\nabla_i^2 - \sum_{i}^{n}\sum_{I}^{N}\frac{Z_I}{r_{iI}} + \sum_{I<J}^{N}\frac{Z_I Z_J}{r_{IJ}} + \sum_{i<j}^{n}\frac{1}{r_{ij}} \qquad (1.24)$$

where m_I and Z_I are the mass and atomic numbers of the I^{th} atom and r_{ij}, r_{IJ}, and r_{iI} are electron-electron, nucleus-nucleus, and electron-nucleus distances, respectively. The Schrödinger equation is solvable exactly for one-electron atoms only. For many-electron atoms and molecular systems, approximations must be introduced.

One of the most popular approximations for solving the Schrödinger equation is the Born-Oppenheimer approximation.[81,82] This approximation makes it possible to solve the Schrödinger equation exactly for some one-electron molecules. Moreover, the Born-Oppenheimer approximation, or another similar approximation, is needed for defining the molecular potential energy surface, which is a fundamental concept in chemistry.

Nuclei are much heavier than electrons, and thus their movement is much slower. The Born-Oppenheimer approximation assumes that electrons' response to the movement of nuclei is instantaneous and electrons don't move on the same timescale as the nuclei, and therefore the two movements can be separated. Therefore electrons can be treated as moving while nuclei are fixed. Mathematically, this corresponds to separating the total

molecular wave function into electronic and nuclear wave functions. In the electronic Hamiltonian, the kinetic-energy and potential-energy of the nuclei can be neglected,

$$\hat{H}_e = -\frac{1}{2}\sum_i^n \nabla_i^2 - \sum_i^n \sum_I^N \frac{Z_I}{r_{iI}} + \sum_{i<j}^n \frac{1}{r_{ij}} \tag{1.25}$$

The electronic energy is the eigenvalue of the electronic Hamiltonian. Adding the nucleus-nucleus repulsion energy to the electronic energy gives the molecular potential energy surface. Finding various approximations to the potential energy surface is one of the fundamental problems in theoretical quantum chemistry. Most computational chemistry methods involve computing the potential energy surface and using it to elucidate chemical phenomena.

1.4.3 Hartree-Fock Approximation

Further approximations for the molecular wave function are required because, except for a few very special cases, the electronic Schrödinger equation cannot be solved for many-electron systems. One of the most fundamental and earliest approximations is the Hartree-Fock (HF) method.[83] Like other approximate wave function methods that are suitable for large systems, in Hartree-Fock the problematic electron-electron repulsion potential in the molecular Hamiltonian, Eq. (1.25), is replaced with a one-electron effective potential operator. The resulting Hartree-Fock equations are easily solvable for systems with hundreds, or even thousands, of electrons.

The Hartree-Fock method is the basis for molecular orbital (MO) theory. In this theory, the motion of an electron is described by a single-particle function (orbital) that isn't explicitly dependent on the instantaneous motion of the rest of the electrons. Although the orbital picture is only a mathematical construct that approximates reality, the prevalence of the orbital picture in chemistry is an indication of the predictive power and appeal of the Hartree-Fock theory.

The Hartree-Fock method is simply explained as describing the many-body electron wave function by a single Slater determinant constructed from one-electron molecular orbitals. Therefore, the Hartree-Fock wave function of an *N*-electron system will have the form

$$\psi_{HF}\left(\mathbf{r}_1,\mathbf{r}_2,...,\mathbf{r}_N\right)=\frac{1}{\sqrt{N!}}\begin{vmatrix}\phi_1(\mathbf{r}_1) & \phi_2(\mathbf{r}_1) & ... & \phi_N(\mathbf{r}_1)\\ \phi_1(\mathbf{r}_2) & \phi_2(\mathbf{r}_2) & ... & \phi_N(\mathbf{r}_2)\\ ... & ... & ... & ...\\ \phi_1(\mathbf{r}_N) & \phi_2(\mathbf{r}_N) & ... & \phi_N(\mathbf{r}_N)\end{vmatrix} \tag{1.26}$$

where $\frac{1}{\sqrt{N!}}$ is a normalization constant. Exchanging two electrons in a Slater determinant changes the sign of the wave function, which satisfies the anti-symmetry requirements of a wave function and conforms to the Pauli principle. The electronic Hamiltonian is replaced by the Fock operator,

$$\hat{F}\left[\left\{\phi_j\right\}\right](1)=\hat{H}^{core}(1)+\sum_{j=1}^{n/2}\left[2\hat{J}_j(1)-\hat{K}_j(1)\right] \tag{1.27}$$

where $\hat{F}\left[\{\phi_j\}\right](1)$ is the one-electron Fock operator, comprising the one-electron core Hamiltonian,

$$\hat{H}^{core}(1) = -\frac{1}{2}\nabla_1^2 - \sum_A \frac{Z_A}{r_{1A}} \tag{1.28}$$

the Coulomb operator,

$$\hat{J}_j(\mathbf{r}_1) = \int d\mathbf{r}_2 \left|\phi_j(\mathbf{r}_2)\right|^2 r_{12}^{-1} \tag{1.29}$$

the exchange operator,

$$\hat{K}_j(1) = \int d\mathbf{r}_2 \phi_j^*(\mathbf{r}_2)\phi_i(\mathbf{r}_2) r_{12}^{-1} \tag{1.30}$$

where $r_{12} = |\mathbf{r}_1 - \mathbf{r}_2|$.

Using the one-electron Fock operator as a Hamiltonian to solve the one-electron Schrödinger equation gives one-electron wave functions for the system called the Hartree-Fock spin-orbitals $\phi_i(1)$,

$$\hat{F}(1)\phi_i(1) = \varepsilon_i \phi_i(1) \tag{1.31}$$

The Hartree-Fock wave function is a Slater determinant, and the electronic energy (for a normalized wave function) is given by the integral

$$E_{el} = \langle \Psi_{HF} | \hat{H} | \Psi_{HF} \rangle \tag{1.32}$$

The variational principle states that the energy is always an upper bound to the true energy. Therefore, better Slater determinants are obtained by varying the molecular orbitals to minimize the energy. The correct set of molecular orbitals in a Slater determinant, $\{\phi_i\}_{i=1}^{N}$, is the one that minimizes the electronic energy E_{el}. These molecular orbitals are usually expressed as linear combinations of atomic orbital basis functions in the form,

$$\phi_k(r) = \sum_i c_k^i \varphi_i(r) \tag{1.33}$$

where φ_i is an atomic orbital basis function which is commonly written as atom-centered Gaussian type functions. For example, the *1s*-type Gaussian orbital has the form

$$\varphi(r) = (2\alpha/\pi)^{3/4} e^{-\alpha r^2} \tag{1.34}$$

where α is the Gaussian orbital exponent. Gaussian basis sets have the advantage that the integrals that appear in Eqs. (1.29), (1.30), and (1.32) can be evaluated analytically, instead of numerically.

The main deficiency of the Hartree-Fock approximation is the absence of electron correlation: in the Hartree-Fock approximation, electrons move in an effective one-body potential, and the explicit electron-electron interactions (the two-electron repulsion term in the exact Hamiltonian) is neglected. The correlation energy is defined as

$$E_{corr} = E_{exact} - E_{HF} \tag{1.35}$$

where E_{exact} is the true energy of the system, E_{HF} is the Hartree-Fock energy.

Many post-Hartree-Fock methods have been proposed for including electron correlation, and the Hartree-Fock method is usually a good starting point for these more sophisticated methods for molecules near their equilibrium geometry. As discussed in the next sections, some of the widely-used post-Hartree-Fock methods include Møller-Plesset perturbation theory, configuration interaction, and coupled cluster methods.

1.4.4 Perturbation Theory

Perturbation theory is a widely used approach in quantum chemistry to describe the state of complicated systems using a simpler system.[84] The starting point of the theory is a simple and solvable system; a perturbation Hamiltonian that represents a (hopefully small) change to this system is then added. If the perturbations are small enough, quantities associated with the perturbed system, such as energy, can be written as corrections to those of the model system. In Møller-Plesset perturbation theory, better approximations to the true Hamiltonian of a system are obtained from the simpler Hartree-Fock Hamiltonian.

In perturbation theory the Hamiltonian is written as

$$\hat{H} = \hat{H}^{(0)} + \lambda \hat{H}^{(1)} \tag{1.36}$$

where $\hat{H}^{(0)}$ is a model Hamiltonian (e.g., Hartree-Fock; cf. Eq. (1.27)) with known eigenfunctions, $\hat{H}^{(1)}$ is a perturbing Hamiltonian, and λ is a parameter that controls the size of the perturbation. The perturbation expansion of the ground-state wave function and energy can be expressed as power series

$$\Psi_i = \Psi_i^{(0)} + \lambda\Psi_i^{(1)} + \lambda^2\Psi_i^{(2)} + ... \tag{1.37}$$

$$\varepsilon_i = \varepsilon_i^{(0)} + \lambda\varepsilon_i^{(1)} + \lambda^2\varepsilon_i^{(2)} + ... \tag{1.38}$$

where $\Psi_i^{(n)}$ and $\varepsilon_i^{(n)}$ are the *n*th-order correction to the model's wave function and energy, $\Psi_i^{(0)}$ and $\varepsilon_i^{(0)}$, respectively.

Substituting these equations into the Schrödinger equation and equating terms, order-by-order, in λ gives the working equations of perturbation theory. This approach allows for the approximation of the energies and wave functions of a difficult-to-solve Hamiltonian (like the exact electronic Hamiltonian) from an easier-to-solve model Hamiltonian (like the Hartree-Fock Hamiltonian). When the model Hamiltonian is the Hartree-Fock Hamiltonian, this approach is called Møller-Plesset perturbation theory.[85,86] Møller-Plesset perturbation theory, like all post Hartree-Fock methods, is more computationally demanding than Hartree-Fock. Developing numerical strategies for using Møller-Plesset perturbation theory for large systems is an area of active research in electronic structure theory. Without specialized software, it is difficult to routinely

compute the second-order Møller-Plesset energy for molecules containing more than about 50 atoms.

1.4.5 Configuration Interaction

The configuration interaction (CI)[87] theory extends the Hartree-Fock (HF) method by modelling the wave function as a linear combination of multiple Slater determinants, rather than the single Slater determinant used in HF.

The coefficients of the Slater determinants, which are different for each excited state *j*, are obtained by solving the eigenvalue problem

$$\hat{H}\Psi_j(\mathbf{r};\boldsymbol{R}) = E_j\Psi_j(\mathbf{r};\boldsymbol{R}) \tag{1.39}$$

where

$$\left|\Psi_j\right\rangle = \sum_{i=1}^{M} c_{ij}\left|\Phi_i\right\rangle \tag{1.40}$$

For HF theory, this sum has only a single term: one Slater determinant constructed from the occupied HF one-electron orbitals. If $\{\Phi_i\}$ is a complete set of determinants within the basis of occupied and unoccupied Hartree-Fock orbitals, then Eq. (1.40) is called the full-configuration interaction (full-CI) method. This is an exact solution to the Schrödinger equation within this basis, but it is computationally intractable for systems with more than about 10 electrons. Developing algorithms and software for computing

the full-CI theory for larger systems (up to maybe 100 electrons) is an extremely active area of research in electronic structure theory.

For larger molecules, it is traditional to truncate the CI expansion in Eq. (1.40) by including only low-order excitations of the Hartree-Fock reference determinant. Consider the full-CI wave function, written in terms of the Hartree-Fock determinant, Φ_{HF}, and its single, double, etc. excitations:

$$\Psi = c_0 \Psi_{HF} + \sum_{i}^{occ.} \sum_{a}^{vir.} c_i^a \Psi_i^a + \sum_{i<j}^{occ.} \sum_{a<b}^{vir.} c_{ij}^{ab} \Psi_{ij}^{ab} + ... \quad (1.41)$$

Here *i*, *j*, … denote occupied orbitals, *a*, *b*, … denote virtual orbitals, and Ψ_i^a is a singly-excited Slater determinant generated by replacing a spin orbital *i* with a spin orbital *a* (or exciting one electron from orbital *i* to orbital *a*). It is common to truncate the expansion in Eq. (1.41) after double-excitations; this is called the configuration interaction with single and double excitations (CISD) method. CISD is routinely applied to molecules with a few tens of atoms.

The CI method can be applied to excited states and open-shell systems; it can simulate systems far from their equilibrium geometries. In many cases, however, one needs to include some highly excited determinants. Finding accurate but computationally efficient ways to truncate the CI expansion in Eq. (1.41) is another research topic in electronic structure theory.

1.4.6 Coupled Cluster

The coupled cluster (CC) method is a mathematically elegant scheme and among the most popular methods for estimating the electron correlation energy.[88] It is commonly used to benchmark other methods, like the density functional theory methods described below. The most popular coupled cluster methods are applicable for small to medium-sized molecules (up to a few tens of atoms), though there has been significant recent progress on extending coupled cluster techniques to systems with a few hundred atoms.

In the coupled cluster method, the full-CI wave function is constructed using the exponential ansatz,

$$\Psi = e^{\hat{T}} \Psi_{HF} \tag{1.42}$$

As before, Ψ_{HF} is a Slater determinant and $\hat{T}$, the cluster operator that is used to account for electron correlation, is defined with the expansion

$$\hat{T} = \hat{T}_1 + \hat{T}_2 + \hat{T}_3 + ... + \hat{T}_n \tag{1.43}$$

Here *n* is the total number of electrons in the system, and the operator $\hat{T}_i$ generates all possible determinants with *i* excitations from the reference HF wave function. For example, $\hat{T}_1$ and $\hat{T}_2$, the operators for all single and double excitations, respectively, are written as

$$\hat{T}_1 = \sum_{i}^{occ.} \sum_{a}^{vir.} t_i^a \Psi_i^a \tag{1.44}$$

$$\hat{T}_2 = \sum_{i<j}^{occ.} \sum_{a<b}^{vir.} t_{ij}^{ab} \Psi_{ij}^{ab} \tag{1.45}$$

where *i*, *j*, … denote occupied orbitals and *a*, *b*, … denote unoccupied orbitals. Finding the coupled cluster wave function requires solving for the cluster amplitudes, t_i^a , t_{ij}^{ab} , *etc*.

Applying the one- and two-particle excitation operators, $\hat{T}_1$ and $\hat{T}_2$, to the reference wave function Ψ_{HF} transforms it into a linear combination of singly- and doubly-excited Slater determinants, respectively. That is, the CISD wave function could be rewritten as

$$\Psi_{CISD} = \left(1 + \hat{T}_1 + \hat{T}_2\right) \Psi_{HF} \tag{1.46}$$

and full-CI corresponds to applying the entire operator, $\left(1+\hat{T}\right) = \left(1+\hat{T}_1+\hat{T}_2+\hat{T}_3+\cdots\right)$ to the Hartree-Fock wave function.

The advantage of CC's exponential ansatz over the CI expansion is realized when one truncates the excitation level. For example, if one considers only double excitations, the CCD wave function is

$$\begin{aligned} \Psi_{CCD} &= e^{\hat{T}} \Psi_{HF} \\ &= \left(1 + \hat{T}_2 + \frac{\hat{T}_2^2}{2!} + \frac{\hat{T}_2^3}{3!} + \ldots\right) \Psi_{HF} \end{aligned} \tag{1.47}$$

where CCD denotes coupled cluster with the double excitation operator only. In this expression, each application of $\hat{T}_2$ gives a double excitation. So $\hat{T}_2^2$, the product of two consecutive double excitations, generates quadruple excitations; $\hat{T}_2^3$ generates hextuple excitations, and so on. Therefore, with only the double-excitation operator, more than doubly-excited Slater determinants contribute to the cc wave function. This approximation is preferable to "leaving out" these excitations (as is done in the corresponding CID method) as long as the excitations can be considered independently.

Substituting the coupled cluster wave function into the Schrödinger equation gives

$$\begin{aligned} He^{\hat{T}} \left|\Psi_{HF}\right\rangle &= Ee^{\hat{T}} \left|\Psi_{HF}\right\rangle \\ \left\langle\Psi_{HF}\right| He^{\hat{T}} \left|\Psi_{HF}\right\rangle &= E_{cc} \left\langle\Psi_{HF}\right| e^{\hat{T}} \Psi_{HF} \Big\rangle \\ &= E_{cc} \left\langle\Psi_{HF}\right| \left(1+\hat{T}_1+\hat{T}_2+...\right) \Psi_{HF} \Big\rangle \end{aligned} \tag{1.48}$$

And the coupled cluster energy is

$$E_{cc} = \left\langle\Psi_{HF}\right| He^{\hat{T}} \left|\Psi_{HF}\right\rangle \tag{1.49}$$

If the excitations are limited to single and double excited Slater determinants, the coupled cluster energy becomes

$$E_{cc} = E_{HF} + \sum_{i}^{occ}\sum_{a}^{vir} t_i^a \left\langle\Psi_{HF}\right| H \left|\Psi_i^a\right\rangle + \sum_{i<j}^{occ}\sum_{a<b}^{vir} \left(t_{ij}^{ab} + t_i^a t_j^b - t_i^b t_j^a\right) \left\langle\Psi_{HF}\right| H \left|\Psi_{ij}^{ab}\right\rangle \tag{1.50}$$

Coupled cluster methods are classified according to the highest number of excitations in the cluster operator $\hat{T}$. CCSD means coupled cluster with single and double excitations. Adding triple excitations explicitly to CCSD makes it too computationally demanding and restricts its application only to very small molecules. This led to the development of several approaches to estimate the effects of triple excitations using perturbation theory. The most robust and widely used method is called CCSD(T), a coupled cluster with single and double excitations, with the contribution of triple excitations are estimated by perturbation theory. The method is very effective in producing accurate results and is often called the "gold standard" for quantum chemistry calculations.

1.4.7 Density Functional Theory

Density functional theory (DFT) is the most popular quantum chemistry method for modelling systems in chemistry, physics, and materials science.[89-91] Like post Hartree-Fock methods, DFT provides an approximate treatment of the electron correlation. However, while post Hartree-Fock methods are obviously more computationally expensive than the underlying Hartree-Fock approximation, DFT methods have comparable computational cost to Hartree-Fock. This makes DFT one of the most efficient and versatile methods for studying the electronic structures of many-body systems. It is widely used to study organic reactions, biological processes, and solid-state materials.

Unlike post-Hartree-Fock methods, DFT does not treat electron correlation using a complicated wave function, but instead uses only the ground-state electron density. The electron density is a simpler mathematical formalism than the many-electron wave function because it depends on only three variables: the three Cartesian coordinates *x*, *y*, and *z*, while the wave function depends on three spatial and one spin coordinates for every electron when nuclear positions are fixed. The fact that the electron density is a physical observable makes it a simpler conceptual object, unlike the many-body wave function which is essentially uninterpretable and can't be grasped intuitively.

The central quantity of DFT, the ground-state electron density, $\rho(\mathbf{r})$, can be obtained from the ground-state *N*-electron wave function by

$$\rho(\mathbf{r}) = N \int ... \int \left| \psi(\mathbf{x}_1, \mathbf{x}_2, ..., \mathbf{x}_N) \right|^2 d\mathbf{s}_1 d\mathbf{x}_2 ... \mathrm{d}\mathbf{x}_N \tag{1.51}$$

Here $\rho(\mathbf{r})$ is the probability of finding an electron within the volume element $d\mathbf{r}$, $\mathbf{r}$ is a spatial variable, $\mathbf{s}$ is a spin variable, and $\mathbf{x}$ denotes both spatial and spin variables. For a molecule, the electron density is nonnegative, vanishes at infinity, and integrates to the number of electrons

$$N = \int \rho(\mathbf{r}) d\mathbf{r} \tag{1.52}$$

The first Hohenberg-Kohn theorem[92] indicates that the ground-state electron density completely specifies all molecular properties, including the electronic energy, many-

electron wave function, and molecular potential energy surface. The exact electronic energy, E_{el}, of a system can therefore be written as a functional of the electron density,

$$E_{el} = E\left[\rho(\mathbf{r})\right] \tag{1.53}$$

It is convenient to expand the energy functional as a sum of two pieces, one of which can be evaluated exactly from the electron density and the other of which needs to be approximated,

$$E\left[\rho(\mathbf{r})\right] = \int V_{ext}(\mathbf{r})\rho(\mathbf{r})d\mathbf{r} + F\left[\rho(\mathbf{r})\right] \tag{1.54}$$

The first term, which is known exactly, represents the interactions of electrons with an external potential $V_{ext}(\mathbf{r})$ typically due to nuclei. The second term is the sum of the kinetic energy of electrons and electron-electron interactions. According to the second Hohenberg-Kohn theorem, the ground-state energy is obtained by the variational minimization of the energy expression in Eq. (1.54) with respect to the electron density.

DFT replaces the difficult problem of solving the electronic Schrödinger equation with the problem of approximately determining the Hohenberg-Kohn function, $F[\rho(\mathbf{r})]$. The problem is that there are no known explicit mathematical expressions for the Hohenberg-Kohn functional. In 1965 Kohn and Sham[93] suggested replacing the correct Hamiltonian, which contains the problematic electron-electron interaction term, with the Hamiltonian of a non-interacting system of electrons that has the same ground-state electron density as the correct Hamiltonian. Like the Hartree-Fock Hamiltonian, the

Kohn-Sham Hamiltonian can be described as a sum of one-electron operators, its eigenfunctions are Slater determinants, and its eigenvalues are the sum of one-electron eigenvalues.

The next key idea is that the exact energy can be written as the energy of the fictitious system of noninteracting electrons, plus correction factors that account for the interactions between electrons,

$$E\left[\rho(\mathbf{r})\right] = T_S\left[\rho(\mathbf{r})\right] + \int V_{ext}(\mathbf{r})\rho(\mathbf{r})\,d\mathbf{r} + J\left[\rho(\mathbf{r})\right] + \Delta T\left[\rho(\mathbf{r})\right] + \Delta V_{ee}\left[\rho(\mathbf{r})\right] \tag{1.55}$$

Here $T_S\left[\rho(\mathbf{r})\right]$ is the kinetic energy of the fictitious system of non-interacting electrons, which is the sum of the kinetic energy of occupied Kohn-Sham orbitals; $J\left[\rho(\mathbf{r})\right]$ is the classical electron-electron repulsion, $\Delta T\left[\rho(\mathbf{r})\right]$ is the difference between the kinetic energy of the real and the non-interacting systems, and $\Delta V_{ee}\left[\rho(\mathbf{r})\right]$ is the non-classical portion of the electron-electron repulsion, including exchange (from the Pauli exclusion principle) and electron correlation effects. The last two terms, $\Delta T\left[\rho(\mathbf{r})\right]$ and $\Delta V_{ee}\left[\rho(\mathbf{r})\right]$, are difficult to approximate explicitly, so they are combined together to form a single unknown function called the exchange-correlation energy,

$$E_{XC}\left[\rho(\mathbf{r})\right] = \Delta T\left[\rho(\mathbf{r})\right] + \Delta V_{ee}\left[\rho(\mathbf{r})\right] \tag{1.56}$$

Eq (1.55) becomes

$$E\left[\rho(\mathbf{r})\right] = T_S\left[\rho(\mathbf{r})\right] + V_{ne}\left[\rho(\mathbf{r})\right] + V_{ee}\left[\rho(\mathbf{r})\right] + E_{XC}\left[\rho(\mathbf{r})\right] \tag{1.57}$$

This last term, the exchange-correlation energy functional, is the only term that is unknown. Current research in DFT focuses on designing improved approximations to E_{XC}.

The Kohn-Sham energy functional, Eq. (1.57), can be written as an orbital expression for the density as

$$E\left[\rho(\mathbf{r})\right] = \sum_{i=1}^{n} \int \psi_i(\mathbf{r}) \left(-\frac{\nabla^2}{2}\right) \psi_i(\mathbf{r}) d\mathbf{r} + \int V_{ext}(\mathbf{r}) \rho(\mathbf{r}) d\mathbf{r} + \frac{1}{2} \int\int \frac{\rho(\mathbf{r}_1)\rho(\mathbf{r}_2)}{|\mathbf{r}_1 - \mathbf{r}_2|} d\mathbf{r}_1 d\mathbf{r}_2 + E_{XC}\left[\rho(\mathbf{r})\right] \tag{1.58}$$

where n is the number of electrons. The electron density is just the sum of the occupied orbital densities,

$$\rho(\mathbf{r}) = \sum_{i=1}^{n} |\psi_i(\mathbf{r})|^2 \tag{1.59}$$

Similar to Hartree-Fock, the orbitals that minimize E satisfy the one-electron Kohn-Sham equations

$$\hat{G}_i \psi_i(\mathbf{r}_1) = \varepsilon_i \psi_i(\mathbf{r}_1) \tag{1.60}$$

where $\hat{G}_i$ is the Kohn-Sham one-electron operator

$$\hat{G}\left[\{\psi\}\right](1) = -\frac{\nabla_1^2}{2} - \sum_{A=1}^{N} \frac{Z_A}{r_{1A}} + \int \frac{\rho(\mathbf{r}_2)}{r_{12}} d\mathbf{r}_2 + V_{XC}\left[\mathbf{r}_1\right] \tag{1.61}$$

Here the exchange-correlation potential, $V_{XC}(\mathbf{r})$, is defined as the functional derivative of the exchange-correlation energy functional,

$$V_{XC}(\mathbf{r}) = \frac{\delta E_{xc}[\rho]}{\delta \rho(\mathbf{r})} \tag{1.62}$$

As in Hartree-Fock, the Kohn-Sham orbitals are expanded using basis functions, {ϕ}, and then the energy expression, Eq. (1.58) is minimized. This amounts to self-consistently solving the Kohn-Sham equations (1.60). The Kohn-Sham equations can be solved using the same iterative solvers that are used in Hartree-Fock theory, simply by replacing the Fock operator $\hat{F}$ by the Kohn-Sham operator $\hat{G}$.

Solving the Kohn-Sham equations has about the same computational cost as solving the Hartree-Fock equations, but DFT approximately includes the effects of electron correlation, which the Hartree-Fock method lacks. A key philosophical difference between HF and DFT is that while in Hartree-Fock one approximates the wave function, and then solves the resulting equations exactly. In DFT, the exchange-correlation energy functional is approximated, and then the resulting (approximate) equations are solved. Unlike HF, DFT is in principle exact: it is only limited by the difficulty of constructing effective exchange-correlation energy functionals.

DFT methods offer an excellent combination of computational cost and accuracy. The affordability of DFT is enabling computational chemistry to make the transition from

describing small molecules to designing large systems like proteins, supramolecular structures, and materials with specific properties.

1.4.8 Exchange-Correlation Functionals

The first Hohenberg-Kohn theorem is an existence theorem: they proved that all molecular properties, including the ground-state electronic energy and the exchange-correlation energy, can be written as a density functional. They did not present the form of this functional and, indeed, it is debatable whether an explicit expression for the functional exists.[94] Kohn-Sham DFT is limited, therefore, by our ability to approximate the unknown term in the Kohn-Sham energy functional, the exchange-correlation energy E_{XC}. E_{XC} includes the effects of electron exchange and correlation, the correction for self-interaction between electrons, and the difference in kinetic energy between the real and fictitious non-interacting systems. Different types of approximations for E_{XC} are discussed in the next sections.

1.4.8.1 The Local Density Approximation

Most approximate exchange-correlation functionals are based upon the local density approximation (LDA). LDA assumes that the energy of an electron at a point **r** depends only on the electron density at this point. Typically functionals of this type are derived from the uniform electron gas, a system with constant electron density where the external

potential is a constant neutralizing positive background charge, so that the net charge of this infinite system is zero.

Within the LDA approximation, the exchange-correlation energy, E_{XC}, can be written as

$$E_{XC}^{LDA}[\rho] = \int \rho(\mathbf{r})\ \varepsilon_{XC}\left(\rho(\mathbf{r})\right) d\mathbf{r} \tag{1.63}$$

where $\varepsilon_{XC}\left(\rho(\mathbf{r})\right)$ is the exchange-correlation energy per electron for the uniform electron gas. The quantity $\varepsilon_{XC}\left(\rho(\mathbf{r})\right)$ can be split into exchange and correlation contributions

$$\varepsilon_{XC}\left(\rho(\mathbf{r})\right) = \varepsilon_{X}\left(\rho(\mathbf{r})\right) + \varepsilon_{C}\left(\rho(\mathbf{r})\right) \tag{1.64}$$

Dirac[95] derived the exchange part as

$$\varepsilon_{X} = -\frac{3}{4}\left(\frac{3\rho(\mathbf{r})}{\pi}\right)^{1/3} \tag{1.65}$$

This term represents the exchange energy of one electron in the uniform electron gas. For the correlation part, however, no explicit expression is known.

The LDA gives bond lengths for molecules and solids with high accuracy (~2%). However, its accuracy for ionization energies of atoms and dissociation energies is

inferior to Hartree-Fock and it can fail in systems with strong electron correlation. The level of accuracy provided by LDA is not suitable for most applications in chemistry.

1.4.8.2 The Generalized Gradient Approximation

The LDA approximation assumes that the exchange-correlation energy density at the point **r** depends only on the electron density at that point, so it fails when the electron density changes rapidly, as it does in atoms and molecules. To include the effects of changes in the electron density at the point, one can express the exchange-correlation energy density as a function of the magnitude of the gradient of the density as well as the density at the point. This is the generalized gradient approximation (GGA), and corresponds to the expression

$$\varepsilon^{GGA}\left[\rho;\mathbf{r}\right]=\varepsilon^{GGA}\left(\rho\left(\mathbf{r}\right),\left|\nabla\rho\left(\mathbf{r}\right)\right|\right) \tag{1.66}$$

Including the gradient of the density leads to significant improvements over the LDA functionals. It was the first density functional approximation that had sufficient accuracy for many chemical applications. Any functional that is an explicit functional of the electron density and its derivatives are called pure density functionals. LDA and GGAs are the most popular types of pure functionals. GGAs are the most popular functionals for simulating condensed matter like solids, liquids, and complex materials.

1.4.8.3 Hybrid Functionals

Another class of approximations to the exchange-correlation energy is the hybrid functionals. These functionals combine a portion of exact exchange from the Hartree-Fock method with a more traditional density functional, typically a GGA. Hybrid functionals have the general form

$$E_{XC}^{hyb} = \alpha E_X^{HF} + (1-\alpha) E_X^{DFT} + E_C^{DFT} \tag{1.67}$$

This approach generally performs better than pure functionals, helps in correcting the "shortsightedness" of DFT potential, and reduces the self-interacting error. It provides more accurate results for many molecular properties such as bond lengths, atomization energies, reaction rates, and vibrational frequencies. Hybrid-GGAs are the most popular functionals for molecular quantum chemistry.

1.4.8.4 Long-range Corrected Functionals

Pure DFT exchange-correlation functionals use the electron density and its derivatives at the point **r** to construct the exchange-correlation energy density at that point. This tends to underestimate long-range electron exchange-correlation, and leads to significant self-interaction errors, especially in many-electron systems. Long-range exchange corrections help overcome this problem.

In the long-range corrected functionals, the two-electron operator $\frac{1}{r_{12}}$ is generally separated into short-range and long-range parts using an Ewald-inspired decomposition,

$$\frac{1}{r_{12}} = \frac{1-erf\left(\lambda r_{12}\right)}{r_{12}} + \frac{erf\left(\lambda r_{12}\right)}{r_{12}} \tag{1.68}$$

where *erf* is the standard error function, and λ is a parameter that determines the characteristic distance that separates the long-range (the first term in Eq. (1.68)) and short-range (the second term in Eq. (1.68)) contributions. Traditional pure density functionals are accurate for the short-range functional, while Hartree-Fock is more reliable for the long-range functional. If exact HF exchange is used at long range, then asymptotic decay of DFT potential is correct.

Long-range corrected functionals give better molecular properties, including equilibrium geometries, ionization energies, charge transfer excitations, and response properties, for a wide range of molecules, including long chains of π-conjugated molecules, which are known for their nonlinear optical properties. CAM-B3LYP, a long-range corrected functional used in this work, predicts accurate geometries and bond-length alternation for conjugated systems.

1.5 Summary

In chapter two we present what is, to our knowledge, the first thorough investigation of the reliability of the finite field method for evaluating the polarizability and hyperpolarizabilities of atoms and molecules; we also propose ways to reduce the numerical error of these calculations. The dependence of the calculated FF property on field strengths is investigated, and we observe that, for each molecule there is a region of feasible field strengths which depends on the structure of the molecule, the order of the response property, and the presence of diffuse basis functions. Calculations done using fields below the feasible region suffer from too large round-off errors; fields that are stronger than the feasible region are also problematic, probably because they cause a cross-over between the zero-field ground and excited state energies.

Within the feasible field region, the main source of error is the contribution of these higher-order derivatives in the Taylor expansion. We observe that the first two refinement steps by Richardson extrapolation reduce the error by one or two orders of magnitude for the second hyperpolarizability, γ. (Additional refinement steps don't lead to further improvement of the accuracy due to the accumulation of numerical errors.) We also show that the conventional choice of a factor of two when generating the geometric progression of field strengths used for the calculation of the FF properties is suboptimal. Based on our dataset of 120 molecules, a common ratio of $x < 2$ and two steps of refinements give the most precise results for γ.

Chapter 2 uses a thorough, but computationally costly, search to find the optimal field strength. In practical calculations one wishes to find a nearly optimal field very quickly. Chapter 3 presents the first protocol for predicting optimal field strengths for calculating the second hyperpolarizabilities γ. First we search for correlations between the optimal field strength with various molecular descriptors. In general, strong correlations were found between the optimal field strength of γ and descriptors of the size of the molecule. The best correlation was the maximum internuclear distance within a molecule in the direction of the applied field.

A protocol to estimate the optimal field strength for γ was developed based on these findings. This protocol was used successfully to predict the optimal field strength for ten molecules. Predicting the optimal field through a cheap and readily available structural parameter like the longitudinal distance reduces the number of field-dependent energy evaluation and removes the requirement for human intervention in finite field calculations.

The optimal field for calculating β, an odd-order derivative of energy, however, shows very different behaviour than γ, an even-order energy derivative. This field doesn't depend on molecular size and depends, instead, on the structure of the molecule. Categorizing molecules by the functional groups they contain was the best way to estimate the optimal field for calculating β.

Chapter four presents a benchmark study of various DFT functionals against CCSD(T) for calculating the second hyperpolarizability γ for a data set of 30 molecules. This study shows the limitation of conventional DFT functionals for evaluating the second hyperpolarizability of organic molecules and oligomers. The error of these functionals depends on the size of the molecule, which leads to disastrous results for medium-sized and large molecules.

The performance of different DFT functionals depends on the system under consideration. Pure functionals perform better than other models only for aromatic molecules. For the rest of the dataset, hybrid functionals, which contain exact HF and DFT exchange, perform better than pure ones, but still have errors that increase linearly with the size of the molecule. Long-range corrected hybrid functionals perform better than the rest of functions; this is probably because these functionals give better band gaps, have better long-range behaviour for the Kohn-Sham potential, and provide a more accurate treatment of electron delocalization in and through bonds.

Chapter 4 also sheds light on the contribution of electron correlation to the calculated γ values. Hartree-Fock consistently underestimates γ because it lacks electron correlation. The study examines the validity of using CCSD(T) as a benchmarking method for π-conjugated systems. We report a progressive deviation of CCSD from CCSD(T) for conjugated systems as the chain lengthens, which indicates that either the connected

triples excitations have significant contribution to γ values or the overestimation of triples contribution by perturbation theory.

Chapter five presents a variation of the finite field method for calculating dipole polarizability and the first and second hyperpolarizabilities using a rational function model, instead of the Taylor expansion (as in the preceding chapters). We detected the optimal form of the rational model, determined the optimal distribution of fields, and showed a reliable way to choose the initial field strength for the accurate calculation of response properties.

The rational function model and the polynomial model have similar errors. However, the rational functions, unlike polynomial models, do not need further (Richardson-like) refinements. This gives rational functionals a lower computational cost and ease of implementation. Moreover, the rational function model is less sensitive to the choice of the initial field strength and has wider feasible field regions.

In addition to the work included in this thesis, I also conducted three other studies in my current group (at McMaster University). The first was extending our investigation of γ (chapters 2 and 3) to the dipole polarizability, α, and the first hyperpolarizability, β. α showed a very similar behaviour to that of γ, because both of them are even-order energy derivatives. Two steps of refinements by Richardson extrapolation increased the accuracy of α by about two orders of magnitude. The calculated α values, being lower energy derivatives than γ, were stable over a wide range of common ratios. Nonetheless, using *x*

< 2 for the geometric progression of field strengths in the refinement steps is favourable. The optimal field strength for calculating α has the strongest correlations with maximum internuclear distance in the direction of the applied field as well. A similar protocol to estimate the optimal field was developed and successfully tested.

The first hyperpolarizability, β, on the other hand, being an odd-order energy derivative, shows a different pattern from α and γ. Similar to γ, β values benefit from using a common ratio $x < 2$ for the geometric progression of field strengths. The values gain about one order of magnitude in precision from the first step of refinement, without any systematic increase in precision with further steps. This study is in preparation for publication.

Second, I conducted a study on a new pH-responsive molecular tweezer that has been proposed for drug delivery. This study supported the experimental finding that the tweezer can potentially be used as a drug carrier and provided new insights into the preferred conformation of the protonated tweezer. The study showed that the tweezer is flexible with small barriers for conformational changes, that the preferred conformation depends on the protonation state of the tweezer, and that the tweezer can hold aromatic molecules between its arms through noncovalent interactions. We were able to observe the dynamics of pH-induced conformational change and the drug release process through molecular dynamics simulations. The barrier to conformation change, the pH required to open the tweezer, and the drug binding energy can be tuned by substitution with

functional groups. This study provides a protocol to test tweezers for desirable properties. This study was published in the Journal of Computational Chemistry.[96]

Third, I tested the adequacy of cluster models to predict pK_a values of amino acid residues in proteins. Results for this model were compared to other approaches such as the numerical solution of Poisson-Boltzmann equation and those obtained by numerical fitting. The cluster model predicts far too low pK_a values. This underestimation is due to the overestimation of the stabilizing effect of nearby residues with positive charges and the underestimation of the hydrophobic effect by continuum solvation models. This study shows the importance of including the hydrophobic environment of protein residues in calculating pK_as. This study was published as a book chapter (*in press*).[97]

1.6 References

1. N. Bloembergen, *Nonlinear Optics* (1965).
2. R. Fisher, *Optical Phase Conjugation* (Academic, New York, 1983).
3. R. W. Boyd, *Nonlinear Optics* (Academic press, San Diego CA, 1992).
4. H. Nalwa, S. Miyata, *Nonlinear Optics of Organic Molecules and Polymers* (CRC Press, Boca Raton, 1996).
5. P. Franken, A. Hill, C. Peters, G. Weinreich, Phys. Rev. Lett. **7**, 118 (1961).
6. T. H. Maiman, Nature **187**, 493 (1960).
7. R. J. Collins, D. F. Nelson, A. L. Schawlow, W. Bond, C. G. B. Garrett, W. Kaiser, Phys. Rev. Lett. **5**, 303 (1960).
8. D. R. Kanis, M. A. Ratner, T. J. Marks, Chem. Rev. **94**, 195 (1994).
9. J. L. Brédas, C. Adant, P. Tackx, A. Persoons, B. M. Pierce, Chem. Rev. **94**, 243 (1994).
10. B. Kirtman, in *Theoretical and Computational Modeling of NLO and Electronic Materials*, edited by S. P. Karna, A. T. Yeates, (ACS, Washington, D.C., 1996), Vol. 628, pp. 58.
11. B. Kirtman, B. Champagne, Int. Rev. Phys. **16**, 389 (1997).
12. D. M. Bishop, P. Norman, in *Handbook of Advanced Electronic and Photonic Materials and Devices, Nonlinear Optical Materials* Vol. 9, Edited by H. S. Nalwa (Academic, San Diego, 2001).
13. B. Champagne, B. Kirtman, in *Handbook of Advanced Electronic and Photonic Materials and Devices, Nonlinear Optical Materials* Vol. 9, Edited by H. S. Nalwa (Academic, San Diego, 2001), pp. 63.
14. K. Y. Suponitsky, T. V. Timofeeva, M. Y. Antipin, Russ. Chem. Rev. **75**, 457 (2006).

15. M. de Wergifosse, B. Champagne, J. Chem. Phys. **134**, 074113 (2011).
16. S. Wouters, P. A. Limacher, D. Van Neck, P. W. Ayers J. Chem. Phys. **136**, 134110 (2012).
17. S. Wouters, V. Van Speybroeck, D. Van Neck J. Chem. Phys. **145**, 054120 (2016).
18. M. B. Oviedo, N. V. Ilawe, B. M. Wong, J. Chem. Theory Comput. **12**, 3593 (2016).
19. A. A. K. Mohammed, P. A. Limacher, P. W. Ayers, Chem. Phys. Lett. **682**, 160 (2017).
20. B. J. Coe, J. A. Harris, L. A. Jones, B. S. Brunschwig, K. Song, K. Clays, J. Garin, J. Orduna, S. J. Coles, M. B. Hursthouse, J. Am. Chem. Soc. **127**, 4845 (2005).
21. F. Mançois, L. Sanguinet, J.-L. Pozzo, M. Guillaume, B. Champagne, V. Rodriguez, F. Adamietz, L. Ducasse, F. Castet, J. Phys. Chem. B **111**, 9795 (2007).
22. J. F. Lamère, I. Malfant, A. Sournia-Saquet, P. G. Lacroix, J. M. Fabre, L. Kaboub, T. Abbaz, A.-K. Gouasmia, I. Asselberghs, K. Clays, Chem. Mater. **19**, 805 (2007).
23. M. C. Ruiz Delgado, J. Casado, V. Hernandez, J. T. Lopez Navarrete, J. Orduna, B. Villacampa, R. Alicante, J.-M. Raimundo, P. Blanchard, J. Roncali, J. Phys. Chem. C **112**, 3109 (2008).
24. E. C. Brown, T. J. Marks, M. A. Ratner, J. Phys. Chem. B **112**, 44 (2008).
25. O. Loboda, R. Zalesny, A. Avramopoulos, J. M. Luis, B. Kirtman, N. Tagmatarchis, H. Reis, M. G. Papadopoulos, J. Phys. Chem. A **113**, 1159 (2009).
26. H. Nagai, M. Nakano, K. Yoneda, R. Kishi, H. Takahashi, A. Shimizu, T. Kubo, K. Kamada, K. Ohta, E. Botek, B. Champagne, Chem. Phys. Lett. **489**, 212 (2010).
27. D. S. Chemla, J. Zyss, *Nonlinear Optical Properties of Organic Molecules and Crystals* (Academic, New York, 1987).

28. J. Zyss, *Molecular Nonlinear Optics: Materials, Physics, and Devices* (Academic, New York, 1994).

29. W. Blau, H. Byrne, W. M. Dennis, J. M. Kelly, Opt. Commun. **56**, 25 (1985).

30. R. A. Norwood, J. R. Sounik, Appl. Phys. Lett. **60**, 295 (1992).

31. H. S. Nalwa, Adv. Mater. **5**, 341 (1993).

32. C. Li, L. Zhang, M. Yang, H. Wang, Y. Wang, Phys. Rev. A **49**, 1149 (1994).

33. K. P. Unnikrishnan, J. Thomas, V. P. N. Nampoori, C. P. G. Vallabham, Chem. Phys. **27**, 209 (2002).

34. J. M. Hales, S. Zheng, S. Barlow, S. R. Marder, J. W. Perry, J. Am. Chem. Soc. **128**, 11362 (2006).

35. J. C. Chien, *Polyacetylene: Chemistry, Physics and Material Science* (Academic, Orlando, 1984).

36. H. Kahlert, O. Leitner, G. Leising, Synth. Met. **17**, 467 (1987).

37. I. Krivoshein, V. Skorogobatov, *Polyacetylene and Polyarylenes: Synthesis and Conductive Properties* (Gordon & Breach, Philadelphia, 1991).

38. H. Shirakawa, Rev. Mod. Phys. **73**, 713 (2001)

39. P. Kerkoc, M. Zgonik, K. Sutter, Ch. Bosshard, P. Günter, J. Opt. Soc. Am. B **7**, 333 (1990).

40. M. G. Vivas, D. L. Silva, R. D. F. Rodriguez, S. Canuto, J. Malinge, E. Ishow, C. R. Mendonca, L. De Boni J. Phys. Chem. C **119**, 12589 (2015).

41. R. Morales, K. D. Belfield, J. M. Hales, E. W. Van Stryland, D. J. Hagan, Chem. Mater. **18**, 4972, (2006).

42. Z. J. Liu, T. Chen, B. Liu, Z. L. Huang, T. Huang, S. Y. Li, J. G. Qin, J. Mater. Chem. **17**, 4685 (2007).

43. Y. H. Jiang, Y. C. Wang, J. L. Hua, S. Y. Qu, S. Q. Qian, H. Tian, J. Polym. Sci. Part A: Polym. Chem. **47**, 4400, (2009).

44. L. L. Xue, J. T. He, X. Gu, Z. F. Yang, B. Xu, W. J. Tian, J. Phys. Chem. C **113**, 12911 (2009).

45. J. L. Wang, Q. Xiao, J. Pei, Org. Lett. **12**, 4164 (2010).

46. V. Hrobáriková, P. Hrobárik, P. Gajdoš, I. Fitilis, M. Fakis, P. Persephonis, P. Zahradnìk, J. Org. Chem. **75**, 3053 (2010).

47. S. Kawata, H.-B. Sun, T. Tanaka, K. Takada, Nature **412**, 697 (2001).

48. W. Zhou, S. M. Kuebler, K. L. Braun, T. Yu, J. K. Cammack, C. K. Ober, J. W. Perry, S. R. Marder, Science **296**, 1106 (2002).

49. D. Gao, R. R. Agayan, H. Xu, M.A. Philbert, R. Kopelman, Nano Lett. **6**, 2383 (2006).

50. M. C. Skala, J. M. Squirrell, K. M. Vrotsos, V. C. Eickhoff, A. Gendron-Fitzpatrick, K. W. Eliceiri, N. Ramanujam, Cancer Res. **65**, 1180 (2005).

51. U. Hohm, J. of Mol. Struct. **1054-1055**, 282 (2013).

52. S. A. Korff, G. Breit, Rev. Mod. Phys. **4**, 471 (1932).

53. M. Born, *Optik*, Springer, Berlin, 1933.

54. H. Scheffers, J. Stark, Phys. Z **35**, 625 (1934).

55. C. R. Ekstrom, J. Schmiedmayer, M. S. Chapman, T. D. Hammond, D. E. Pritchard, Phys. Rev. A **51**, 3883 (1995).

56. C. Szmytkowski, G. Kasperski, P. Mo_zeiko, J. Phys. B: At. Mol. Opt. Phys. **28**, L629 (1995).

57. K. Clays, A. Persoons, Phys. Rev. Lett. **66**, 2980 (1991).

58. K. Clays, A. Persoons, Rev. Sci. Instrum. **63**, 3285 (1992).

59. P. M. Felker, A. H. Zewail, J. Chem. Phys. **86**, 2460 (1987).

60. B. Jansik, P. Salek, D. Jonsson, O. Vahtras, H. Agren, J. Chem. Phys. **122**, 054107 (2005).

61. T. Helgaker, S. Coriani, P. Jørgensen, K. Kristensen, J. Olsen, K. Ruud, Chem. Rev. **112**, 543 (2012).

62. R. M. Stevens, R. Pitzer, W. N. Lipscomb, J. Chem. Phys. **38**, 550 (1963).

63. J. Gerratt, I. M. Mills, J. Chem. Phys. **49**, 1719 (1968).

64. T. C. Caves, M. Karplus, J. Chem. Phys. **50**, 3649 (1969).

65. M. H. Alexander, R. G. Gordon, J. Chem. Phys. **56**, 3823 (1972).

66. M. Schindler, W. Kutzelnigg, J. Chem. Phys. **76**, 1919 (1982).

67. R. Fournier, J. Andzelm, D. R. Salahub, J. Chem. Phys. **90**, 6371 (1989).

68. A. Komornicki, G. Fitzgerald, J. Chem. Phys. **98**, 1398, (1993).

69. B. Champagne, E. A. Perpète, S. J. A. van Gisbergen, E.-J. Baerends, J. G. Snijders, C. Soubra-Ghaoui, K. A. Robins, B. Kirtman, J. Chem. Phys. **109**, 10489 (1998).

70. M. Kamiya, H. Sekino, T. Tsuneda, K. Hirao J. Chem. Phys. **122**, 234111 (2005).

71. R. Ditchfield, N. S. Ostlund , J. N. Murrell, M. A. Turpin, Mol. Phys. **18**, 433 (1970).

72. F. Meyers, S. R. Marder, B. M. Pierce, J. L. Bredas J. Am. Chem. Soc. **116**, 10703 (1994).

73. B. Champagne, B. Kirtman, J. Chem. Phys. **125**, 024101 (2006).

74. H. D. Cohen, C. C. J. Roothaan, J. Chem. Phys. **43**, S34 (1965).

75. A. A. K. Mohammed, P. A. Limacher, B. Champagne, J. Comput. Chem. **34**, 1497 (2013).

76. L. F. Richardson, J. A. Gaunt, Phil. Trans. R. Soc. Lond. A **226**, 299 (1927).

77. C. J. Cramer, *Essentials of Computational Chemistry: Theories and Models*. (John Wiley & Sons Inc., Hoboken, NJ, second edition, 2004).

78. A. R. Leach, *Molecular Modelling: Principles and Applications*, (Pearson Education Limited, second edition, 2001).

79. T. Schlick, *Molecular Modeling and Simulation: An Interdisciplinary Guide*, (Springer, New York, second edition, 2002).

80. C. J. Cramer, Potential Energy Surfaces, in *Essentials of Computational Chemistry: Theories and Models*. (John Wiley & Sons Inc., Hoboken, NJ, second edition, 2004), pp 6-10.

81. V. M. Born, R. Oppenheimer, Annalen der Physik **389**, 457 (1927).

82. D. J. Wales, The Born-Oppenheimer Approximation and Normal Modes. In *Energy Landscapes*, (Cambridge University Press, 2003), pp 119-160.

83. A. Szabo, N. S. Ostlund, The Hartree-Fock Approximation, in *Modern Quantum Chemistry: Introduction to Advanced Electronic Structure Theory*. (Dover Publishing, Mineola, New York, 1996), pp108-230.

84. C. J. Cramer, Perturbation Theory, in *Essentials of Computational Chemistry: Theories and Models*. (John Wiley & Sons Inc., Hoboken, NJ, second edition, 2004), pp 216-224.

85. C. Møller, M. S. Plesset, Phys. Rev. **46**, 618 (1934).

86. M. Head-Gordon, J. A. Pople, M. J. Frisch, Chem. Phys. Lett. **153**, 503 (1988).

87. A. Szabo, N. S. Ostlund, Configuration Interaction in *Modern Quantum Chemistry: Introduction to Advanced Electronic Structure Theory*. (Dover Publishing, Mineola, New York, 1996), pp. 231-270.

88. C. J. Cramer, Coupled-cluster Theory, in *Essentials of Computational Chemistry: Theories and Models*. (John Wiley & Sons Inc., Hoboken, NJ, second edition, 2004), pp. 224–227.

89. P. W. Ayers, W. Yang, Density Functional Theory, in P. Bultinck, H. de Winter, W. Langenaeker, J. P. Tollenaere (Eds.) *Computational Medicinal Chemistry for Drug Discovery*, (Dekker, New York, 2003), pp. 571-616.

90. R. G. Parr, W. Yang, *Density-Functional Theory of Atoms and Molecules*, (Oxford University Press, New York, 1989).

91. A. Hinchliffe, Density Functional Theory, in *Modelling Molecular Structures*, (John Wiley & Sons Ltd, Baffins Lane, Chichester, West Sussex, second edition, 2001), pp 218-229.

92. P. Hohenberg, W. Kohn, Phys. Rev. **136**, B864 (1964).

93. W. Kohn, L. J. Sham, Phys. Rev. **140**, A1133 (1965).

94. P. W. Ayers, R. G. Parr, Indian J. Chem. A **53**, 929 (2014).

95. P. A. M. Dirac, Proc. Cambridge Phil. Soc. **26**, 376 (1930).

96. A. A. K. Mohammed, S. K. Burger, P. W. Ayers. J. Comput. Chem. **35**, 1545 (2014).

97. A. A. K. Mohammed, S. K. Burger, P. W. Ayers, Failures of Embedded Cluster Models for pKa Shifts Dominated by Electrostatic Effects, in *Conceptual Density Functional Theory* (*in press*).

Chapter 2

Finding Optimal Finite Field Strengths Allowing for a Maximum of Precision in the Calculation of Polarizabilities and Hyperpolarizabilities[*]

2.1 Motivation

The finite field (FF) method is a fast and easy-to-implement numerical technique that is widely used for calculating the static dipole polarizabilities and hyperpolarizabilities of molecules and polymers. Although the FF method has been extensively used for calculating nonlinear optical properties of molecules, there are no systematic investigations of its performance or comparisons with more accurate methods. A well-known drawback of the FF approach is the dependence of the calculated quantity on the initial field strength. Nonetheless, there are no thorough examinations of the nature of this dependence or schemes to guarantee reliable calculations. Another problem of the FF

[*] This chapter was originally published as A. A. K. Mohammed, P. A. Limacher, B. Champagne, *J. Comput. Chem.* **34**, 1497 (2013).
[†] This chapter was originally published as A. A. K. Mohammed, P. A. Limacher, P. W. Ayers,

methods is the contamination of the FF results from higher order terms in the Taylor expansion. A few iterations of Richardson extrapolation are widely used to reduce this effect. But it is not clear if there is an optimal number of iterations.

This chapter presents a thorough investigation of the FF method. An overview of the method is outlined and the equations required for calculating response properties are derived. The two main problems of the FF method, dependence on field strength and the need for refinement, are explored. A range of feasible field strengths that guarantee reliable numerical results is established. The quality of different types of meshes to screen the feasible region is assessed. Extrapolation schemes are presented that reduce the truncation error and increase the precision of the finite field calculations.

2.2 Introduction

Nonlinear optical (NLO) properties of molecules and polymers are a subject of high importance in organic chemistry and materials sciences.[1] The theoretical prediction of NLO properties based on quantum chemical calculations is challenging and the development of new, along with improvement of existing, methodology remains a substantial demand for computational chemistry.[2,3] The difficulties that occur in such calculations are related to the fact that the NLO properties render themselves very fragile quantities being high-order derivatives of the energy or of lower-order response

properties. If the dependence of the energy E on an external homogeneous static electric field F is written as a Taylor expansion of the form

$$E(F) = E(0) + \left.\frac{\partial E}{\partial F}\right|_0 F + \frac{1}{2!}\left.\frac{\partial^2 E}{\partial F^2}\right|_0 F^2 + \frac{1}{3!}\left.\frac{\partial^3 E}{\partial F^3}\right|_0 F^3 + \frac{1}{4!}\left.\frac{\partial^4 E}{\partial F^4}\right|_0 F^4 + \ldots \qquad (2.1)$$

$$E(F) = E(0) - \mu F - \frac{1}{2}\alpha F^2 - \frac{1}{6}\beta F^3 - \frac{1}{24}\gamma F^4 + \ldots \qquad (2.2)$$

the nonlinear responses, namely the first and second hyperpolarizabilities β and γ, are the third and fourth derivatives of E with respect to F. The other quantities are the permanent dipole moment μ and the dipole polarizability α.

The finite field (FF) method is a straightforward, easy-to-implement technique for the calculation of hyperpolarizabilities. In contrast to other methods such as the sum over states approach, coupled-perturbed Hartree-Fock, or response theory, the property of interest can be calculated simply from the knowledge of the energy at certain field strengths, and no additional information is needed about excited states or analytical derivatives with respect to the field components. These benefits render the FF method an universally applicable technique to any level of theory, with no additional requirements to a quantum chemical program other than to allow for an extra electric field term in the Hamiltonian.[4] It is thus common practice to first implement the FF method for the evaluation of hyperpolarizabilities in newly designed programs or homebuilt quantum chemistry codes.[5-12]

On the other hand, the FF method has also certain down-sides. It is, for example, limited to the evaluation of static molecular properties, as time-dependent fields cannot be handled in a straightforward manner. Most crucial, however, is the dependence of the outcome of an FF calculation on the initially chosen field strength. It is well-known that too small fields introduce numerical noise on the calculated properties due to the finite convergence thresholds for the energy and wave function optimization. These parameters are thus generally tightened by orders of magnitude for hyperpolarizability evaluations compared to an ordinary single point energy calculation. The problem with too small fields persists, however, due to the finite precision arithmetics of every computer, and can only be mitigated at most.

At the other end of the scale, there is also an upper bound for feasible field strengths. A field chosen too strong leads to an inaccurate evaluation of molecular properties driven by two different factors: First of all, the higher-order terms in the Taylor expansion of Eq. (2.2) lead to non-negligible contributions to the overall energy with increasing field strength. This effect is systematic and can be cancelled out by linear combination of properties obtained at different field strengths, which is usually applied in literature.[13-18]

A second, more cumbersome effect is the change in the electron configuration of the system at a certain field strength.[19] The perturbative potential associated with an external homogeneous electric field modifies the Hamiltonian of a system in such a way that its spectrum becomes unbound and, as a consequence, the true ground state would

correspond to a completely ionized molecular core with all electrons located at minus infinity. In practice however, the use of finite, atom-centered basis sets prevents such behaviour. If the field strength in such a calculation is chosen decently enough, the ground state, corresponding to a metastable state in the infinite basis set description, will closely resemble the ground state of a zero field calculation. For too strong fields however, an excited state at zero field could become favourable in energy and changes place with the former ground state. Hence, all properties evaluated at such field strengths reflect the behaviour of this excited state. Moreover, quantum chemical methods lacking multireference character often fail to converge in the vicinity of the intersection between these states.

In conclusion, choosing a reasonable field strength for an FF calculation requires coping with a rather delicate balance between the two extremes of too weak fields, leading to numerical errors that can be several orders of magnitude larger than the actual property of interest, and too strong fields causing the calculation of properties for an excited state.

This study intends to analyze the FF method in details for a broad range of field strengths, to characterize the behaviour of the noise at the low field limit, and to give prescriptions about how to find a critical upper limit for the field. Once the region of feasible field strengths is identified, the issue will be addressed of how to reach a maximum of precision using different FF meshes and extrapolation techniques. The final

section contains the application of the different extrapolation schemes to some exemplary molecules.

2.3 Methods

2.3.1 FF equations for the electric field derivatives

The FF formulae needed to compute the different tensor elements of the successive electric properties are straightforward to derive and treated in-depth in many excellent text books and articles.[6,20] Nevertheless, they are quickly recapitulated here as certain aspects should be highlighted to provide useful insights exploited in later sections.

The Taylor expansion of Eq. (2.2) can be split into an even and an odd part introducing symmetric and antisymmetric linear combinations of the energy at equal positive and negative fields:

$$E_S(F) = \frac{E(F)+E(-F)}{2} = E(0) - \frac{1}{2}\alpha F^2 - \frac{1}{24}\gamma F^4 + O(F^6) \tag{2.3}$$

$$E_A(F) = \frac{E(F)-E(-F)}{2} = -\mu F - \frac{1}{6}\beta F^3 - \frac{1}{120}\delta F^5 + O(F^7) \tag{2.4}$$

This allows a completely separate treatment of the polarizabilities and even order hyperpolarizabilities decoupled from any effects of the dipole moment and all odd order

hyperpolarizabilities, which characterize noncentrosymmetric molecules. The dipole moments and polarizabilities can be obtained directly, rearranging these equations to

$$\mu(F) = -\frac{E_A(F)}{F} = \mu + \frac{1}{6}\beta F^2 + \frac{1}{120}\delta F^4 + O(F^6) \tag{2.5}$$

$$\alpha(F) = 2\frac{E(0) - E_S(F)}{F^2} = \alpha + \frac{1}{12}\gamma F^2 + \frac{1}{360}\varepsilon F^4 + O(F^6) \tag{2.6}$$

which are already good estimates for μ and α under the assumption that F is chosen small enough.

For the evaluation of β and γ, the energy has to be known at two different field strengths, chosen here to be F and $2F$, besides the energy at zero field. This allows to eliminate μ and α from Eqs. (2.5) and (2.6) to yield

$$\beta(F) = 2\frac{\mu(2F) - \mu(F)}{F^2} = \frac{2E_A(F) - E_A(2F)}{F^3} = \beta + \frac{1}{4}\delta F^2 + O(F^4) \tag{2.7}$$

$$\gamma(F) = 4\frac{\alpha(2F) - \alpha(F)}{F^2} = \frac{-2E_S(2F) + 8E_S(F) - 6E(0)}{F^4} = \gamma + \frac{1}{6}\varepsilon F^2 + O(F^4)$$

(2.8)

The last equality in Eqs. (2.5)–(2.8) shows that all electric properties can be formulated as Taylor expansions in the same fashion as the energy in Eq. (2.2). Any quantity may thus be calculated as well from analytical dipole moments $\mu(0)$ and

$\mu(\pm F)$ using Eq. (2.5), or analytical polarizabilities $\alpha(0)$ and $\alpha(\pm F)$ using Eq. (2.6), etc. This leads to less and less finite differences to take and consequently to more precise results. There are, however, other methods to reduce the numerical error based on different extrapolation schemes.

2.3.2 Error reduction

A well-established method to lift the scaling of the error in Eqs. (2.5)–(2.8) to higher orders is based on Richardson extrapolation.[21] Specifically in quantum chemistry, this approach is equally well known as Romberg differentiation due to its similarity with the numerical integration scheme of the same name.[13] Both approaches are in fact exactly the same and were successfully applied in the past.[15,16,22]

Two given Taylor expansions of an arbitrary quantity *q* evaluated at different field strengths *F* and *xF*

$$q(F) = q(0) + aF + bF^2 + cF^3 + \ldots \tag{2.9}$$

$$q(xF) = q(0) + axF + bx^2F^2 + cx^3F^3 + \ldots \tag{2.10}$$

can be combined to obtain

$$x^m q(F) - q(xF) = (x^m - 1)q(0) + (x^m - x)aF + (x^m - x^2)bF^2 + \ldots. \tag{2.11}$$

in order to remove a certain power of *F* from the expansion by a proper choice of *m*. If *q* is evaluated for a number of field strengths following a geometric progression $q_{n,0} = q\left(x^n F\right)$ with common ratio *x*, then all the $\left\{q\left(x^n F\right)\right\}$ form a set of zero-order approximations for $q(0)$. Refined values for $q(0)$ are obtained by acting on this set with the recursive relation

$$q_{n,m} = \frac{x^m q_{n,m-1} - q_{n+1,m-1}}{x^m - 1} \tag{2.12}$$

For every refinement step *m*, the scaling power of the error is increased by one. Thus, if numerical values of $q_{n,0}$ are known for a geometric progression of, for example, five field strengths, the final $q_{0,4}$ is an approximation for $q(0)$ with the error scaling only as $O(F^4)$.

Richardson extrapolation is widely used in literature to refine the precision of FF properties, especially for the higher-order derivatives β and γ, which significantly improve during the first few iterations.[23] Further refinement, however, is not possible, as the quality of the result drops, once the range of field strengths spanned by the geometric progression extends beyond the feasible region.

A remedy for this is to shrink the ratio *x* of the progression such that more data points lie within the feasible region. Although it is common practice to work with *x* = 2,

values of $x < 2$ were found to improve the precision.[13] To this end, formulae (2.7) and (2.8) have to be generalized to

$$\beta(F) = \frac{6}{x^2-1} \cdot \frac{\mu(xF)-\mu(F)}{F^2} = \frac{6}{F^3 x} \cdot \frac{xE_A(F)-E_A(xF)}{x^2-1} \qquad (2.13)$$

$$\gamma(F) = \frac{12}{x^2-1} \cdot \frac{\alpha(xF)-\alpha(F)}{F^2} = \frac{24}{F^4 x^2}\left(\frac{x^2 E_S(F)-E_S(xF)}{x^2-1} - E(0) \right) \qquad (2.14)$$

which is achieved using Eq. (2.11), this time to remove the lower-order terms from the energy expansion. Setting $x = 2$, the conventional expressions (2.7) and (2.8) are retrieved.

For the subsequent Richardson extrapolation, the occurrence of solely even powers of F in the Taylor expansions (2.5)–(2.8) makes it more convenient to change the definition of m in Eq. (2.12) to

$$q_{n,m} = \frac{x^{2m} q_{n,m-1} - q_{n+1,m-1}}{x^{2m}-1} \qquad (2.15)$$

with $q = \{ \mu,\ \alpha,\ \beta,\ \gamma \}$.

2.3.3 Polynomial fitting

Another way to extrapolate α and γ from an FF calculation toward the values at zero field is to fit an appropriate function of order r to a given set $\{F_i, E_i\}$ of field strengths

and energies.[20] For centrosymmetric systems, α and γ are obtained by fitting a polynomial of the form

$$E(F) \approx E_{fit} - \frac{1}{2}\alpha_{fit}F^2 - \frac{1}{24}\gamma_{fit}F^4 + ... = \sum_{k=0}^{r} q_{k,fit}\frac{F^{2k}}{(2k)!} \quad (2.16)$$

to these data using the least-squares method. Note that only even powers of F are needed, if the symmetrized energy of Eq. (2.3) is used. Thus, choosing r = 1 allows the determination of E_{fit} and α_{fit}, an order of r = 2 yields E_{fit}, α_{fit}, and γ_{fit}, etc., also if the inspected molecule is not centrosymmetric. Naturally, the precision of the extrapolated values depends on the choice of r for the polynomial as well as on the number of data in the set. As a general rule, r has to be larger, the broader the considered range $\{F_i\}$ is. The optimal choice of r, however, depends on the nature and precision of the data, and is not trivial to find.

2.3.4 Field grid

A fine grid was used to find the optimal common ratio x for the geometric progression of field strengths for calculating γ of the 120 molecule benchmark (Figure 2.6) according to Eq. (2.14). For each molecule, energy calculations were performed at field strengths

$$F_n = F_0 \cdot 2^{n/100} \quad (2.17)$$

with n ranging from 0 to 800 and F_0 = 0.0005 au, which yields a maximum field strength > 0.1 au. This fine grid allowed us to test 200 different common ratios and determine the optimal x value with precision. The choice of x = 2 corresponds to setting n = 100. Choosing n = 50 gives $x = \sqrt{2}$, and $x = \sqrt[4]{2}$ is obtained by n = 25.

2.3.5 Electronic structure calculations

Geometry optimizations of the 120 molecules of the benchmark were done using the Gaussian 09 program[24] at the CAM-B3LYP/6-31G* level of theory. The rest of the calculations in this study were performed with the DALTON quantum chemistry program.[25] The reference values to which the FF properties are compared were obtained using response theory (RT).[26,27] Molecular geometries were optimized at the same level of theory as the subsequent evaluation of the hyperpolarizabilities unless otherwise noted.

Assessing the quality of finite differences requires the comparison of many almost identical numbers. For a maximal precision of these small numerical differences, care was taken that all wave functions, molecular energies, and property parameters were tightly converged. All the energies presented in this study are exact up to at least $2 \cdot 10^{-12}$ au = 2e-12 au. As the smallest molecules considered here have absolute energies above 40 au, we end up with a relative precision of at least 1e-13 for the energy or, alternatively stated, 13 significant digits.

The convergence criteria for the response equations were chosen such that at least 10 significant digits for α_{RT} can be guaranteed. For β_{RT} and γ_{RT}, it is nine and eight significant digits, respectively. The errors on the FF properties investigated in the present study are orders of magnitude higher, so that all the response properties can essentially be considered as the correct reference values.

2.4 Results and Discussion

2.4.1 Field dependence of the FF quantities

Figure 2.1 and Figure 2.2 show γ_{FF} of the neon atom as a function of the field strength, as calculated using Eq. (2.8). Independent of the quantum chemical method used, all the curves of Figure 2.1a have the same characteristics: After an initial noisy region below 0.001 au, values for γ_{FF} begin to stabilize before excited states become similar in energy and start to alter the slope at ~0.05 au. Moreover, contributions from higher order terms in the Taylor expansion become non-negligible at higher fields. Finally, all the curves drop down to zero after the field reaches ionizing strength, which cannot be accounted for by atom-centered basis sets.

In Figure 2.1b, the window for stable calculations of γ can be seen to vary if different basis sets are applied. It is well-known that basis sets lacking diffuse functions only recover a small fraction of the actual γ (for instance, the cc-pVDZ value is about four orders of magnitude too small when compared to t-aug-cc-pVQZ) which goes along with

the need for stronger fields before reaching the stable region. For the same reasons, when going toward large values of *F*, the end of the stable region occurs at smaller field strengths for more diffuse basis sets.

More insight on the field dependence of γ_{FF} can be gained if an accurate reference value for γ is known. In our case, response theory was applied to obtain a γ_{RT} from an unrelaxed CCSD calculation (Figure 2.2a) and a HF calculation (Figure 2.2b). The unsigned relative error $|\varepsilon_\gamma| = \left|\frac{\gamma_{FF}}{\gamma_{RT}} - 1\right|$ reveals more details about the accuracy of γ_{FF}: There is a critical field strength, corresponding to ionization or state inversion below which the error is well-behaved and, while moving toward smaller *F*, γ_{FF} approaches more and more the γ_{RT} value. This is the region of field strengths for which extrapolation schemes are meaningful. Then, for even smaller field strengths, there is a clear point where the noise starts to drop in, systematically worsening the precision on γ_{FF}. The aforementioned shift of optimal field strengths for different basis sets is also visible here. Nevertheless, the relative precision is the same for all basis sets and reaches a maximum of about three significant digits. This is generally sufficient for investigations focusing on predicting and interpreting γ values.

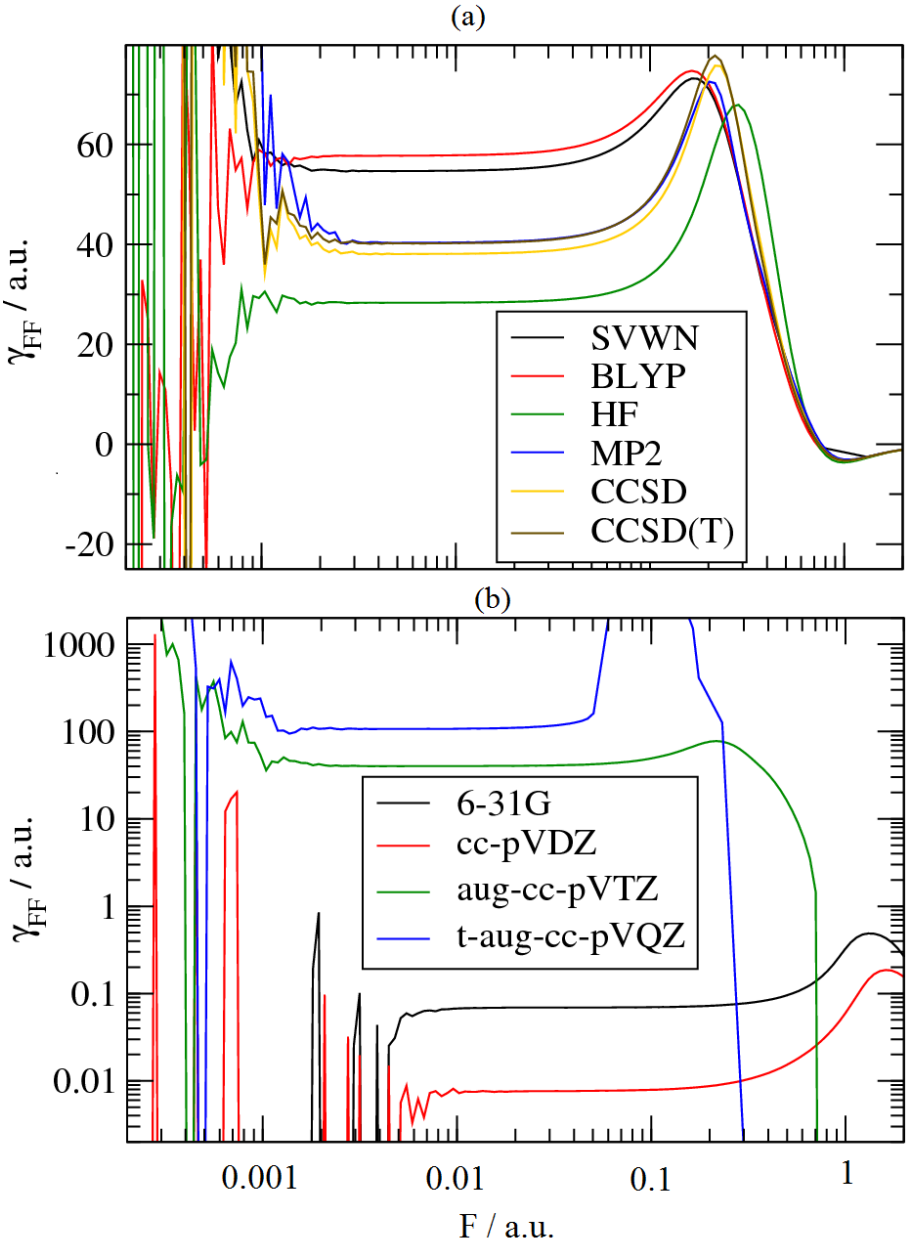

Figure 2.1. Finite field second hyperpolarizabilities γ_{FF} for the neon atom as a function of the field strength F using Eq. (8). (a) compares different quantum chemical methods using the aug-cc-pVTZ basis set. (b) shows values for γ_{FF} from relaxed CCSD(T) calculations using different basis sets.

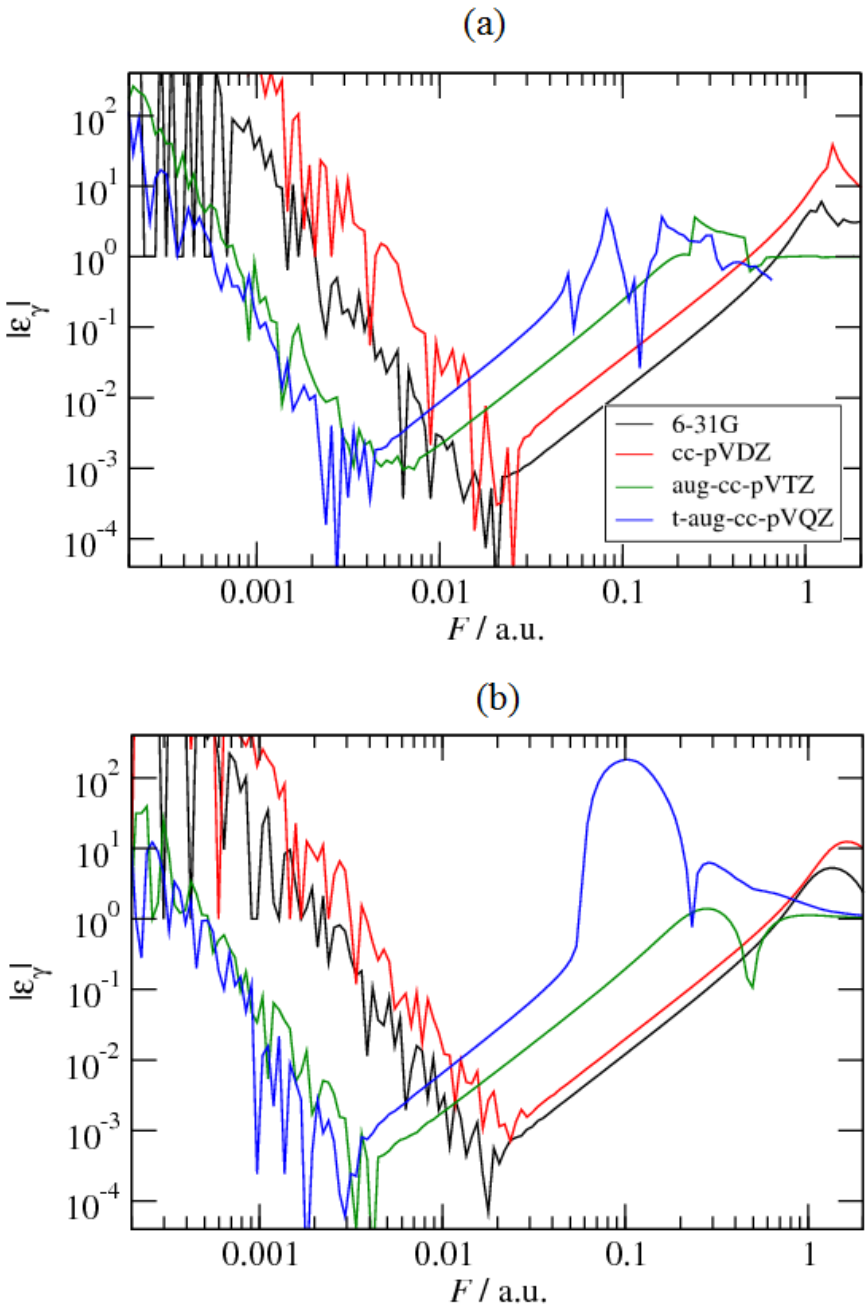

Figure 2.2. The unsigned relative error of finite field second hyperpolarizabilities γ_{FF} of (a) unrelaxed CCSD, (b) HF method in comparison to response theory for the same basis sets as in Figure 2.1.

If the study is extended to polar molecules such as water, similar observations can also be made for the first hyperpolarizability β. In fact, as is shown in Figure 2.3a, using Eqs. (2.5)–(2.8), all the properties that are derivatives of the energy with respect to the electric field follow the same pattern. The threshold field strength at which noise starts to corrupt precise calculations is naturally larger for higher-order derivatives and the overall precision thus drops to less significant digits. At the same time, the critical field strength defining an upper bound for meaningful FF quantities remains unchanged or is shifted to smaller values as energies acquired at twice the field strength will enter the calculations, according to Eqs. (2.7) and (2.8). This leads to an overall shrinking of the interval of acceptable field strengths when going to higher-order derivatives.

Figure 2.3b points out that, within the same order of derivatives, any tensor element can be evaluated to the same precision over the same interval of acceptable field strengths. This allows us to focus on one distinct tensor element only (γ_{xxxx} in the following). The findings for this quantity can then be generalized to any other tensor element. Nevertheless, an optimal field strength in *x*, *y*, and *z* direction has to be found individually for very prolate or oblate molecules (e.g., planar, π conjugated systems) if mixed tensor elements such as γ_{xxyy} are calculated.

It should further be noted from Figure 2.3 that all the slopes in the region of acceptable field strengths are nearly parallel for all quantities and correspond to a quadratic deviation (i.e., a slope of two in the double-logarithmic representation) from the

reference value. This means that the error due to the usage of finite fields in this region is almost exclusively related to the contribution of the next term in the odd/even power expansion, which is the quantity's second-order derivative (e.g., β in the case of μ, or γ in the case of α) and is thus straightforward to eliminate. In the low field regions of Figure 2.3, the noise takes overhand. Its characteristic scaling correlates with the order of the derivative. The constant round-off error on the energy differences is made field-dependent through the division by a specific power of the field strength, according to Eqs. (2.5)–(2.8), which causes the error-increase at low fields. The choice of plotting the unsigned error in Figure 2.3 has the benefit of illustrating this noise rather nicely, but on the other hand also leads to artificial peaks on the high field side, whenever (γ_{FF}-γ_{RT}) changes sign (visible e.g., around 0.2 au for μ, or around 0.05 au for β).

2.4.2 The low field limit

As the energy is only correct up to a certain threshold δE, the finite differences in Eqs. (2.5)–(2.8) cannot be more precise than that. As all the FF quantities (q) are divided by a certain power of F, the following relations holds for their absolute precision (δq):

$$\left|\delta E\right| \approx \left|F\delta\mu\right| \approx \left|F^2\delta\alpha\right| \approx \left|F^3\delta\beta\right| \approx \left|F^4\delta\gamma\right| \tag{2.18}$$

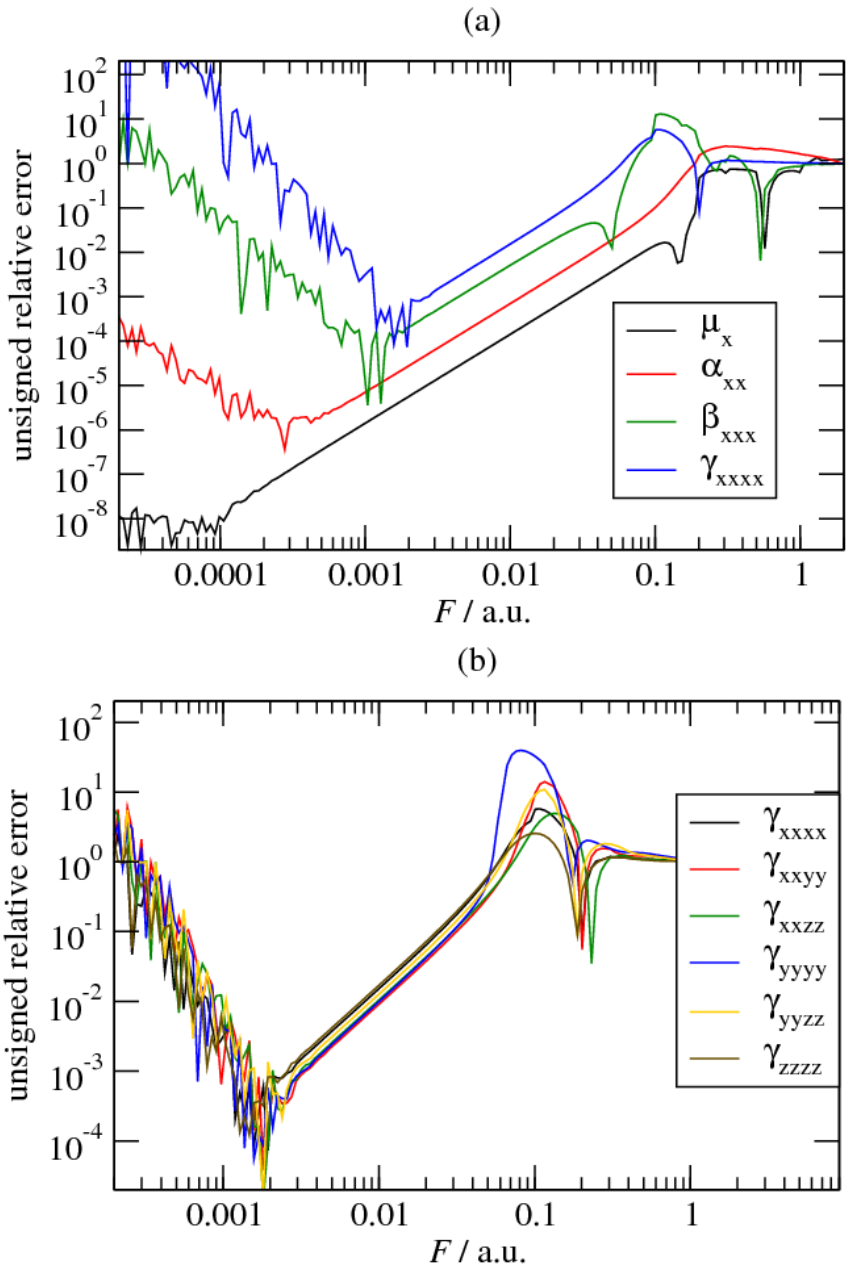

Figure 2.3. Relative error of finite field properties in comparison to response theory for different tensor elements of water at the HF/aug-cc-pVTZ level of theory. (a) shows the dipole moment μ, polarizability α, and first and second hyperpolarizabilities β and γ along the direction of the dipole. (b) shows all nonzero tensor elements for γ. The water molecule is oriented such that the dipole moment points along the x axis, and z corresponds to the out-of-plane axis.

That the noise scales indeed as inverse powers of F can be seen from Figure 2.3a. Relation (2.18) defines an ultimate limit of how precise an FF quantity can be known. If, for example, for a molecule α and γ are evaluated at F = 0.001 au and its energy is computed to a precision of δE=1e-10 au, then the absolute error introduced on α is of the order 0.0001 au and likewise γ cannot be more precise than ±100 au, independent of its absolute magnitude.

2.4.3 The high field limit

Taking only the numerical noise into consideration, it would be profitable to choose the field strength as high as possible. However, this is prohibited by non-negligible higher-order terms in the Taylor expansion (2.2) and an eventual change in the electronic configuration. Figure 2.4 illustrates the interplay between the ground and excited state energies for neon at rather strong fields and its effect on α and γ. It holds in general that the more diffuse a basis set, the smaller the required field strength to cause an abrupt change of the slope of $E(F)$, which corresponds to an inversion of the electronic ground state with the first excited state.[19] This relation is well-established and is confirmed by Figure 2.4a for basis sets up to quadruple augmentation. At zero field, the energy is essentially the same (within 0.0001 au) for all but the nondiffuse cc-pVDZ basis. Applying weak fields below 0.05 au, the ground state energy changes are mostly described by the $-\frac{1}{2}\alpha F^2$ term and are, therefore, systematic and similar for all basis sets.

Beyond that point, the energy of the q-aug-cc-pVDZ calculation suddenly starts to drop rapidly. In the same way, although sometimes less visible, all the other basis sets have a characteristic field strength at which the energy starts to behave differently.

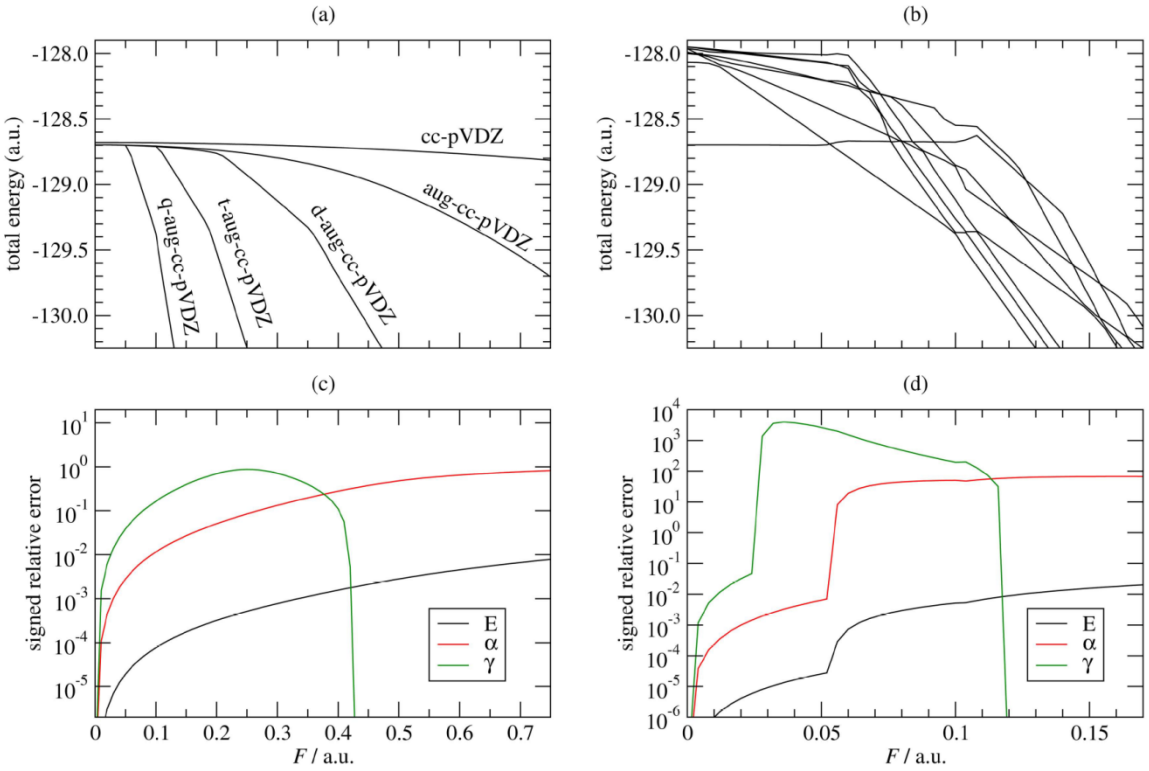

Figure 2.4. Ground and excited state energies of neon obtained by a CASSCF(8,13) calculation as a function of the external electric field. (a) The ground state energy using cc-pVDZ with varying amounts of diffuse basis functions. (b) Ground and several excited state energies, applying the q-aug-cc-pVDZ basis set. (c) The relative energy difference ($E(F)/E(0)$-1), as well as the relative error on the polarizability (α_{FF}/α_{RT}-1) and on the second hyperpolarizability (γ_{FF}/γ_{RT}-1) obtained with aug-cc-pVDZ. (d) The same data as in (c) for q-aug-cc-pVDZ.

This sudden drop originates from some excited states that stabilize faster than the ground state when F increases so that, beyond a certain field amplitude, they are successively replacing the ground state. This is depicted in Figure 2.4b for the q-aug-cc-pVDZ basis where the first state inversion happens at ~0.05 au followed by another one at ~0.1 au. The steeper slope in the interval [0.05 au, 0.1 au] is attributed to the larger α value for that state.[28,29] The second inversion happens with a highly excited state whose zero field energy certainly lies beyond the ionization potential of neon at $E_{IP} \approx 0.8$ au, such that its corresponding α is physically meaningless.

It is, however, possible to go beyond this point with less augmented basis sets, and Figure 2.4c shows proof that indeed reasonable values for α_{FF} and γ_{FF} can be obtained for $F > 0.05$ au using the aug-cc-pVDZ basis (The same is visible in Figure 2.1b for other basis sets). Figure 2.4d shows what happens to the polarizability calculated above the critical field strength. At each crossing point of the ground state, $F > 0.05$ au, α jumps to a new value approximately corresponding to the polarizability of that new state (visible as a large error in Figure 2.4d). As γ_{FF} is calculated according to Eq. (2.8), it contains also the energy at twice the field strength and the critical point thus appears at half the value of the first ground state crossing. At even stronger fields, γ_{FF} changes sign and is thus not depicted in the figure anymore.

The comparison of Figure 2.4c and Figure 2.4d reveals that it can be difficult to find the critical field strength only based on inspection of the ground state energy. In

Figure 2.4a, the graph for the aug-cc-pVDZ basis set possesses no obvious kink from an intersection with excited states. Nevertheless, γ_{FF} in Figure 2.4c is only acceptable for $F <$ 0.1 au. For stronger fields, the error is of the same magnitude or even larger than γ itself.

For small molecules, it is usually affordable to add another layer of diffuse basis functions in order to clearly locate the intersection of two states and thus easily define the upper bound for feasible field strengths. The problem looks different for cases where the use of diffuse basis sets is discouraged or even prohibited due to near-linear dependences within the overlap matrix.[30] A famous, well studied example are polyynes (PY), linear chains of alternating carbon–carbon single and triple bonds.[31] In these extended systems, even nondiffuse basis sets such as cc-pVTZ can have convergence issues because of the relatively small triple bond length. The basis sets used to investigate NLO properties are thus usually of double-, maximally triple-zeta quality with few or no diffuse and polarization functions, also in the most recent literature.[15,16,32,33] In Figure 2.5, FF calculations are performed at the HF/6-31G* level for PY chains containing 1 (Figure 2.5a), 5 (Figure 2.5b), and 10 (Figure 2.5c) triple bonds, respectively. For the small molecule of Figure 2.5a, the usage of a nondiffuse basis set makes it difficult to locate any kink in the field dependence of the ground state energy that could be assigned to an intersection with excited states. However, additional information, such as the HOMO-LUMO gap, is of great assistance in tracking such a change. Indeed, the minimum value of the gap around F = 0.2 au corresponds to soft kinks in the relative error for α, and also for γ at half that field strength.

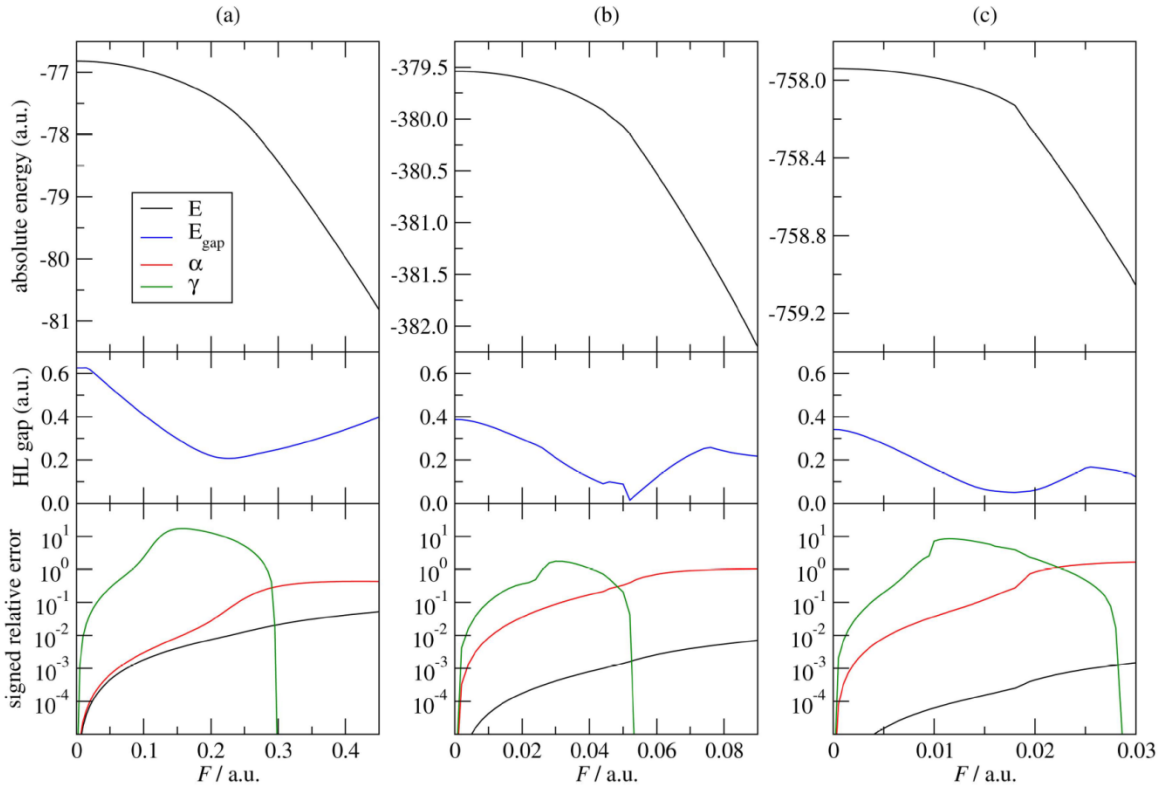

Figure 2.5. Field dependence of several quantities for PY chains of 1, 5, and 10 triple bonds, obtained at the HF/6-31G* level of theory. (a) shows the results for C_2H_2, (b) for $C_{10}H_2$, and (c) for $C_{20}H_2$. The upper row shows the absolute energy. In the middle, the energy difference between the highest occupied and the lowest unoccupied canonical molecular orbital (HOMO-LUMO gap) is depicted. On the bottom, the relative energy difference, as well as the error on α and γ is shown for each molecule analog to Figure 2.4c and Figure 2.4d.

If the chain length is increased, a certain "diffuseness" of the basis is generated by the fact that neighbouring atomic basis functions overlap substantially and thus account for some missing features of a small basis set. This effect is also the reason why accurate values for the NLO properties of elongated systems can be obtained without the aid of diffuse basis functions.[34] Figure 2.5b and Figure 2.5c are a verification of that statement. For $C_{20}H_2$, a kink at ~0.018 au is easily visible for the ground state energy. The discontinuities in the relative error on α and γ are more expressed than in the smaller chains, such that an overall localization of the critical field strength is facilitated. $C_{10}H_2$ presents an intermediate behaviour with a change of slope in $E(F)$ around $F = 0.05$ au.

In conclusion, (i) the upper limit for an electric field that will lead to meaningful FF quantities is usually found in a straightforward manner, if the basis set contains enough diffuse functions, (ii) extended molecular chains behave well without diffuse basis functions, and (iii) in problematic cases, additional quantities such as the excitation energies or the HOMO-LUMO gap may help to locate the critical field strength.

2.4.4 Extrapolating FF quantities

We now turn to Richardson extrapolation, which has the advantage over the polynomial fit that no additional parameters, such as the order r, need to be chosen. The effects of this kind of extrapolation are studied for the second hyperpolarizability of a large set of molecules shown in Figure 2.6. For every molecule, a minimal relative error is found by varying the field strength, while the common ratio x and the degree of

refinement *m* in Eq. (2.15) are fixed. Although very noisy for individual molecules, the average over multiple molecules produces smooth graphs that show significant trends.

It is found that the first two refinement steps reduce the relative error by more than one order of magnitude. Going beyond $m = 2$ does not lead to further improvement anymore as the lowering of the truncation error is superseded by the accumulated round-off error in Eq. (2.15). The dependence of the error on *x* is increased for large *m* and leads to best results for $x = [1.2, 1.8]$. Values for $x < 2$, in particular $x = \sqrt{2}$, were already suggested in Ref. [13] based on inspection of an analytical function and one numerical example. These findings are greatly confirmed here based on a broad data set of 120 molecules.

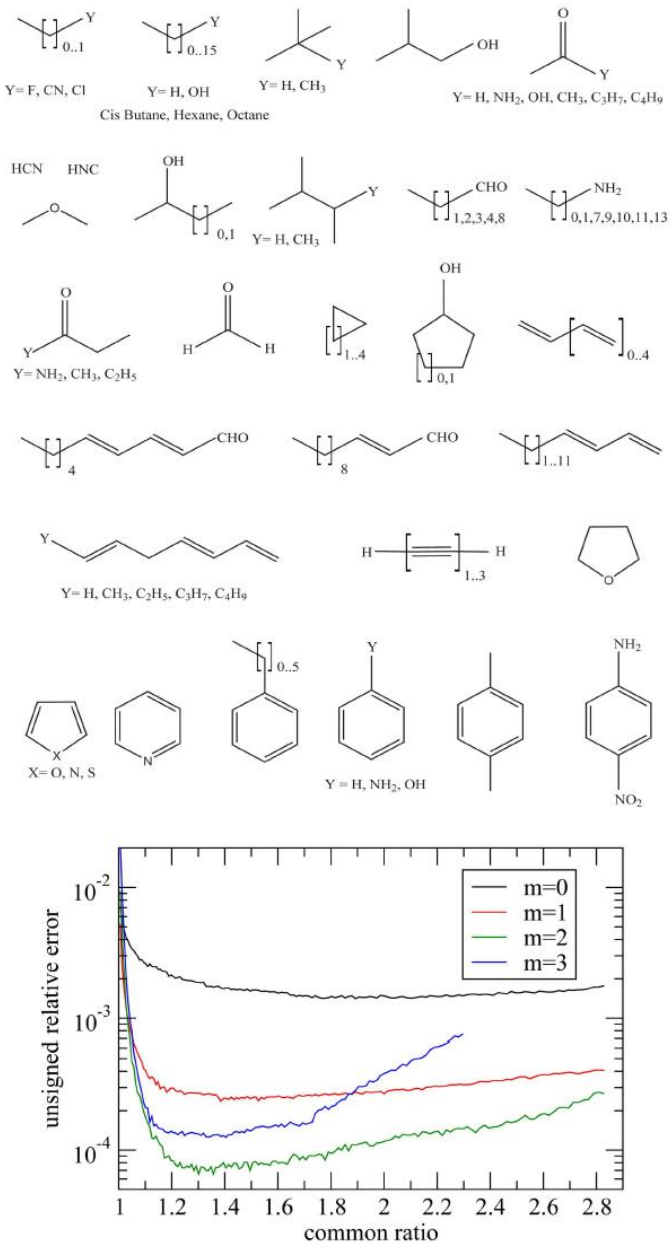

Figure 2.6. The minimal relative error $|\varepsilon_\gamma|$ as a function of common ratio x and refinement step m (all dimensionless quantities), averaged over a data set of 120 molecules shown on the top. The FF calculations were done with HF/6-31G* based on CAM-B3LYP/6-31G* geometries. For each molecule, various $\gamma_{n,m}$ were calculated using Eq. (2.15). The minimal relative error is found, by picking that n which leads to the smallest deviation from the reference value γ_{RT}, while m and x stay fixed. The averaging over the molecules is done by taking the logarithmic mean.

2.4.5 Exemplary cases

We finally show the gain in precision that can be achieved using the methods of polynomial fitting and Richardson extrapolation for some exemplary molecules. Table 2.1 contains the relative error for α, β, and γ of tetrachloromethane and acetonitrile, two reference molecules for NLO measurements.[22] Table 2.2 shows similar data for increasing chains of cumulene (C_nH_4). These conjugated systems have huge NLO properties with the peculiarity that a sign change for γ can occur depending on the level of theory.[35] This leads to a rather small γ_{RT} for C_6H_4, whereas all the other properties like α and the higher-order derivatives of the Taylor expansion are extremely large. Hence, the precision on γ_{FF} is very limited with only one significant digit in the unrefined case.

As a general observation, the improvement due to extrapolation is larger for α (up to three orders of magnitude increase for the precision) than for β and γ (one to two orders of magnitude). Comparing the different extrapolation schemes, no preference can be given. However, Richardson extrapolation with m = 1 needs only four energy calculations, at optimally chosen fields $\{0, F, xF, x^2F\}$, that return a precision similar to a polynomial fit with 14 data points. The only time when the polynomial fit outperforms Richardson extrapolation is the special case of C_6H_4 where apparently the precision benefits from the larger array of data points.

Table 2.1. The relative error ε_q for different electric-field response properties of tetrachloromethane (CCl_4) and acetonitrile (CH_3CN) computed at the HF/aug-cc-pVTZ level of theory.

		Reference	Raw value[(a)]	Polynomial fit[(b)]	Richardson extrapolation[(c)]		
Molecule[(d)]	q	q_{RT}/au	ε_q	$\varepsilon_{q,fit}$	x=2	$x=\sqrt{2}$	$x=\sqrt[4]{2}$
CCl_4	α_{xx}	65.67	8.0e-6	5.5e-8	2.9e-8	7.4e-9	1.7e-8
CCl_4	γ_{xxxx}	6119	6.4e-3	3.2e-4	2.4e-4	1.4e-4	2.1e-4
CH_3CN	α_{xx}	36.68	8.2e-6	1.1e-9	1.7e-8	2.0e-10	1.1e-9
CH_3CN	β_{xxx}	12.41	8.6e-4	3.3e-5	9.0e-5	8.0e-5	3.9e-5
CH_3CN	γ_{xxxx}	3572	1.6e-3	6.5e-6	1.4e-4	3.3e-5	4.8e-5

Different extrapolation schemes are tested for a set containing the energies for 13 field strengths defining a geometric progression in the range [0.001 au, 0.008 au] (and another 13 fields of opposite sign for the noncentrosymmetric CH_3CN) plus the zero field energy.

(a) Properties calculated by Eqs. (2.6)–(2.8) for F = 0.001 au.

(b) A polynomial fit of order r=3 (i.e., including terms up to F^6 with the coefficients of odd powers set equal zero) was used for α_{fit} and γ_{fit}. For β_{fit}, a polynomial of order r=2 (including terms up to F^4) was fitted to the field dependent dipole moments of Eq. (2.5).

(c) Smallest error achievable within above set of 14 data points using a refinement step m=1 and different choices of x.

(d) Only tensor elements along the x axis are reported. For CCl_4, this coincides with one of the molecule's C_2 axes. In CH_3CN, the x axis is defined as the line connecting all heavy atoms.

Table 2.2. The relative error ε_γ for methane, ethylene and cumulene chains computed at the HF/aug-cc-pVDZ level of theory.

	Reference	Raw value	Polynomial fit		Richardson extrapolation		
Molecule	γ_{RT}/au	ε_γ	r=3	r=4	x=2	$x=\sqrt{2}$	$x=\sqrt[4]{2}$
CH_4	1350	1.0e-3	2.9e-6	4.9e-5	2.4e-5	3.0e-6	1.6e-5
C_2H_4	1757	6.7e-4	1.6e-5	1.7e-4	6.7e-5	2.1e-5	3.2e-5
C_3H_4	5820	5.2e-4	7.4e-5	1.4e-4	1.5e-5	7.8e-5	5.5e-5
C_4H_4	10633	1.7e-3	2.2e-4	3.9e-5	3.4e-5	1.3e-4	1.6e-5
C_5H_4	11523	4.3e-3	9.1e-4	1.8e-4	2.6e-4	5.6e-5	2.5e-4
C_6H_4	1587	7.2e-2	2.1e-2	1.7e-4	1.7e-3	2.2e-3	3.5e-2
C_7H_4	30383	7.9e-3	2.4e-3	3.1e-5	3.3e-4	2.7e-5	3.7e-4

The same field strengths and settings described in Table 2.1 and footnotes apply also here.

It should finally be mentioned that the best extrapolation estimates shown in Table 2.1 and Table 2.2 are all obtained for field strengths between 0.001 au and 0.004 au with a tendency toward the lower value for the elongated chains of Table 2.2. On the other hand, the critical field strength lies beyond 0.02 au for all cases. So it seems essential to stay at least a factor of 10 below the critical field strength for performing the most precise calculations of NLO properties.

2.5 Conclusions

The present study assesses the reliability of the finite field (FF) method for evaluating the polarizabilities and hyperpolarizabilities and proposes ways to reduce the numerical error of such calculations. It is found that for every molecule, an individual region of feasible field strengths can be highlighted, which is defined by an upper and a lower bound. Fields chosen below that region suffer from a too large round-off error when taking the finite energy differences. This error scales proportionally to the convergence threshold of the energy and some inverse power of the field strength, dependent on the property. The upper bound is imposed by the critical field strength originating from intersections between the ground and excited state energies and depends on molecule-specific factors, but also strongly on the augmentation level of the basis set.

Within the feasible region, the main source of error stems from higher-order derivatives of the Taylor expansion that can be removed by means of Richardson

extrapolation. The first two refinement steps reduce the error by one or two orders of magnitude for γ and up to three orders for α. Additional steps, however, do not lead to further improvement. A benchmark on 120 molecules confirms that a common ratio of $x < 2$ and a refinement step of $m = 2$ yields the most precise results.

A polynomial fit for different meshes of field strengths within the feasible region reveals the same preference for values of $x < 2$. Although a polynomial of sufficiently high order provides good estimates over the whole range of feasible field strengths, a clear tendency to improved results is discernible, when values close to the critical field strength are discarded from the fit. Similar observations from Richardson extrapolation lead to the conclusion that a factor of about a 10th of the critical field strength should be the upper limit for an extrapolation leading to a maximum of precision.

2.6 References

1. H. Nalwa, S. Miyata, *Nonlinear Optics of Organic Molecules and Polymers*, CRC Press: Boca Raton, 1996.

2. J. L. Bredas, C. Adant, P. Tackx, A. Persoons, B. M. Pierce, Chem. Rev. **94**, 243 (1994).

3. Y. Luo, H. Agren, P. Jorgensen, K. V. Mikkelsen, Adv. Quantum Chem. **26**, 165 (1995).

4. H. D. Cohen, C. C. J. Roothaan, J. Chem. Phys. **43**, S34 (1965).

5. R. J. Bartlett, G. D. Purvis, Phys. Rev. A **20**, 1313 (1979).

6. H. A. Kurtz, J. J. P. Stewart, K. M. Dieter, J. Comput. Chem. **11**, 82 (1990).

7. M. Nakano, I. Shigemoto, S. Yamada, K. Yamaguchi, J. Chem. Phys. **103**, 4175 (1995).

8. G. Maroulis, J. Chem. Phys. **108**, 5432 (1998).

9. K. Kamada, M. Ueda, H. Nagao, K. Tawa, T. Sugino, Y. Shmizu, K. Ohta, J. Phys. Chem. A **104**, 4723 (2000).

10. F. A. Bulat, A. Toro-Labbe, B. Champagne, B. Kirtman, W. Yang, J. Chem. Phys. **123**, 014319 (2005).

11. T. Touma, M. Kobayashi, H. Nakai, Theor. Chem. Acc. **130**, 701 (2011).

12. S. Wouters, P. A. Limacher, D. Van Neck, P. W. Ayers, J. Chem. Phys. **136**, 134110 (2012).

13. M. Medved, M. Stachova, D. Jacquemin, J.-M. Andre, E. A. Perpete, THEOCHEM **847**, 39 (2007).

14. B. Champagne, B. Kirtman, Int. J. Quantum Chem. **109**, 3103 (2009).

15. M. de Wergifosse, B. Champagne, J. Chem. Phys. **134**, 074113 (2011).

16. P. A. Limacher, Q. Li, H. P. Luthi, J. Chem. Phys. **135**, 014111 (2011).

17. L. M. Abreu, T. L. Fonseca, M. A. Castro, J. Chem. Phys. **136**, 234311 (2012).

18. J. B. Robinson, P. J. Knowles, J. Chem. Phys. **137**, 054301 (2012).

19. D. M. Bishop, S. A. Solunac, Chem. Phys. Lett. **122**, 567 (1985).

20. F. Sim, S. Chin, M. Dupuis, J. E. Rice, J. Phys. Chem. **97**, 1158 (1993).

21. L. F. Richardson, J. A. Gaunt, Phil. Trans. R. Soc. Lond. A **226**, 299 (1927).

22. F. Castet, E. Bogdan, A. Plaquet, L. Ducasse, B. Champagne, V. Rodri-guez, J. Chem. Phys. **136**, 024506 (2012).

23. B. Champagne, B. Kirtman, In *Handbook of Advanced Electronic and Photonic Materials and Devices*, Vol. 9; H. S. Nalwa, Ed.; Academic Press: Burlington, 2001, pp. 63–126.

24. Gaussian 09, Revision C.01, M. J. Frisch, G. W. Trucks, H. B. Schlegel, G. E. Scuseria, M. A. Robb, J. R. Cheeseman, G. Scalmani, V. Barone, B. Mennucci, G. A. Petersson, H. Nakatsuji, M. Caricato, X. Li, H. P. Hratchian, A. F. Izmaylov, J. Bloino, G. Zheng, J. L. Sonnenberg, M. Hada, M. Ehara, K. Toyota, R. Fukuda, J. Hasegawa, M. Ishida, T. Nakajima, Y. Honda, O. Kitao, H. Nakai, T. Vreven, J. A. Montgomery, Jr., J. E. Peralta, F. Ogliaro, M. Bearpark, J. J. Heyd, E. Brothers, K. N. Kudin, V. N. Staroverov, T. Keith, R. Kobayashi, J. Normand, K. Raghavachari, A. Rendell, J. C. Burant, S. S. Iyengar, J. Tomasi, M. Cossi, N. Rega, J. M. Millam, M. Klene, J. E. Knox, J. B. Cross, V. Bakken, C. Adamo, J. Jaramillo, R. Gomperts, R. E. Stratmann, O. Yazyev, A. J. Austin, R. Cammi, C. Pomelli, J. W. Ochterski, R. L. Martin, K. Morokuma, V. G. Zakrzewski, G. A. Voth, P. Salvador, J. J. Dannenberg, S. Dapprich, A. D.

Daniels, O. Farkas, J. B. Foresman, J. V. Ortiz, J. Cioslowski, and D. J. Fox, Gaussian, Inc., Wallingford CT, 2009.

25. DALTON, a molecular electronic structure program, Release 2.0 (2005), Available at: http://www.kjemi.uio.no/software/dalton/dalton.html

26. B. Jansik, P. Salek, D. Jonsson, O. Vahtras, H. Agren, J. Chem. Phys. **122**, 054107 (2005).

27. T. Helgaker, S. Coriani, P. Jørgensen, K. Kristensen, J. Olsen, K. Ruud, Chem. Rev. **112**, 543 (2012).

28. M. Urban, A. J. Sadlej, Theor. Chim. Acta **78**, 189 (1990).

29. M. Merawa, M. Rerat, J. Chem. Phys. **108**, 7060 (1998).

30. P. A. Limacher, K. V. Mikkelsen, H. P. Luthi, J. Chem. Phys. **130**, 194114 (2009).

31. S. Eisler, A. D. Slepkov, E. Elliott, T. Luu, R. McDonald, F. A. Hegmann, R. R. Tykwinski, J. Am. Chem. Soc. **127**, 2666 (2005).

32. J.-W. Song, M. A. Watson, H. Sekino, K. Hirao, J. Chem. Phys. **129**, 024117 (2008).

33. J.-W. Song, M. A. Watson, H. Sekino, K. Hirao, Int. J. Quantum Chem. **109**, 2012 (2009).

34. G. J. B. Hurst, M. Dupuis, E. Clementi, J. Chem. Phys. **89**, 385 (1988).

35. J. O. Morley, J. Phys. Chem. **99**, 10166 (1995).

Chapter 3

Predicting Optimal Finite Field Strengths for Calculating the First and Second Hyperpolarizabilities Using Simple Molecular Descriptors[†]

3.1 Motivation

The previous chapter explored the general performance of the finite field method, with an emphasis on its dependence on the choice of initial field strength. The optimal common ratio for the geometric progression of the field and the optimal scheme of refinement of the second hyperpolarizability were determined. But an important question that remains is: given a molecular structure, how could the initial field for calculating accurate hyperpolarizabilities be determined *a priori*? In this chapter, we show that the

[†] This chapter was originally published as A. A. K. Mohammed, P. A. Limacher, P. W. Ayers, Chem. Phys. Lett. **682**, 160 (2017).

optimal field strength depends on the molecular structure and should be chosen for each molecule individually. We, then, propose a protocol to predict the optimal field strength for calculating the second hyperpolarizability and suggest a way of estimating the optimal field for the first hyperpolarizability.

3.2 Introduction

The finite field (FF) method is a standard technique in quantum chemistry for calculating electric response properties of molecules like the static dipole polarizabilities (α) and higher order derivatives thereof (e.g., the first and second hyperpolarizabilities, β and γ).[1-4] The main advantage of the FF method is its low computational cost and ease of implementation, compared to other approaches like the sum over states formalism, coupled-perturbed Hartree-Fock, or response theory (RT).[5,6] Whereas these methods need additional information such as analytical gradients or excited state information, the FF method simply requires the calculation of the electronic energy in the presence of various external electric fields.[7] As such it is usually the method of choice for newly developed theories, but also for high level ab initio correlated calculations.

However, there are also serious drawbacks of the FF method, the most crucial being the dependence of the result on the initially chosen field strength *F*. The higher order derivatives, β and γ, are especially sensitive quantities, with a rather narrow range of suitable field strengths. This sensitivity arises because the FF method is effectively a way

of numerically differentiating the energy of a molecule with respect to the magnitude of the electric field, and as such suffers from finite-precision artifacts when the value of F is too small. On the other hand, if one chooses a value of F that is too large the higher-order derivatives become nonnegligible and contaminate the lower-order derivatives of interest. Worse, after a certain critical field strength has been passed, a field-induced state inversion, where an excited state at zero-field becomes lower in energy than the ground state occurs.[8] The first effect can be mitigated using Richardson extrapolation, which combines calculations at several different field strengths in order to reduce the finite difference error.[9,10] This procedure has been successfully applied in the literature.[11-13]

In a recent article, we illustrated how to maximize the benefits of such refinement procedures.[14] Using Richardson extrapolation, significant improvements of the precision are obtained when the applied field strengths follow a geometric progression with a common ratio smaller than two.[15] Another finding is that the precision only benefits from the first one or two steps of iterative Richardson refinement. Subsequent Richardson steps lead to an accumulation of numerical noise.

An open question so far is, how an optimal field strength, F_{opt}, which is the field strength that corresponds to the minimum relative error of the calculated FF quantity, should be chosen for a particular molecule. It is clear that molecules of different size and shape react differently to the applied external electric field. Intuitively, one can understand that large and extended molecules are exposed to much higher potential

changes when placed in an external field and thus are expected to have a much smaller F_{opt} than small molecules. Similarly, it is conceivable that molecules of the same size, but different electronic structure (e.g., saturated vs. conjugated hydrocarbon chains) might have very different optimal field strengths. The purpose of this study is to find correlations between the optimal field strength and other molecule-specific descriptors that allow one to make straightforward, *a priori*, predictions for F_{opt}. This is important because it allows one to avoid the (computer) time-consuming search for the optimal field strength.

3.3 Methods

3.3.1 Finite field method

The energy E of a molecule for a small external homogenous static electric field F can be approximated with a McLaurin series,

$$E(F) = E(0) + \left.\frac{\partial E}{\partial F}\right|_0 F + \frac{1}{2!}\left.\frac{\partial^2 E}{\partial F^2}\right|_0 F^2 + \frac{1}{3!}\left.\frac{\partial^3 E}{\partial F^3}\right|_0 F^3 + \frac{1}{4!}\left.\frac{\partial^4 E}{\partial F^4}\right|_0 F^4 + \ldots \qquad (3.1)$$

$$E(F) = E(0) - \mu F - \frac{1}{2}\alpha F^2 - \frac{1}{6}\beta F^3 - \frac{1}{24}\gamma F^4 + \ldots \qquad (3.2)$$

where μ and α denote the dipole moment and the dipole polarizability, respectively. The higher-order nonlinear responses are the first hyperpolarizability (β) and the second hyperpolarizability (γ).

Eq. (3.2) can be split into even and odd powers of *F*, which leads to symmetric and antisymmetric combinations of energies at equal positive and negative field strength

$$E_S(F) = \frac{E(F) + E(-F)}{2} = E(0) - \frac{1}{2}\alpha F^2 - \frac{1}{24}\gamma F^4 + O(F^6) \tag{3.3}$$

$$E_A(F) = \frac{E(F) - E(-F)}{2} = -\mu F - \frac{1}{6}\beta F^3 - \frac{1}{120}\delta F^5 + O(F^7) \tag{3.4}$$

This allows the polarizabilities and the even-order hyperpolarizabilities to be treated separately from the dipole moment and the odd-order hyperpolarizabilities. By rearranging Eqs. (3.3) and (3.4), the dipole moment (μ) and polarizability (α) can be obtained directly as

$$\mu(F) = -\frac{E_A(F)}{F} = \mu + \frac{1}{6}\beta F^2 + \frac{1}{120}\delta F^4 + O(F^6) \tag{3.5}$$

$$\alpha(F) = 2\frac{E(0) - E_S(F)}{F^2} = \alpha + \frac{1}{12}\gamma F^2 + \frac{1}{360}\varepsilon F^4 + O(F^6) \tag{3.6}$$

If *F* is chosen small enough, Eqs. (3.5) and (3.6) are good estimate for μ and α, respectively.

To evaluate β and γ, μ and α have to be eliminated from Eqs. (3.5) and (3.6), respectively. This can be achieved if the energy is known at two different field strengths, e.g., F and $2F$, besides the energy at zero field

$$\beta(F) = 2\frac{\mu(2F)-\mu(F)}{F^2} = \frac{2E_A(F)-E_A(2F)}{F^3} = \beta + \frac{1}{4}\delta F^2 + O(F^4) \qquad (3.7)$$

$$\gamma(F) = 4\frac{\alpha(2F)-\alpha(F)}{F^2} = \frac{-2E_S(2F)+8E_S(F)-6E(0)}{F^4} = \gamma + \frac{1}{6}\varepsilon F^2 + O(F^4) \qquad (3.8)$$

More generally, for any two values of field strengths (say F and xF), Eqs. (3.7) and (3.8) can be generalized to

$$\beta(F) = \frac{6}{x^2-1}\cdot\frac{\mu(xF)-\mu(F)}{F^2} = \frac{6}{F^3x}\cdot\frac{xE_A(F)-E_A(xF)}{x^2-1} \qquad (3.9)$$

$$\gamma(F) = \frac{12}{x^2-1}\cdot\frac{\alpha(xF)-\alpha(F)}{F^2} = \frac{24}{F^4x^2}\left(\frac{x^2E_S(F)-E_S(xF)}{x^2-1} - E(0)\right) \qquad (3.10)$$

The common practice to work with field strengths F and $2F$, corresponds to the choice $x = 2$ in Eq. (3.10).[16,17] However, in a recent study we showed that using $x < 2$ improves the accuracy of FF calculations because it allows for more points lying in the acceptable region of field strengths.[14] Motivated by the results of that study, we always use $x = \sqrt{2}$ in our calculations of γ. Eq. (3.10) then simplifies to

$$\gamma(F) = \frac{12}{F^4}\left(-E_S\left(\sqrt{2}F\right)+2E_S(F)-E(0)\right) \qquad (3.11)$$

For β, we use $x = \sqrt[4]{2}$. Eq. (3.9) becomes

$$\beta(F) = \frac{6}{F^3\sqrt[4]{2}} \cdot \frac{\sqrt[4]{2}E_A(F) - E_A\left(\sqrt[4]{2}F\right)}{\sqrt{2}-1} \tag{3.12}$$

3.3.2 Error reduction

The scaling of the error in Eqs. (3.7) and (3.8) can be lifted to a higher order by Richardson extrapolation.[9] This method is widely applied to improve the precision of FF quantities by reducing the error from truncating the Taylor expansion, and it is known to improve the precision of the higher order derivatives β and γ in the first few iterations. A detailed description of the recursive Richardson extrapolation can be found in Ref. 14. Based on these results, we use at most two iterations of refinement (m=0, 1, 2). Eq. (3.11) corresponds to the unrefined $\gamma_{m=0}$ case. Combining two or three instances of $\gamma_{m=0}$ with adjusted fields, we obtain

$$\gamma_{m=1}(F) = \frac{3}{F^4}\left(E_S(2F) - 10E_S\left(\sqrt{2}F\right) + 16E_S(F) - 7E(0)\right) \tag{3.13}$$

and

$$\gamma_{m=2}(F) = \frac{1}{4F^4}\begin{pmatrix} -E_S\left(2^{3/2}F\right) + 26E_S(2F) - 176E_S\left(\sqrt{2}F\right) \\ +256E_S(F) - 105E(0) \end{pmatrix} \tag{3.14}$$

For β, we use only one step of Richardson extrapolation and $x = \sqrt[4]{2}$

$$\beta_{m=1}(F) = \frac{3}{F^3\left(\sqrt{2}-1\right)^2}\left(E_A\left(\sqrt{2}F\right) - 3\sqrt[4]{2}E_A\left(\sqrt[4]{2}F\right) + 2\sqrt{2}E_A(F)\right) \qquad (3.15)$$

3.3.3 Field grid

In this work we use a fine grid to find the optimal field strength F_{opt}. For each molecule, energy calculations are performed at field strengths

$$F_n = F_0 \cdot 2^{n/100} \qquad (3.16)$$

with n ranging from 0 to 800 and F_0=0.0005 au which yields a maximum field strength >0.1 au. Within this array of fields, many geometric progressions with a common ratio of $x = \sqrt{2}$ can be generated, simply by picking a particular field strength F_{p} and the fields $F_{\text{p+50}}$, $F_{\text{p+100}}$ and $F_{\text{p+150}}$. The energies at these field strengths have to be inserted into Eqs. (3.11), (3.13), and (3.14) together with the energy at zero field to determine the value of γ_{FF} at field strength F_{p}. For β, calculations are done at fields F_{p}, $F_{\text{p+25}}$, $F_{\text{p+50}}$ using equation (3.15).

3.3.4 Molecular descriptors

For every molecule the optimal field strength F_{opt} is correlated to other descriptors of structural or electronic nature. Besides quantities like maximum distances within the molecule, molecular weight, moments of inertia, HOMO-LUMO gap, Hartree-Fock energy, transition moments, and the magnitude of β and γ themselves, we also define five

descriptors, which are constructed from the atomic positions $\boldsymbol{r}_i$ and charges q_i within a molecule. We call them

$$A = \left(\frac{1}{N_{atoms}} \sum_{i=1}^{N_{atoms}} \left| \mathbf{r}_i - \bar{\mathbf{r}} \right|^p \right)^{1/p} \tag{3.17}$$

$$B = \left(\frac{1}{N_{atoms}} \sum_{i=1}^{N_{atoms}} q_i^p \left| \mathbf{r}_i - \bar{\mathbf{r}} \right|^p \right)^{1/p} \tag{3.18}$$

$$C = \left| \sum_{i=1}^{N_{atoms}} q_i^p \left(\mathbf{r}_i - \bar{\mathbf{r}} \right) \right| \tag{3.19}$$

$$D = \sum_{i=1}^{N_{atoms}} q_i^p \left| \mathbf{r}_i - \bar{\mathbf{r}} \right| \tag{3.20}$$

$$E = \sum_{i>j} \tanh \left| \frac{q_i - q_j}{\mathbf{r}_i - \mathbf{r}_j} . p \right| \tag{3.21}$$

In these equations $\bar{\mathbf{r}}$ is defined as

$$\bar{\mathbf{r}} = \frac{1}{N_{atoms}} \sum_{i=1}^{N_{atoms}} \mathbf{r}_i \tag{3.22}$$

and p is an arbitrary exponent. Here, we study cases for p between zero and five. Eqs. (3.17)-(3.21) are measures for the spatial extent and charge distribution of a molecule. For example the radius of gyration can be obtained using Eq. (3.17) and p=2.

3.3.5 Electronic structure calculations

For each molecule a geometry optimization was performed using the Gaussian 09 program,[18] using the long-range corrected hybrid density functional CAM-B3LYP,[19-24] which was proven to produce accurate molecular geometries,[25,26] with a 6-31G(d) basis set.[27-30]

All calculations of the response and finite field properties were done with the DALTON quantum chemistry program using the aforementioned optimized geometries.[31] The level of theory was HF/6-31G(d), which is known to supersede DFT polarizabilities in some respects.[12,16,17] We used the natural population analysis method to calculate atomic charges using HF/6-31G(d). As our primary interest is developing *methods* for FF calculations, rather than actually computing accurate hyperpolarizabilities, the level of theory is relatively unimportant to our study. It is more important that (a) reference hyperpolarizabilities are available from response theory and (b) the method is fast enough to allow us to thoroughly explore different FF approaches. The Hartree-Fock method satisfies both these constraints. Diffuse orbitals were not employed because they would introduce another of numerical instabilities.[34,35] The transferability of these HF/6-31(d) results to more advanced levels of theory is straightforward. A change of the quantum chemical method or of the basis set will lead to different values for F_{opt}, and certainly also for γ_{FF}. However, our protocol to determine these values is uninfluenced by this.

Because we compare very small energy differences, tight convergence criteria were applied for the solution of the SCF equations. The energies are calculated to machine precision (15 significant digits). Response theory is used to assess the accuracy of the FF results.[32,33] The convergence criteria in these calculations are chosen such that response theory first and second hyperpolarizabilities, β_{RT} and γ_{RT}, are numerically correct for 8 digits and thus orders of magnitude more accurate than the smallest relative errors for FF encountered in this study. The relative error of a finite field quantity q_{FF} with respect to q_{RT} is given by

$$\varepsilon_q = \frac{q_{FF}}{q_{RT}} - 1, \text{ where } q = \{\beta, \gamma\} \tag{3.23}$$

All hyperpolarizabilities are evaluated for time-independent (static) fields. Results are shown for the longitudinal component of the first and second hyperpolarizability tensor β_{xxx} and γ_{xxxx} with x indicating the molecular axis with the smallest moment of inertia. The subscript x will be dropped for simplicity.

3.4 Results and Discussion

The molecules investigated for γ and β are presented in Figure 3.1 and Figure 3.2, respectively. The data sets contain cyclic and linear alkanes, (poly)alkenes, aromatic rings, and includes heteroatoms and functional groups to obtain a variety of molecules

with a wide range of values for γ (from -21.3 (methane) to 6.2 x 10^5 au (decapentaene)) and β (from 1.2 (pyrrole) to 6261.4 au (4-amino-4'-nitro-diphenylethylene)).

3.4.1 Field dependence of hyperpolarizabilities

In the reliable field region, the numerical error is well-behaved and can be used for extrapolation and error minimization.[14] The exact range of fields for which results are reliable is not only dependent on the level of theory, but also on the molecule under investigation, as seen from Figure 3.3 and Figure 3.4. For γ, the beginning of the reliable field region has a minimal relative error and occurs at lower field strengths for larger molecules (decapentaene < hexylbenzene < hexane < acetonitrile < propane). For β, the reliable field region of push-pull π-conjugated systems clearly starts at lower field strengths than that of saturated hydrocarbons. In both figures, the reliable field region is bordered by a noisy region at low fields (where numerical errors accumulate) and meaningless results at fields that are strong enough to ionize the system. Choosing field strengths within the reliable region is crucial for obtaining meaningful FF results. Figure 3.3 and Figure 3.4 demonstrate the need to find F_{opt} for each molecule individually.

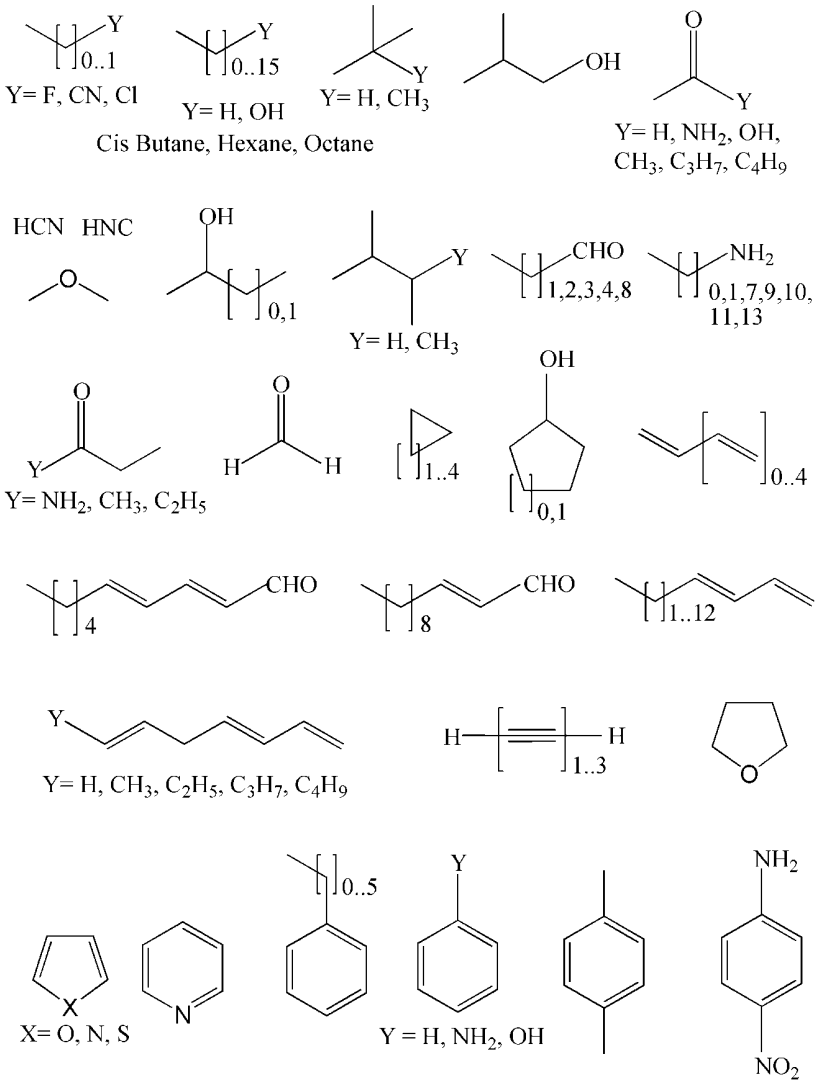

Figure 3.1. Schematic representation of the 120 molecules that were used for the calculation of the second hyperpolarizability.

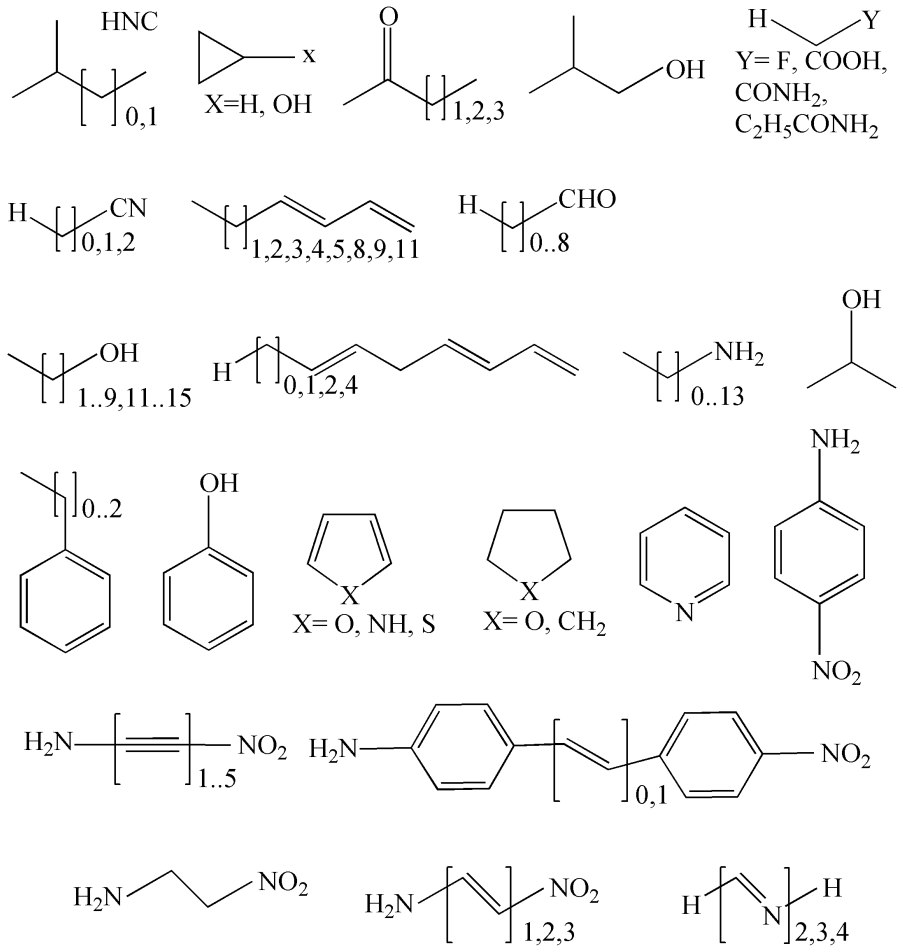

Figure 3.2: Schematic representation of the 91 molecules that were used for the calculation of the first hyperpolarizability.

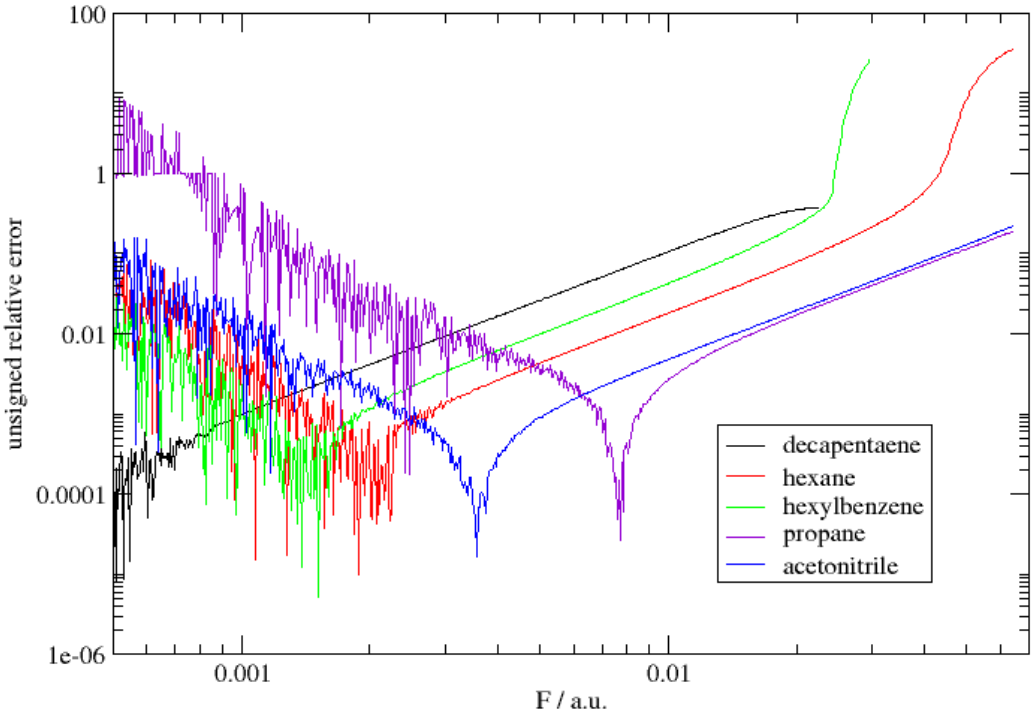

Figure 3.3. Unsigned relative error for γ, $|\varepsilon_\gamma|$, for selected molecules as a function of the field strength *F* using Eq. (3.11).

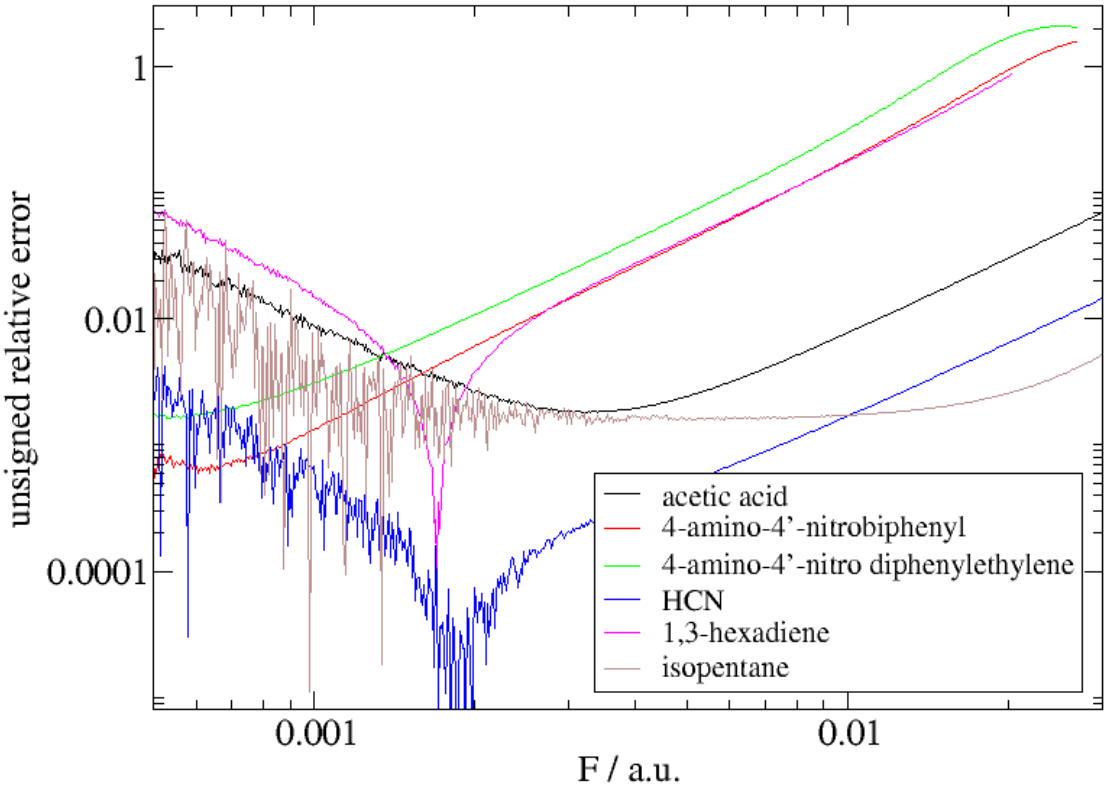

Figure 3.4. Unsigned relative error for β, $|\varepsilon_\beta|$, for selected molecules as a function of the field strength *F* using Eq. (3.12)

3.4.2 Correlation of the optimal field strengths with molecular descriptors

In order to predict the optimal finite fields for first and second hyperpolarizability calculations, we tabulated $F_{opt,\gamma}$ for 111 molecules (Figure 3.1), and $F_{opt,\beta}$ for 91 molecules (Figure 3.2), and correlated them with several molecular descriptors. For this, a linear regression between the logarithm of F_{opt} and the logarithms of each descriptor was performed, allowing us to identify nonlinear relationships. The correlation coefficients can be found in Table 3.1 and Table 3.2. The excitation energy, transition moment square, and oscillator strength in Table 3.1 are given between the ground state and the first allowed excited state, i.e. the lowest state with a non-zero transition moment along the electric field direction. All three quantities correlate only weakly with F_{opt}. The same holds for the dipole moment and the maximum interatomic distances in *y*- and *z*-direction.

Table 3.1: Correlation coefficients R^2 between the logarithm of the optimal field strength of γ and β, and the logarithm of several molecular descriptors. For γ, R^2 is obtained for a set of 111 molecules; For β, the set contains 91 molecules.

Descriptor	R^2 for γ	R^2 for β
Dipole moment	0.02[a]	0.06
Oscillator strength	0.05	0.00
Maximum distance in z	0.05	0.00
Transition moment square	0.06	0.01
Maximum distance in y	0.11	0.00
Excitation energy	0.14	0.12
HOMO-LUMO gap	0.23	0.12
HF energy	0.64	0.14
Molecular weight	0.74	0.00
Moment of inertia	0.78	0.18
Maximum distance	0.80	0.17
$\lvert\gamma_{RT}\rvert$	0.81	-
$\lvert\beta_{RT}\rvert$	-	0.11
Maximum distance in x (longitudinal distance)	0.82	0.17

[a] Correlation with dipole moment was done with only 88 (noncentrosymmetric) molecules for γ.

Table 3.2: Correlation coefficients R^2 between the logarithm of the optimal field strength of γ and β and the logarithm of descriptors A, B, C, D, and E. $B^{(1,3,5)}$ and $D^{(1,3,5)}$ couldn't be calculated for some molecules.

	γ					β				
P	A	B	C	D	E	A	B	C	D	E
0	N/A	N/A	0.733	0.652	-	N/A	N/A	0.125	0.122	-
0.5	-	-	-	-	0.582	-	-	-	-	0.066
1	0.767	0.033	0.688	0.113	0.593	0.152	-	0.137	-	0.061
2	0.771	0.582	0.589	0.489	0.613	0.158	0.192	0.157	0.153	0.056
3	0.770	-	0.458	0.391	0.628	0.162	-	0.164	-	0.056
4	0.769	0.536	0.340	0.235	0.639	0.164	0.196	0.162	0.158	0.057
5	0.766	-	0.256	0.187	0.648	0.165	-	0.156	-	0.058

The HOMO-LUMO gap is known to depend on the external electric field and thus indicates feasible field strengths for every molecule.[14] For propane, for example, the gap starts at 0.70 au at zero field and drops to 0.20 au at $F = 0.1$ au, while for trans-hexane the gap drops from 0.48 au to 0.07 au for the same field strength. Increasing the field strength further will eventually induce an intersection between the ground state and the first excited state(s) of the molecule and thus indicates an upper bound for feasible field strengths. Nevertheless, the HOMO-LUMO gap shows only a weak correlation with $F_{\mathrm{opt},\gamma}$ and a weaker correlation with $F_{\mathrm{opt},\beta}$.

Whereas β correlates only weakly with any of the proposed descriptors, γ possesses significant correlations with extensive properties like the Hartree-Fock energy, molecular weight, and moment of inertia. Table 3.2 shows that $F_{\mathrm{opt},\gamma}$ correlates best with purely spatial measures of the molecule that do not include atomic charges, like descriptor A. On the other hand, if $F_{\mathrm{opt},\gamma}$ is compared to the magnitude of γ itself, a rather high correlation coefficient of 0.81 is found. This is different for β, where the magnitude of β_{RT} is completely uncorrelated with F_{opt}. Apparently, optimal field strengths follow very different patterns for β and γ. The good correlation in the case of γ is also meaningful, since the regression between these two quantities returns a slope of -4.16, which is in close agreement to $\gamma_{\mathrm{FF}} \propto F^{-4}$ from equation (3.10). This indicates that the optimal field strength of γ for every molecule is attained when the finite energy differences in equation (3.10) are close to a constant, molecule-independent value. Although γ is a good predictor

of the optimal field strength it is impossible to use it: we need an *a priori*, not a *post facto*, method for determining F_{opt}.

The most useful correlations for γ are found for the maximum internuclear distance within the molecule, r_{max}, and the maximum internuclear distance in *x*-direction, x_{max}, the longitudinal distance, with an R^2 value of 0.80 and 0.82, respectively. Figure 3.5 illustrates the correlations for these two quantities. The fact that the longitudinal distance is available up front, at no computational cost, makes it the property of choice as a predictor of F_{opt}. The high correlation with these exclusively geometrical descriptors supports our assertion that the optimal field strength of γ is mainly influenced by the molecular extent in the direction of the applied electric field. Surprisingly, F_{opt} for β does not significantly correlate with any of these geometrical descriptors of a molecule. This indicates that optimal field strengths obey entirely different rules, when even or odd energy derivatives are calculated.

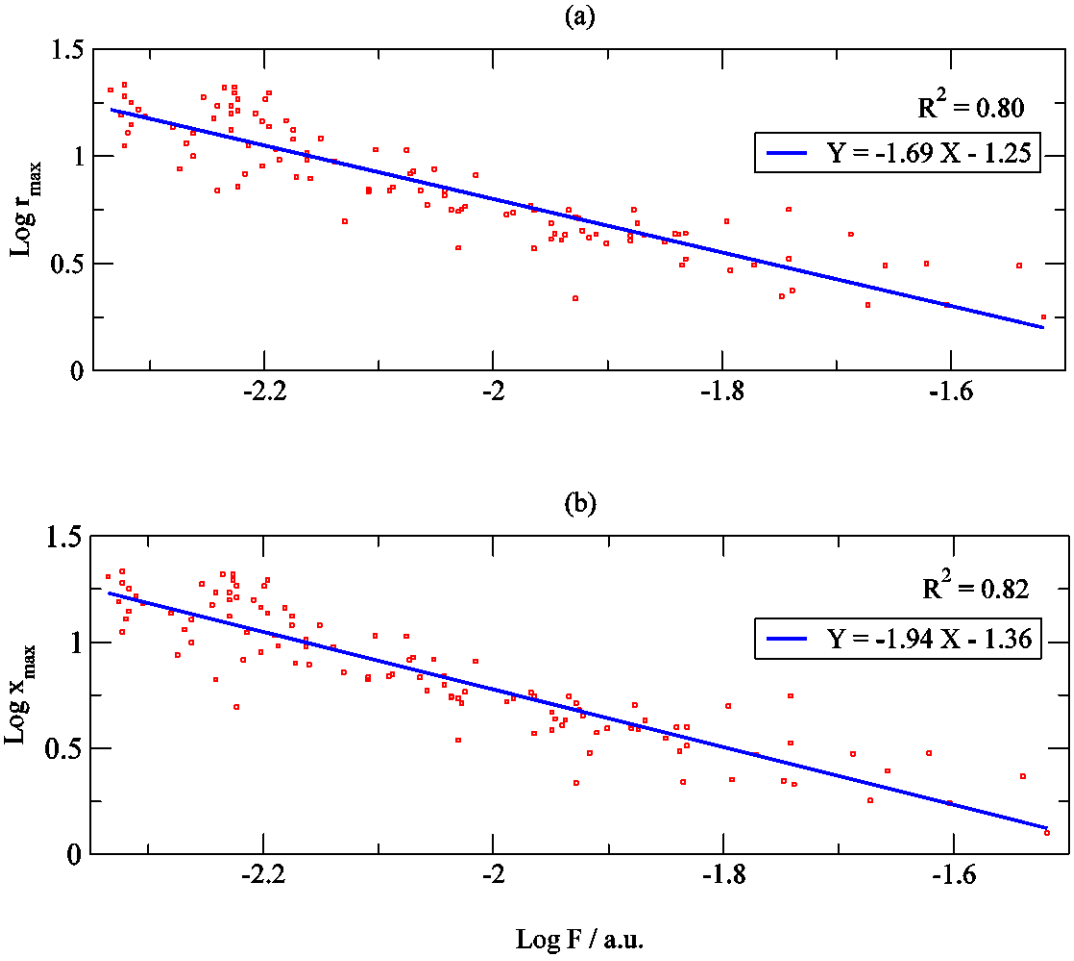

Figure 3.5. Correlations of the logarithm of the optimal field strength of γ with (a) the logarithm of the maximum internuclear distance within the molecule and (b) the logarithm of the maximum internuclear distance in the *x*-direction. γ is calculated using Eq.(3.14).

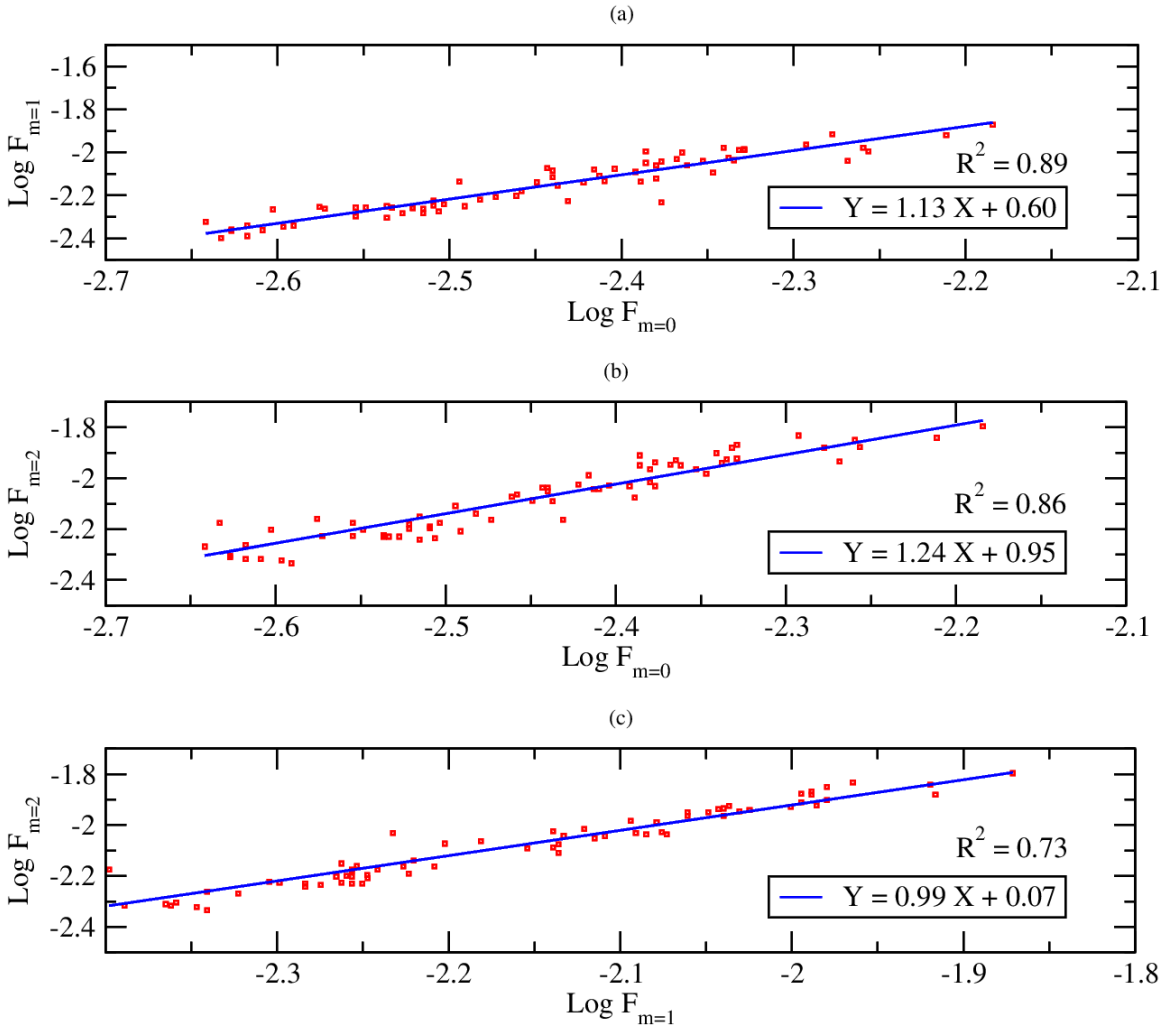

Figure 3.6. Correlations of the logarithm of the optimal field strength of γ obtained with Richardson refinement levels *m*=0, *m*=1, and *m*=2.

In Figure 3.6 it is shown that the optimal field strengths obtained with different expressions for γ_{FF} according to Eqs. (3.11), (3.13), and (3.14) are highly correlated and thus the correlation coefficients presented for m=2 in Table 3.1 and Table 3.2 and Figure 3.5 will hold also for F_{opt} evaluated at the m=0 and m=1 refinement levels. The slope of the linear regression is close to unity in all three cases and thus confirms that either variant of Eqs. (3.11), (3.13), and (3.14) yields the same molecule-specific F_{opt}, up to a constant factor.

3.4.3 Longitudinal distance as a predictor of F_{opt} of γ

To test the efficiency of using the longitudinal distance x_{max} as a predictor for the optimal field strength of γ, a comparison between the predicted and the observed F_{opt} is given in Table 3.3 for ten molecules of different size. The small deviation between the observed and the predicted field strengths verifies the suitability of x_{max} as a powerful predictor of F_{opt}. For all ten molecules, the precision of γ_{FF} obtained with predicted and actual F_{opt} is nearly the same and the predicted F_{opt} is located within the reliable field region. In order to find an accurate F_{opt}, 1600 energy evaluations were performed. Nevertheless we observe cases in Table 3.3 where the predicted values for F_{opt}, which is obtained by only 9 energy evaluations, lead to (slightly) improved values for γ_{FF}. Note that due to additional finite differences in the refinement procedure, F_{opt} is always larger for m=2 in comparison to the unrefined m=0.

Table 3.3: Predicted and calculated optimal field strengths (F_{opt}) for γ and the correspondent unsigned relative errors $|\varepsilon_\gamma|$ for different molecules calculated at the HF/6-31G(d) level of theory. These molecules are not included in the data set used for parameterization. x_{max} is given in angstrom, $|\varepsilon_\gamma|$ is dimensionless, and all other quantities are given in au The prediction is done using the relation Log F_{opt} = -0.73 Log x_{max} – 1.43. The relative errors are given for m=2 only.

Molecule	x_{max}	γ_{RT}	$F^{m=0}_{opt}$ x 10^{-3}		$F^{m=2}_{opt}$ x 10^{-3}		$\|\varepsilon_\gamma\|$	
			predicted	actual	predicted	actual	predicted	actual
acetaldehyde	3.1	720	6.21	5.66	16.5	16.9	8.75E-05	9.17E-05
cyclopropane	3.1	250	6.20	5.78	16.4	14.6	2.51E-04	2.93E-04
neopentane	4.3	905	5.14	5.54	13.0	14.5	3.34E-04	3.11E-04
cyclobutanol	4.4	977	5.10	4.72	12.9	12.0	6.21E-05	8.26E-05
thiophene	4.6	760	4.99	5.58	12.6	13.1	1.84E-03	1.83E-03
aniline	5.8	6867	4.35	3.18	10.6	9.06	4.46E-05	2.17E-05
hexan-2-one	8.1	5846	3.58	3.05	8.33	7.89	2.60E-05	4.99E-05
hexylbenzene	12.1	18268	2.86	2.68	6.31	5.98	5.09E-05	1.53E-05
decatri-1,3,5-ene	12.5	34283	2.81	2.36	6.17	5.39	2.94E-04	1.86E-04
decanal	13.3	13987	2.71	3.16	5.89	6.32	1.27E-04	9.37E-05
average							1.34E-04	1.14E-04

3.4.4 Field dependence of β

The optimal field strengths, F_{opt}, for the 91 molecules of the second data set (Figure 3.2) range from 0.002 to 0.046 au. This means that F_{opt} of β, like that of γ, depends on the structure of the molecule and should be found for each molecule individually as well, as can be seen from Figure 3.4. The dependence of the calculated FF quantity on field strength is qualitatively the same for β and γ.[14] However, we were unable to find any correlations for $F_{opt,\beta}$ with molecular descriptors. This can be partially explained because, unlike γ, the value of β does not explicitly depend on the size of a molecule. Instead β is determined by different functional groups and heteroatoms that add individual contributions, which can also cancel to zero in the case of centrosymmetric molecules. This can explain the poor correlation with descriptors related to molecular size, but still leaves an open question: why isn't there a correlation with the absolute value of beta itself, which is one of the strongest correlations in the case of γ, or with the dipole moment. Instead, we observed that molecules from the data set with the same functional groups have very similar optimal field strengths. For a set of straight-chain alkyl amines that contain 2-14 carbons, there is no systematic change in the optimal field strength as the size of chain grows. Table 3.4 confirms the different behaviour of the optimal field strength for β and γ. It shows that $F_{opt,\gamma}$ systematically decreases with increasing molecule size, whereas $F_{opt,\beta}$ retains a constant value apart from numerical fluctuations. This indicates that only the polar NH_2 group is responsible for $F_{opt,\beta}$ without

influences from the nonpolar alkane tail, whereas $F_{opt,\gamma}$ depends on all parts of the molecule.

Table 3.4: Optimal field strengths $F_{opt,\beta}$ and $F_{opt,\gamma}$ for a set of straight-chain alkyl amines with the structure H-$(CH_2)_n$-NH_2.

n	$F_{opt,\beta}$	$F_{opt,\gamma}$
2	0.005315	0.007362
3	0.005028	0.00721
4	0.004532	0.006869
5	0.004317	0.006543
6	0.004317	0.006498
7	0.004627	0.006453
8	0.005352	0.006409
9	0.005352	0.006453
10	0.005776	0.006364
11	0.005696	0.00619
12	0.006021	0.006105
13	0.005979	0.006021
14	0.005696	0.005938

3.5 Conclusions

An assessment of the optimal field strengths for calculating the first hyperpolarizability, β, using a data set of 91 molecules and the second hyperpolarizability, γ, using a data set of 120 molecules reveals that most precise values for β_{FF} and γ_{FF} are obtained at molecule-specific finite fields.

Calculations with individually tailored field strengths, which range from 0.004 to 0.03 au for the data set and level of theory investigated here, and two iterations of Richardson refinement lead to an average precision for γ_{FF} of four significant digits. This can be compared to an average of only 2 or 3 significant digits when the same computational protocol was used with an intermediate FF value of 0.01 au.

Strong correlations of the optimal field strength for γ_{FF} with various molecular descriptors were found. The most useful correlation was the maximum internuclear distance within a molecule r_{max} and even more so the maximum internuclear distance in the field direction, x_{max}. This longitudinal distance, x_{max}, can be used to predict optimal field strengths for individual molecules. It is straightforward to extend this protocol to different electronic structure methods and basis sets.

Contrary to the even order energy derivatives (α and γ) the odd order derivatives (μ and β) follow a completely different pattern, as optimal field strengths for these quantities are nearly independent of the size of a molecule and do not significantly correlate with

any of the studied descriptors. Instead, molecules with the same functional group have very similar optimal field strengths.

The benefit of predicting the optimal field strength with a method-independent, computationally cheap, and readily available structural parameter like the longitudinal distance lies in the reduction of the number of field-dependent energy evaluations and, more importantly, in the abolition of the human intervention used to “hunt and peck” for the right field strengths and refinement procedures.

3.6 References

1. G. Maroulis, *J. Chem. Phys*. **1998**, 108, 5432-5448.
2. K. Kamada, M. Ueda, H. Nagao, K. Tawa, T. Sugino, Y. Shmizu, K. Ohta *J. Phys.* Chem. A **2000**, 104, 4723-4734.
3. F. A. Bulat, A. Toro-Labbé, B. Champagne, B. Kirtman, W. Yang *J. Chem. Phys*. **2005**, 123, 014319.
4. T. Touma, M. Kobayashi, H. Nakai *Theor. Chem. Acc.* **2011**, 130, 701-709.
5. M. Kamiya, H. Sekino, T. Tsuneda, K. Hirao, *J. Chem. Phys*. **2005**, 122, 234111.
6. T. Helgaker, S. Coriani, P. Jørgensen, K. Kristensen, J. Olsen, K. Ruud, *Chem. Rev*. **2012**, 112, 543-631.
7. H. D. Cohen, C. C. J. Roothaan, *J. Chem. Phys*. **1965**, 43, S34-S39.
8. D. M. Bishop, S. A. Solunac , *Chem. Phys. Lett*. **1985**, 122, 567 –571.
9. L. F. Richardson, J. A. Gaunt, Phil. Trans. R. Soc. Lond. A **1927**, 226, 299-361.
10. B. Champagne, B. Kirtman "Chapter 2 - Theoretical approach to the design of organic molecular and polymeric nonlinear optical materials: in Hari Singh Nalwa Handbook of Advanced Electronic and Photonic Materials and Devices, Academic Press, Burlington, vol. 9, 2001, p 63-126.
11. M. de Wergifosse, B. Champagne, *J. Chem. Phys*. **2011**, 134, 074113.
12. P. A. Limacher, Q. Li, H. P. Lüthi, *J. Chem. Phys*. **2011**, 135, 014111.
13. F. Castet, E. Bogdan. A. Plaquet, L. Ducasse, B. Champagne, V. Rodriguez, *J. Chem. Phys*. **2012**, 136, 024506.

14. A. A. K. Mohammed, P. A. Limacher, B. Champagne, *J. Comput. Chem.* **2013**, 34, 1497-1507.

15. M. Medved, M. Stachová, D. Jacquemin, J.-M. André, E. A. Perpète THEOCHEM **2007**, 847, 39–46.

16. B. Champagne, E. A. Perpète, S. J. A. van Gisbergen, E.-J. Baerends, J. G. Snijders, C. Soubra-Ghaoui, K. A. Robins, B. Kirtman, *J. Chem. Phys.* **1998,** 109, 10489.

17. B. Champagne, E. A. Perpète, D. Jacquemin, S. J. A. van Gisbergen, E.-J. Baerends, C. Soubra-Ghaoui, K. A. Robins, B. Kirtman, *J. Phys. Chem. A* **2000**, 104, 4755.

18. Gaussian 09, Revision C.01, M. J. Frisch, G. W. Trucks, H. B. Schlegel, G. E. Scuseria, M. A. Robb, J. R. Cheeseman, G. Scalmani, V. Barone, B. Mennucci, G. A. Petersson, H. Nakatsuji, M. Caricato, X. Li, H. P. Hratchian, A. F. Izmaylov, J. Bloino, G. Zheng, J. L. Sonnenberg, M. Hada, M. Ehara, K. Toyota, R. Fukuda, J. Hasegawa, M. Ishida, T. Nakajima, Y. Honda, O. Kitao, H. Nakai, T. Vreven, J. A. Montgomery, Jr., J. E. Peralta, F. Ogliaro, M. Bearpark, J. J. Heyd, E. Brothers, K. N. Kudin, V. N. Staroverov, T. Keith, R. Kobayashi, J. Normand, K. Raghavachari, A. Rendell, J. C. Burant, S. S. Iyengar, J. Tomasi, M. Cossi, N. Rega, J. M. Millam, M. Klene, J. E. Knox, J. B. Cross, V. Bakken, C. Adamo, J. Jaramillo, R. Gomperts, R. E. Stratmann, O. Yazyev, A. J. Austin, R. Cammi, C. Pomelli, J. W. Ochterski, R. L. Martin, K. Morokuma, V. G. Zakrzewski, G. A. Voth, P. Salvador, J. J. Dannenberg, S. Dapprich, A. D. Daniels, O. Farkas, J. B. Foresman, J. V. Ortiz, J. Cioslowski, and D. J. Fox, Gaussian, Inc., Wallingford CT, 2009.

19. T. Yanai, D. P. Tew, N. C. Handy, *Chem. Phys. Lett.* **2004**, 393, 51.

20. A. D. Becke, *Phys. Rev. A*, **1988**, 38, 3098-3100.

21. C. Lee, W. Yang, R. G. Parr, *Phys. Rev. B* **1988**, 37, 785-789.

22. A. D. Becke, *J. Chem. Phys.*, **1993**, 98, 5648-5652.

23. T. Leininger, H. Stoll, H.-J. Werner, A. Savin, *Chem. Phys. Lett*. **1997**, 275, 151.

24. A. V. Krukau, G. E. Scuseria, J. P. Perdew, A. Savin, *J. Chem. Phys.* **2008**, 129, 124103.

25. P. A. Limacher, K. V. Mikkelsen, H. P. Lüthi, *J. Chem. Phys.* **2009**, 130, 194114.

26. M. J. G. Peach, E. I. Tellgren, P. Salek, T. Helgaker, D. J. Tozer, *J. Phys. Chem.* A **2007**, 111, 11930.

27. R. Ditchfield, W. J. Hehre, J. A. Pople, *J. Chem. Phys.* **1971**, 54**,** 724.

28. W. J. Hehre, R. Ditchfield, J. A. Pople, *J. Chem. Phys.* **1972**, 56, 2257.

29. P. C. Hariharan, J. A. Pople, *Theor. Chem. Acc.* **1973**, 28, 213.

30. M. J. Frisch, J. A. Pople, J. S. Binkley, *J. Chem. Phys*. **1984**, 80, 3265.

31. DALTON, a molecular electronic structure program, Release 2.0 (2005), see http://www.kjemi.uio.no/software/dalton/dalton.html.

32. B. Jansik, P. Salek, D. Jonsson, O. Vahtras, H. Agren, *J. Chem. Phys.* **2005**, 122, 054107.

33. Y. Luo, H. Agren, P. Jorgensen, K. V. Mikkelsen, *Adv. Quantum Chem.* **1995**, 26, 165.

34. G. J. B. Hurst, M. Dupuis, E. Clementi, *J. Chem. Phys*. **1988**, 89, 385.

35. M. Torrent-Sucarrat, M. Sola, M. Duran, J. M. Luis, B. Kirtman, *J. Chem. Phys*. **2003**, 118, 711.

Chapter 4

Benchmarking Density Functionals for the Second Hyperpolarizability of Organic Molecules

4.1 Motivation

In the last two chapters we determined the optimal conditions for obtaining the most accurate results for the second hyperpolarizability by the finite field method. We determined the optimal choice of initial field and the ratio for the geometric progression of field strengths, as well as the number of refinement steps. In this chapter, we use these conditions to test the performance of several DFT functionals by comparing them to the "gold standard" of quantum chemistry for energy calculations, CCSD(T). Molecules with superior NLO properties are typically oligomers and large systems, and thus DFT, which offer an excellent compromise between accuracy and computational cost, is an ideal

method to calculate response properties for these large systems. The significant role of correlation in obtaining reliable response properties is shown and the shortcomings of DFT for computing the hyperpolarizability are shown.

4.2 Introduction

Nonlinear optical (NLO) properties of molecules and polymers have gained attention from both experimental and theoretical chemists because of their application in various types of optoelectronic devices.[1-9] Theoretical tools have a particularly important role to play in these studies, because they can give insight into the specific molecular features that lead to desirable NLO properties, and therefore guide the design of new NLO molecules and materials.[10-13] Nonetheless, predicting NLO properties and designing new materials with specific response properties remains a challenging and ambitious task for quantum chemistry. Materials with high NLO properties are typically polymers and supramolecular structures. This means that high-accuracy benchmark quantum chemistry methods like coupled cluster approaches are often too expensive. NLO properties are also sensitive to the treatment of electron correlation, and so lower-cost methods like Hartree-Fock and density functional theory (DFT) approaches are unreliable. In this work, we assess the performance of several DFT functionals for calculating the second hyperpolarizability of organic molecules and oligomers by comparing their results to those obtained by the coupled-cluster method. This allows us to suggest which DFT functionals are most reliable.

A thorough understanding of molecular hyperpolarizabilities and their structure-property relationships is still an open and active area of research for theoretical chemistry.[14-23] Comparing the performance of different methods for calculating hyperpolarizabilities should provide more insight into the nature of these properties and reveal the contribution of local molecular factors and structure, and thus help for designing materials with desired electric response properties. It should also be useful for assessing the theoretical methods themselves and provide insights into how one may develop improved electronic structure methods.

Direct comparisons between computed molecular (hyper)polarizabilities and experimental values are difficult because theory and experiment depend on different factors.[24] Theoretical values of the second hyperpolarizability γ are usually obtained as a frequency-independent tensor component in the molecular propagation axis of one molecule; the experimental value is a tensor average $\langle\gamma\rangle$ of an ensemble of interacting molecules that have different conformations and orientations. Moreover, different experimental methods produce different results. Calculations must include vibronic contributions,[25,26] solvent effects,[27] and local field factors to be compared to experimental results. Experimental gas phase data for γ are rare, and nonexistent for some molecules. These factors make direct comparison to experimental results very difficult or unavailable for many molecules. As an alternative, *ab initio* methods of high accuracy can provide reference values for molecular hyperpolarizabilities.

The computed value of the second hyperpolarizabilities is much more sensitive to electron correlation than most molecular properties.[28-32] For a small molecule or oligomer, one often computes reference values for second hyperpolarizability, γ, using coupled-cluster singles and doubles with a perturbative estimations of the triples method, CCSD(T), which is considered the "gold standard" of quantum chemistry. We will use this method in this paper also. However, CCSD(T) is too computationally expensive to be applied to large systems, which are of interest because NLO properties often increase with system size. For example, the second hyperpolarizability for all trans polyacetylene and polyyne oligomers is known to grow with length of the chain according to

$$\gamma \propto n^{a} \tag{4.1}$$

where n is the length of the chain and a is a constant. Therefore, molecules with high NLO properties are typically oligomers.

Density functional theory (DFT) methods provide a favourable compromise between accuracy and computational cost, and thus are widely used for calculating NLO properties of larger molecules. However, the most commonly used DFT functionals are known to fail in the qualitative description of hyperpolarizabilities for large π-conjugated systems.[33]

In the past few years, new DFT functionals have been developed,[34-47] but the performance of these functionals for evaluating NLO properties needs thorough investigation. Conventional DFT functionals (local density approximations (LDAs),

generalized gradient approximations (GGAs), global hybrids (hybrid-GGA)) are known to overestimate the second hyperpolarizabilities of atoms and small molecules because of the incorrect asymptotic behaviour of the exchange-correlation (XC) potential. This effect increases with the size of the system and leads to catastrophic errors for large molecules.[33,48] The disastrous overestimation of γ comes from the incorrect modelling of electric field dependence by the exchange functional.[49] Global hybrid functionals, such as B3LYP, correct this error only partially by including a fraction of exact HF exchange. The optimized effective potential (OEP) has also been proposed to solve this problem, but results were disappointing.[50] Long-range corrected functionals like range-separated hybrid GGAs are superior, however. This is probably because these functionals have much smaller many-electron self-interaction errors.[38,51-57]

The long-range corrected approach has received a considerable attention for calculating molecular properties, including nonlinear responses.[58-63] However, most of these studies were limited to a single family of molecules (e.g. linear π conjugation, push-pull systems), or even one single molecule. Similarly limited studies are available for the relatively new Minnesota family of functionals.

In this study we benchmark the performance of several DFT functionals for static second hyperpolarizability against CCSD(T) method using the finite field (FF) method. The FF method is a straightforward and easy-to-implement approach for calculating longitudinal (hyper)polarizabilities of atoms and molecules using only single-point

energy calculations. Specifically, the value of the (hyper)polarizability is deduced from the value of the energy at different external fields. We use the techniques developed in our recent works on the finite field method to obtain accurate γ values.[21,23] The errors in our FF calculations are significantly less than the errors in the electronic structure methods we are comparing.

4.3 Methods

4.3.1 The finite field method

The energy *E* of a molecule subject to a small external homogenous static electric field *F* can be approximated with a McLaurin series,

$$E(F) = E(0) + \left.\frac{\partial E}{\partial F}\right|_0 F + \frac{1}{2!}\left.\frac{\partial^2 E}{\partial F^2}\right|_0 F^2 + \frac{1}{3!}\left.\frac{\partial^3 E}{\partial F^3}\right|_0 F^3 + \frac{1}{4!}\left.\frac{\partial^4 E}{\partial F^4}\right|_0 F^4 + \ldots \qquad (4.2)$$

$$E(F) = E(0) - \mu F - \frac{1}{2}\alpha F^2 - \frac{1}{6}\beta F^3 - \frac{1}{24}\gamma F^4 + \ldots, \qquad (4.3)$$

where μ is the dipole moment, α is the dipole polarizability, β is first hyperpolarizability, and γ is the second hyperpolarizability.

The expression for α can be obtained by arranging equation (4.3) as

$$\alpha(F) = 2\frac{E(0) - E_S(F)}{F^2} = \alpha + \frac{1}{12}\gamma F^2 + \frac{1}{360}\varepsilon F^4 + O(F^6) \qquad (4.4)$$

where E_S is the symmetric combination of energy

$$E_S(F) = \frac{E(F) + E(-F)}{2} = E(0) - \frac{1}{2}\alpha F^2 - \frac{1}{24}\gamma F^4 + O(F^6) \quad (4.5)$$

This allows the polarizabilities and the even-order hyperpolarizabilities to be treated separately from the dipole moment and the odd-order hyperpolarizabilities. Eq. (4.4) provides a good estimate of α when *F* is small enough.

The second hyperpolarizability γ can be evaluated by eliminating α from Eq. (4.4). This can be achieved if the energy is known at two different field strengths, e.g., *F* and 2*F*, besides the energy at zero field

$$\gamma(F) = 4\frac{\alpha(2F) - \alpha(F)}{F^2} = \frac{-2E_S(2F) + 8E_S(F) - 6E(0)}{F^4} = \gamma + \frac{1}{6}\varepsilon F^2 + O(F^4)$$

(4.6)

Although it is a common practice to work with field strengths *F* and 2*F*, we showed in chapter 2 that using a step smaller than 2 gives better results for γ. In this study we use a step of $\sqrt{2}$, and the expression for γ becomes

$$\gamma(F) = \frac{12}{F^4}\left(-E_S\left(\sqrt{2}F\right) + 2E_S(F) - E(0)\right) \quad (4.7)$$

The precision γ can be improved by using Richardson extrapolation.[64] This scheme is widely used to improve the precision of FF quantities by reducing the error incurred by truncating the Taylor expansion. This method is explained in detail in chapter 2 of this

thesis. In this study we use two iterations of refinement for γ. The expression for the refined γ is

$$\gamma_{m=2}(F) = \frac{1}{4F^4}\begin{pmatrix} -E_S\left(2^{3/2}F\right)+26E_S\left(2F\right)-176E_S\left(\sqrt{2}F\right) \\ +256E_S\left(F\right)-105E\left(0\right) \end{pmatrix} \quad (4.8)$$

In this study, we consider only the time-independent (static) longitudinal second hyperpolarizability, γ_{xxxx}, where *x* denotes the molecular axis with the smallest moment of inertia. Henceforth the subscript *x* will be dropped for simplicity.

4.3.2 Field grid

In this study we used a fine grid to find the optimal field strength F_{opt}. For each molecule, energy calculations are performed at field strengths

$$F_n = F_0 \,.\, 2^{n/8} \quad (4.9)$$

Many geometric progressions with a common ratio of $x = \sqrt{2}$ can be generated within this array of fields, simply by picking a particular field strength F_{p} and the fields $F_{\text{p+4}}$, $F_{\text{p+8}}$ and $F_{\text{p+12}}$. The energies at these field strengths have to be inserted into Eq. (4.8) together with the energy at zero field to determine the value of γ_{FF} at field strength F_{p}.

We showed in chapter 3 that the optimal field strength depends on the structure of the molecule and should be found for each molecule individually. For example, the optimal field strength for polyacetylene chains decreases from 0.0117 au to 0.0023 au as

the chain increases from one unit to five units. Selecting the field strength for each molecule individually generally reduces the error in the calculated γ by one or two orders of magnitude.

4.3.3 Electronic structure calculations

All geometry optimization was performed using the Gaussian 09 program,[65] using the long-range corrected hybrid density functional CAMB3LYP,[66-71] to produce accurate molecular geometries,[8,72] and the cc-pVTZ basis set.[73] Although it is well-known that diffuse basis functions are required to calculate accurate second hyperpolarizabilities,[8,21] diffuse basis sets were not used in this study because they introduce numerical instabilities.[8,74,75] The goal of this study is to compare the performance of DFT functionals to CCSD(T), rather than reproducing accurate second hyperpolarizabilities. The cc-pVTZ basis set is acceptable for this purpose.

Calculations of the finite field properties for CCSD(T) and the Minnesota family of functionals (M06-L, M06, M06-2X, and M06-HF) were performed using Molpro.[76] Finite field properties for the rest of DFT functionals were performed using the DALTON quantum chemistry program[77] and the aforementioned optimized geometries. Because we compare energies with very small differences, tight convergence criteria were applied for the solution of the SCF equations. The energies are converged almost to machine precision (~15 significant digits).

4.3.4 Density functionals

Several types of exchange-correlation functionals have been tested in this study. The exchange-correlation functional SVWN is a local density approximation (LDA).[78,79] The BLYP,[67,68] PBE,[80] and revPBE[81] exchange-correlation functionals are generalized gradient approximations (GGAs). B3LYP,[68,69] B971,[82] B972,[83] and PBE0[84] are global hybrid exchange-correlation functionals; they include various amounts of nonlocal Hartree-Fock exchange.

Hybrid functionals represent an improvement over pure GGA models; this is usually attributed to the fact they have smaller self-interacting error (SIE) than pure functionals like GGAs. However, using fixed amounts of DFT and HF exchange doesn't solve all the problems of pure functionals: the asymptotic decay of the exchange-correlation potential is wrong (giving poor band gaps, excitation energies, and response properties) and there is still substantial many-electron self-interaction error. One can mitigate both of these effects by separating the Coulomb operator into short- and long-range parts. The long-range correction (LC) scheme was first developed by Savin for local density functionals[85] and later extended to GGA functionals.[86] In this scheme the amounts of HF and DFT exchange depend on the interelectronic distance, and are not fixed amounts like they are in hybrid functionals. The ratio of DFT to HF exchange is high when the interelectronic separation is small, where GGAs are usually accurate. When the interelectronic separation is large, the ratio of DFT to HF exchange is low. For example, the

CAMB3LYP[66] functional contains 0.19 HF exchange in the zero-separation limit and 0.65 HF exchange at long range. CAMB3LYP fixes the enormous underestimation of B3LYP of charge transfer excitations.[66]

Another family of meta-GGA functionals (including a dependence on the kinetic energy density) and hybrid-GGA functionals was developed by Truhlar and coworkers and is usually referred to as the Minnesota functionals. M06-L[87] is a local meta-GGA functional that doesn't contain HF exchange. The hybrid functionals M06,[88] M06-2X,[88] and M06-HF[89] contain 27%, 54%, and 100% HF exchange, respectively.

4.4 Results and Discussion

4.4.1 Conjugated systems

The static longitudinal second hyperpolarizabilities of polyacetylene chains calculated by several DFT functionals with the cc-pVTZ basis set along with errors relative to CCSD(T) are shown in Figure 4.1, Figure 4.2, and Figure 4.3, along with Table 4.1. Figure 4.1 shows that the CCSD method gives very similar values to CCSD(T) for small molecules, but the discrepancy increases with the length of the chain. Hartree-Fock consistently underestimates γ and has the highest error among all methods, but the relative error decreases with the chain length. This indicates the importance of electron correlation for calculating accurate γ values, especially for π-conjugated systems.

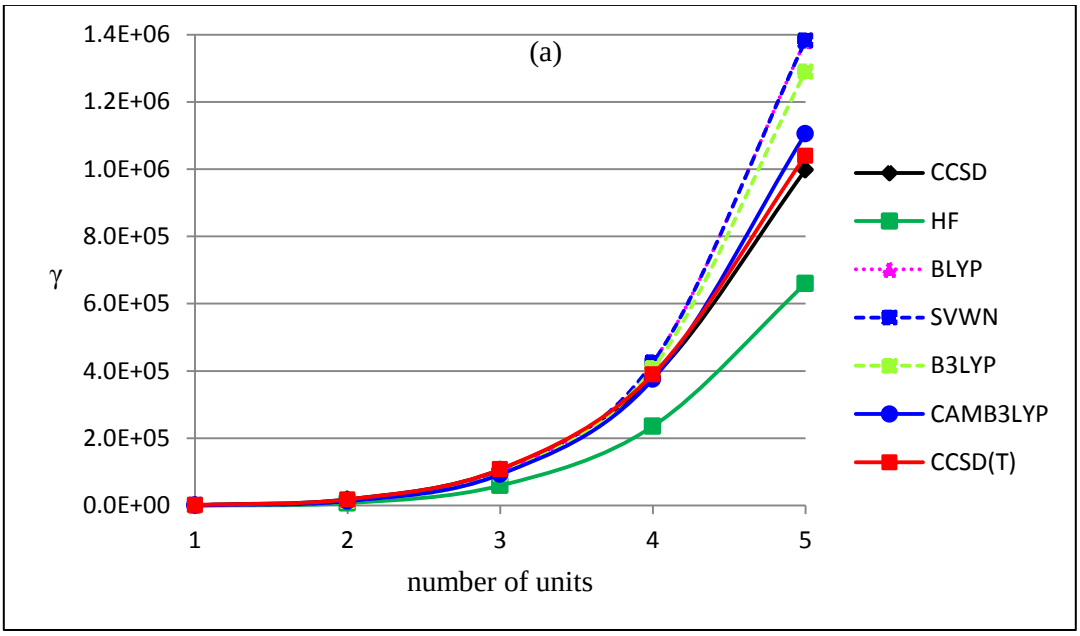

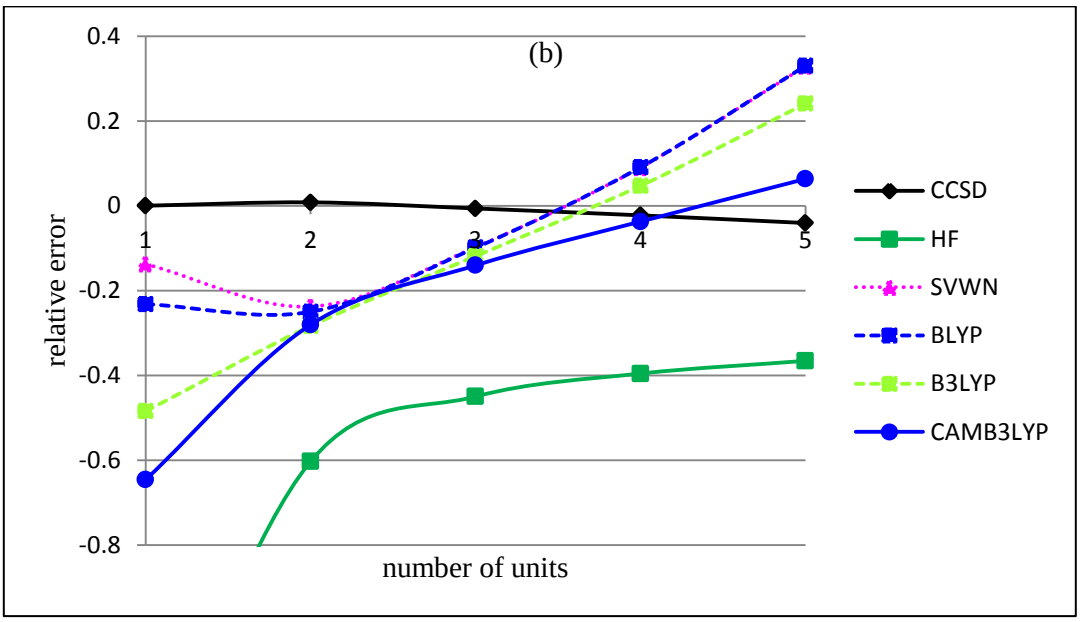

Figure 4.1: (a) Longitudinal second hyperpolarizabilities of polyacetylene chains for several methods as a function of the number of units. (b) Relative error of longitudinal second hyperpolarizabilities of polyacetylene chains for several methods compared to CCSD(T) as a function of the number of units.

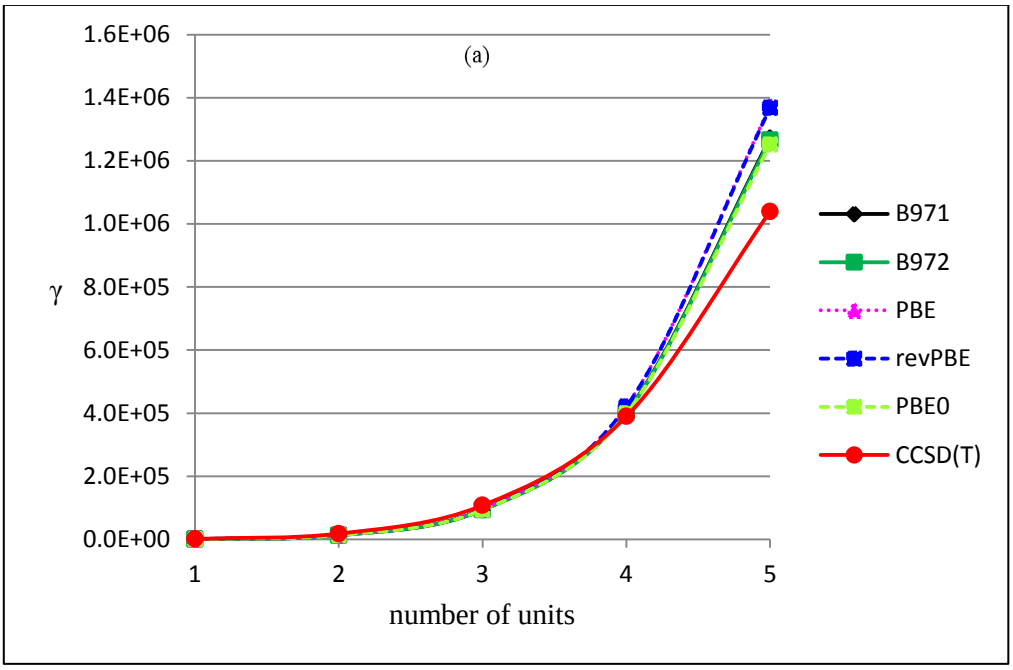

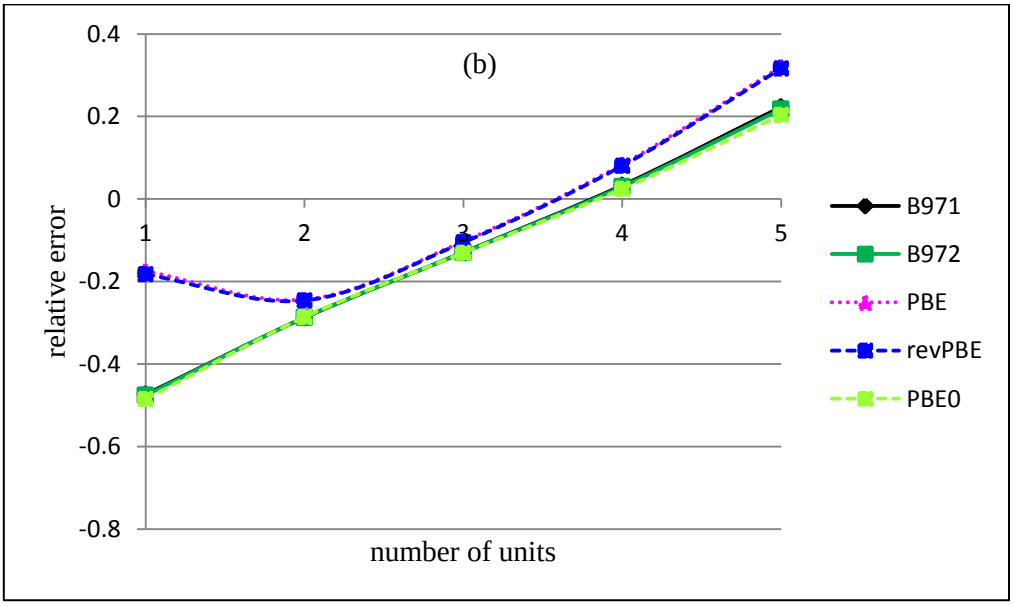

Figure 4.2: (a) Longitudinal second hyperpolarizabilities of polyacetylene chains for several methods as a function of the number of units. (b) Relative error of longitudinal second hyperpolarizabilities of polyacetylene chains for several density functionals compared to CCSD(T) as a function of the number of units.

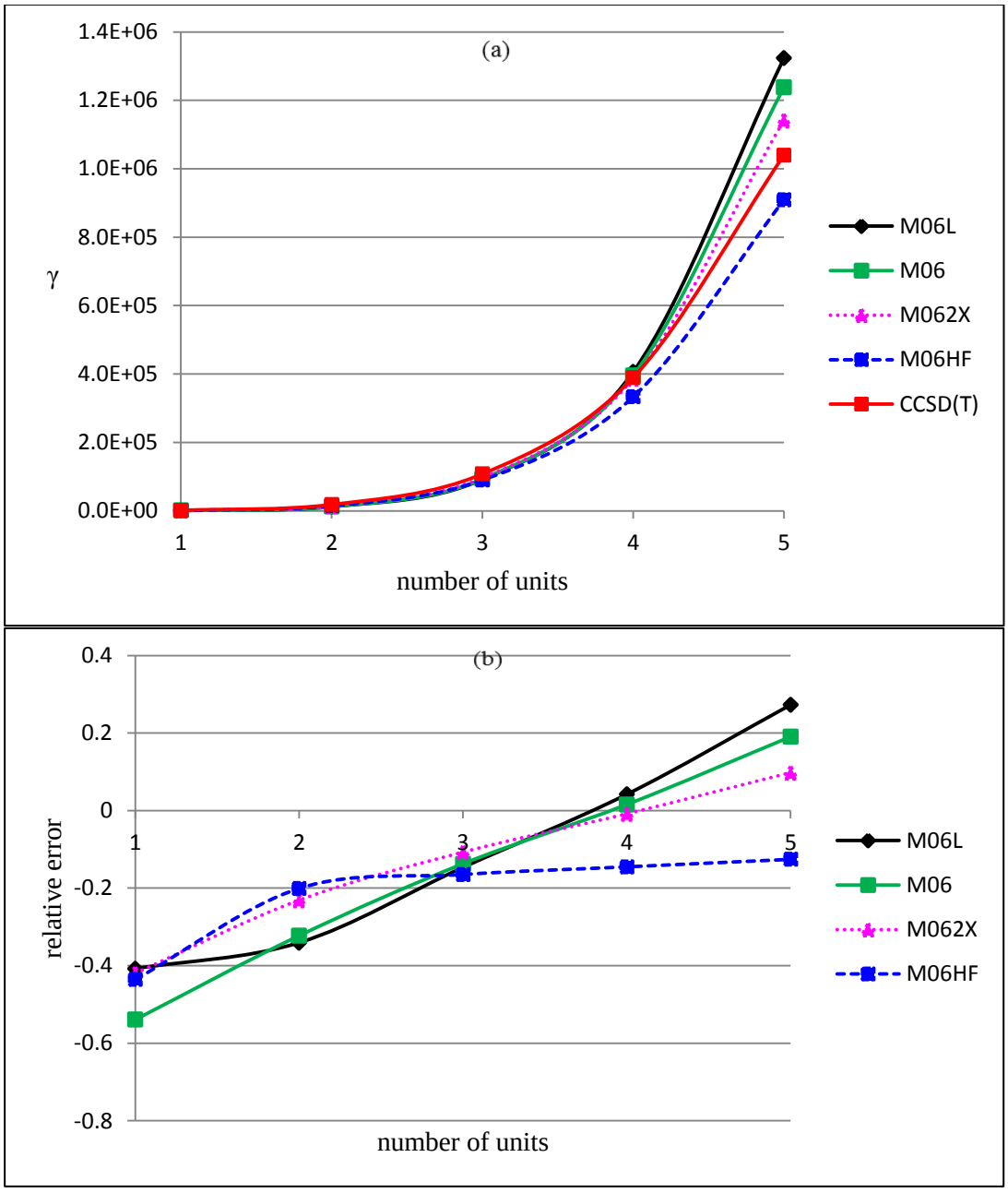

Figure 4.3: (a) Longitudinal second hyperpolarizabilities of polyacetylene chains for several methods as a function of the number of units. (b) Relative error of longitudinal second hyperpolarizabilities of polyacetylene chains for four Minnesota functionals compared to CCSD(T) as a function of the number of units.

Table 4.1: Finite field γ values (in atomic units), relative errors, and average absolute relative errors for polyacetylene units H-(CH=CH)$_m$-H, calculated by different methods using cc-pVTZ basis set. The relative error of a method is calculated by the expression $error = \frac{\gamma_{method}}{\gamma_{CCSD(T)}} - 1.$

	m=1		m=2		m=3		m=4		m=5		avg. error
	γ x10^3	error	γ x10^4	error	γ x10^4	error	γ x10^5	error	γ x10^6	error	
CCSD(T)	1.36		1.83		10.78		3.90		1.04		
CCSD	1.36	0.00	1.84	0.01	10.71	-0.01	3.81	-0.02	1.00	-0.04	0.02
HF	-0.53	-1.39	0.73	-0.60	5.93	-0.45	2.35	-0.40	0.66	-0.37	0.64
SVWN	1.17	-0.14	1.39	-0.24	9.73	-0.10	4.25	0.09	1.38	0.33	0.18
BLYP	1.04	-0.23	1.37	-0.25	9.71	-0.10	4.25	0.09	1.38	0.33	0.20
B3LYP	0.70	-0.48	1.31	-0.28	9.50	-0.12	4.08	0.05	1.29	0.24	0.23
CAMB3LYP	0.48	-0.65	1.31	-0.28	9.26	-0.14	3.75	-0.04	1.11	0.06	0.23
B971	0.71	-0.47	1.30	-0.29	9.39	-0.13	4.02	0.03	1.27	0.22	0.23
B972	0.71	-0.48	1.30	-0.29	9.38	-0.13	4.01	0.03	1.27	0.22	0.23
PBE	1.12	-0.17	1.38	-0.24	9.68	-0.10	4.22	0.08	1.37	0.32	0.19
revPBE	1.11	-0.18	1.38	-0.25	9.65	-0.10	4.21	0.08	1.37	0.32	0.19
PBE0	0.70	-0.48	1.30	-0.29	9.37	-0.13	3.99	0.02	1.25	0.20	0.23
M06-L	0.80	-0.41	1.20	-0.34	9.20	-0.15	4.06	0.04	1.32	0.27	0.24
M06	0.62	-0.54	1.24	-0.32	9.30	-0.14	3.96	0.02	1.24	0.19	0.24
M06-2X	0.79	-0.42	1.40	-0.23	9.62	-0.11	3.86	-0.01	1.14	0.10	0.17
M06-HF	0.77	-0.44	1.46	-0.20	9.00	-0.16	3.33	-0.15	0.91	-0.13	0.21

Both LDA and pure GGA functionals, SVWN and BLYP, respectively, show the same behaviour: underestimation of γ for short chains and overestimation of γ for long chains, with the relative error increasing linearly as the chain lengthens. B3LYP, a hybrid functional, does slightly better than the first two functionals with longer chains because the explicit inclusion of HF exchange partially cancels the overestimation associated with the pure functionals. However, the errors still diverge as the chain grows. The long-range corrected functional CAMB3LYP does significantly better than both hybrid and pure GGA functionals and is very close to CCSD. CAMB3LYP has qualitatively different error behaviour as the chain lengthens and is a considerable improvement over B3LYP for longer chains. CAMB3LYP clearly benefits from using more exact HF exchange at longer distances, but for very long chains, it will still fail. It is clear that 100% long-range Hartree-Fock exchange is essential to describe the hyperpolarizability of long conjugated molecules.

Figure 4.2 confirms the effect of HF exchange on the performance of DFT functionals. The hybrid functionals, B971, B972, and PBE0, have similar behaviour and are slightly better than the GGAs, PBE and revPBE. However, the error increases almost linearly for both types of functionals as the chain grows. The effect of HF exchange is also clear in the Minnesota functionals shown in Figure 4.3. M06-L, which doesn't include HF exchange, has the highest γ values, followed by M06, M06-2X, and M06-HF, which include 27%, 54%, and 100% HF exchange, respectively. For longer chains γ values decrease consistently as the percentage of HF exchange increases, with M06-2X

giving the lowest errors among this family of functionals. In general, there is a significant jump in the error when moving from the four-unit to the five-unit oligomer in most functionals; the only functionals that do not show this error have more than 50% long-range exact exchange (CAMB3LYP, M06-HF, and (to some extent) M06-2X).

Figure 4.4, Figure 4.5, and Figure 4.6, along with Table 4.2, show the values and relative errors of γ for polyyne chains. In general, most methods have the same qualitative behaviour as for the polyacetylene chains. The deterioration in the performance of CCSD method as the chain lengthens is worse than it was for the polyacetylene chains. The underestimation of HF increases with the chain size as well, unlike the polyacetylenes. This makes the single Slater determinant description of this system, especially for longer chains, questionable. However, these chains have a T1 diagnostic between 0.012-0.014, which indicates that the CCSD(T) results should be trustworthy for these systems. (T1 < 0.02 indicates that the system is predominately single-reference and that CCSD and CCSD(T) should be reliable.[90])

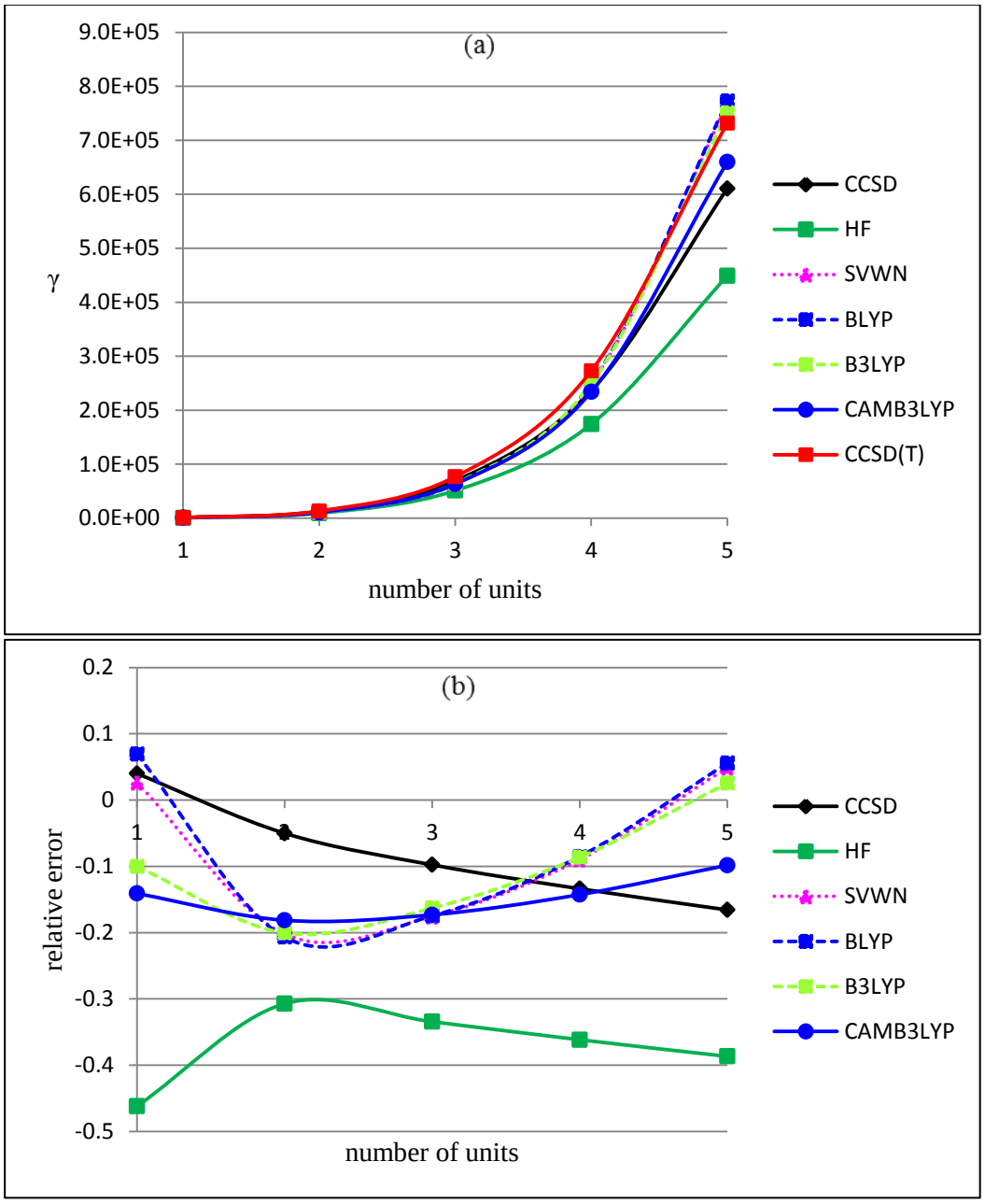

Figure 4.4: Longitudinal second hyperpolarizabilities of polyyne chains for several methods as a function of the number of units. (b) Relative error of longitudinal second hyperpolarizabilities of polyyne chains for several methods compared to CCSD(T) as a function of the number of units.

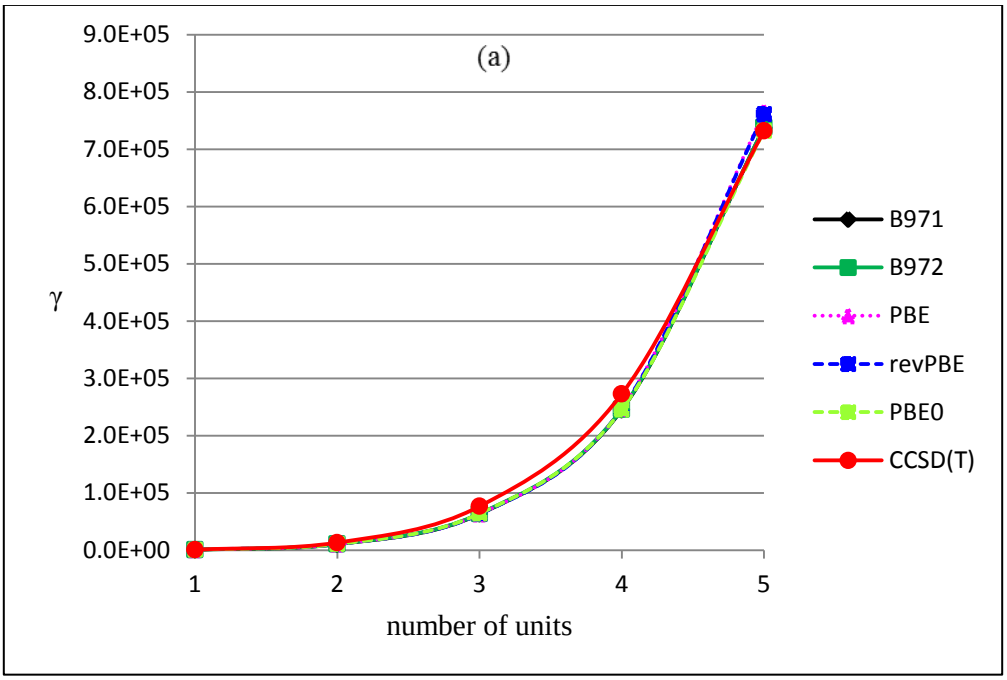

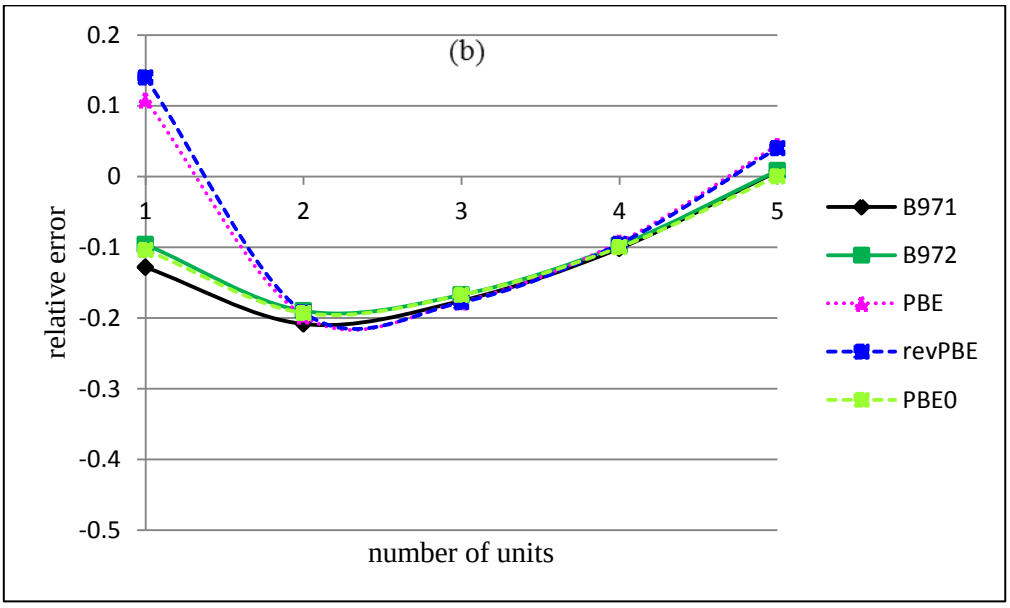

Figure 4.5: Longitudinal second hyperpolarizabilities of polyyne chains for several methods as a function of the number of units. (b) Relative error of longitudinal second hyperpolarizabilities of polyyne chains for several density functionals compared to CCSD(T) as a function of the number of units.

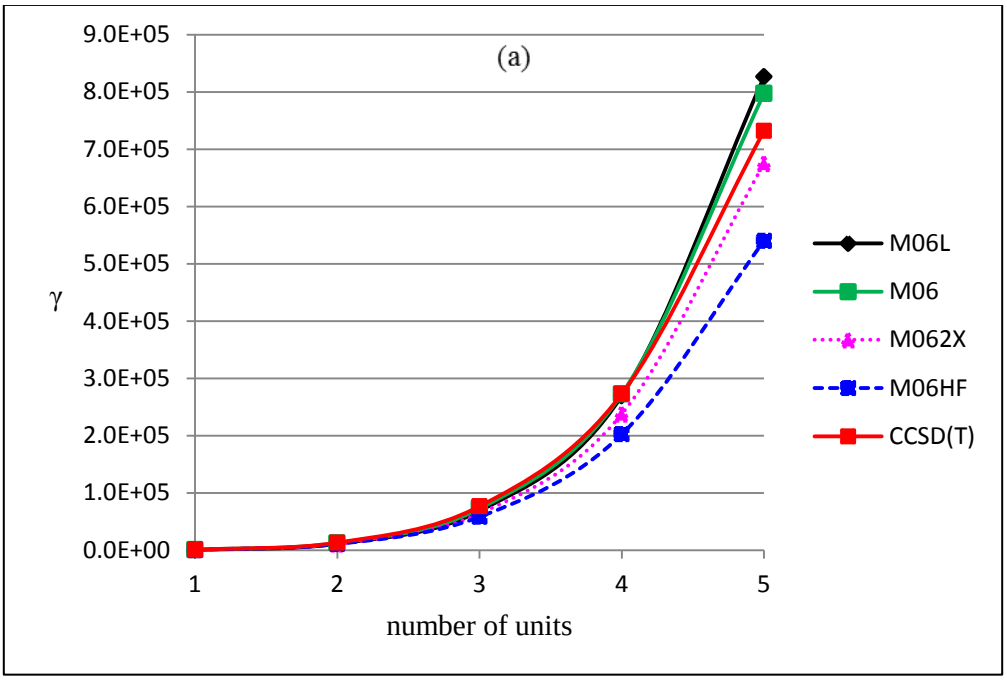

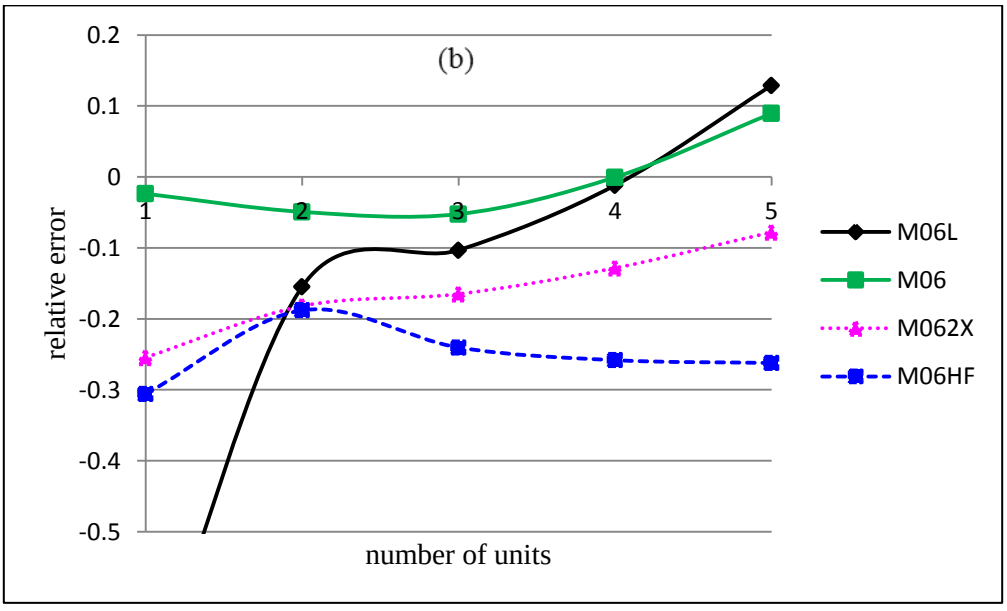

Figure 4.6: (a) Longitudinal second hyperpolarizabilities of polyynes chains for several methods as a function of the number of units. (b) Relative error of longitudinal second hyperpolarizabilities of polyynes chains for four Minnesota functionals compared to CCSD(T) as a function of the number of units.

Table 4.2: Finite field γ values (in atomic units), relative errors, and average absolute relative errors for polyyne chains H-(C≡C)$_m$-H, calculated by different methods using cc-pVTZ basis set. The relative error of a method is calculated by the expression $error = \frac{\gamma_{method}}{\gamma_{CCSD(T)}} - 1$.

	m=1		m=2		m=3		m=4		m=5		avg. error
	γ	error	γ x10^4	error	γ x10^4	error	γ x10^5	error	γ x10^5	error	
CCSD(T)	826		1.32		7.66		2.73		7.32		
CCSD	859	0.04	1.26	-0.05	6.92	-0.10	2.36	-0.13	6.1	-0.17	0.10
HF	444	-0.46	0.92	-0.31	5.1	-0.33	1.74	-0.36	4.49	-0.39	0.37
SVWN	848	0.03	1.06	-0.20	6.32	-0.18	2.48	-0.09	7.67	0.05	0.11
BLYP	883	0.07	1.05	-0.21	6.33	-0.17	2.5	-0.09	7.72	0.06	0.12
B3LYP	743	-0.10	1.06	-0.20	6.41	-0.16	2.49	-0.09	7.5	0.03	0.12
CAMB3LYP	710	-0.14	1.08	-0.18	6.34	-0.17	2.34	-0.14	6.6	-0.10	0.15
B971	720	-0.13	1.05	-0.21	6.32	-0.18	2.45	-0.10	7.37	0.01	0.12
B972	747	-0.10	1.07	-0.19	6.38	-0.17	2.46	-0.10	7.38	0.01	0.11
PBE	915	0.11	1.06	-0.20	6.31	-0.18	2.47	-0.09	7.64	0.04	0.12
revPBE	941	0.14	1.07	-0.19	6.3	-0.18	2.47	-0.1	7.61	0.04	0.13
PBE0	740	-0.10	1.07	-0.19	6.38	-0.17	2.45	-0.10	7.32	0.00	0.11
M06-L	212	-0.74	1.12	-0.15	6.87	-0.10	2.7	-0.01	8.26	0.13	0.23
M06	806	-0.02	1.26	-0.05	7.26	-0.05	2.73	0.00	7.97	0.09	0.04
M06-2X	616	-0.25	1.08	-0.18	6.4	-0.16	2.38	-0.13	6.75	-0.08	0.16
M06-HF	574	-0.31	1.08	-0.19	5.82	-0.24	2.02	-0.26	5.4	-0.26	0.25

Just as in the polyacetylenes, most DFT functionals tested in this study have errors that increase with the length of the polyynes, leading to drastic errors for longer chains. As previously observed, the exceptions are functionals with large HF exchange: CAMB3LYP, M06-2X, and M06-HF. Although CAMB3LYP and M06-2X perform poorly for short chains, the dependence of the error on chain length is different, leading to better results for larger molecules. Both CAMB3LYP and M06-2X underestimate γ for all chain lengths, but they give results between CCSD and CCSD(T) for the longer chains we consider. As before, however, we can see that for very long chains one will still require 100% long-range Hartree-Fock exchange to get accurate results.

Although CCSD(T) is widely accepted as a benchmark method for calculating the hyperpolarizabilities of conjugated systems,[61,62] these results show that the performance of CCSD(T) for conjugated systems, especially with triple bonds, is questionable and requires further investigation. CCSD(T) is considered the "gold standard" for benchmarking other methods because the overestimation of (T) for triples is close to the omitted quadruple excitations, and thus the method benefits from a favoured cancellation of errors.[91] But this effect doesn't necessarily hold for all systems and molecular properties. Electron correlation is known to increase γ, which is clear in the consistent underestimation of HF for all molecules, and thus including more dynamic correlation from the estimate of triple excitation is expected to give higher γ values. However, the contribution of electron correlation is reduced, the ratio $\gamma_{CCSD(T)}/\gamma_{HF}$ decreases, as the polyacetylene chain grows, leading to closer agreement between coupled cluster and the

HF method, which agrees with previous studies.[32,92] The cause of this effect is still not clear. For the polyyne chains, however, we observe the opposite effect of correlation: the ratio $\gamma_{CCSD(T)}/\gamma_{HF}$ increases as the chain lengthens.

Thus, the difference between CCSD and CCSD(T) could reflect the significant contribution of the triples excitations to the second hyperpolarizability.[32] However, MP2 is known to overestimate the second hyperpolarizability of conjugated systems,[93-96] and was shown to give the wrong trend as the chain lengthens.[92] Therefore, the triples estimate could be overestimated. Ref [97] showed that both CCSD(T) and CCSD have a 4% error, overestimation for the former and underestimation for the latter, for calculating γ of a linear chain of 4 hydrogens compared to full-CI. Another study showed that CCSD slightly outperforms CCSD(T) in calculating γ for the same chains.[14] These results are not sufficient to make firm conclusions about the performance of CCSD and CCSD(T) and comparisons with more accurate methods, such as CCSDT, CC3, or DMRG, are required.

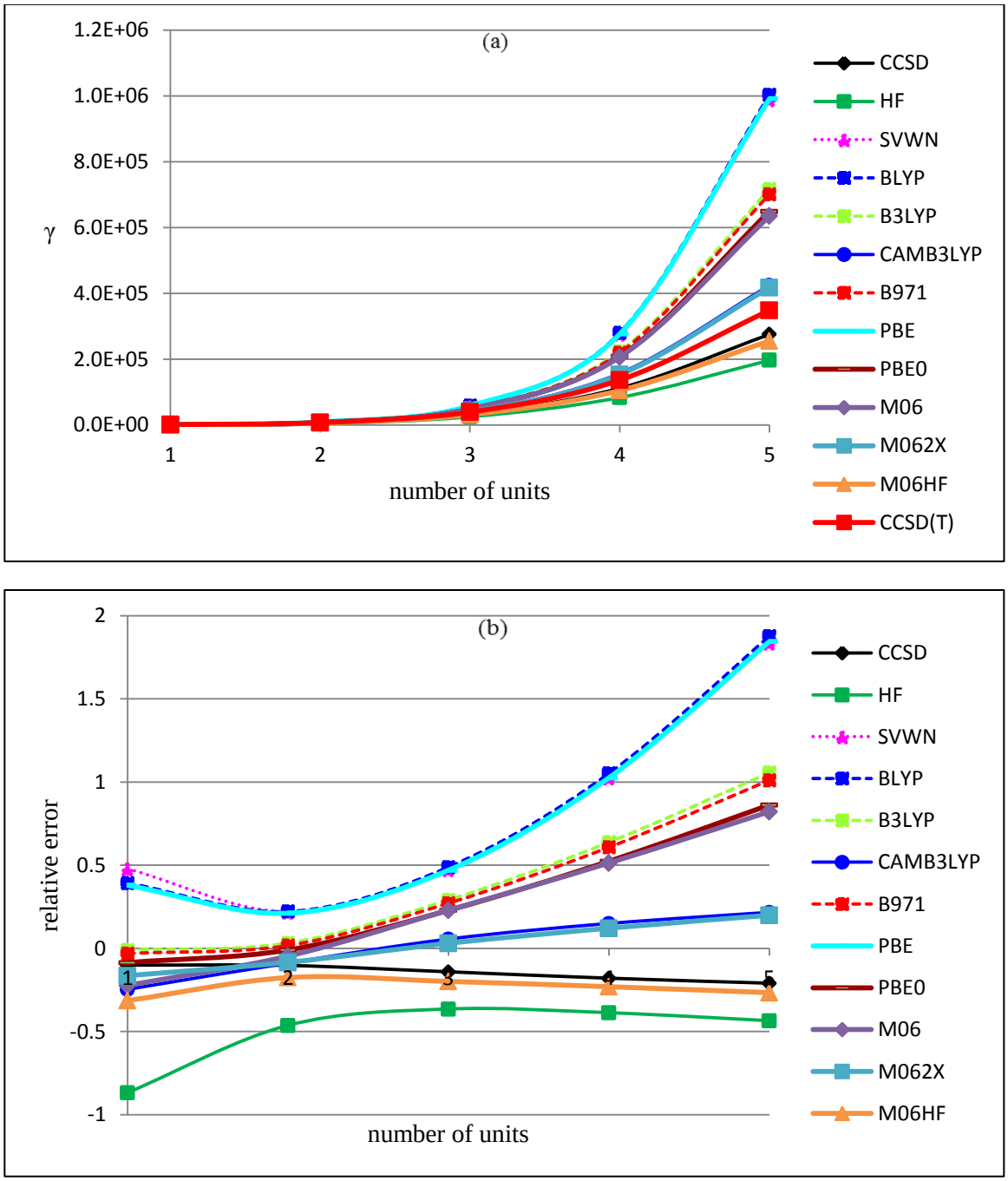

Figure 4.7: (a) Longitudinal second hyperpolarizabilities of polymethineimine chains for several methods as a function of the number of units. (b) Relative error of longitudinal second hyperpolarizabilities of polymethineimine chains for several methods compared to CCSD(T) as a function of the number of units.

Table 4.3: Finite field γ values (in atomic units), relative errors, and average absolute relative errors for polymethineimine H-(CH=N)$_m$-H, calculated by different methods using cc-pVTZ basis set. The relative error of a method is calculated by the expression $error = \frac{\gamma_{method}}{\gamma_{CCSD(T)}} - 1$.

	m=1		m=2		m=3		m=4		m=5		avg. error
	γ x10^3	error	γ x10^3	error	γ x10^4	error	γ x10^5	error	γ x10^5	error	
CCSD(T)	1.21		7.86		3.98		1.37		3.48		
CCSD	1.09	-0.10	7.05	-0.10	3.42	-0.14	1.12	-0.18	2.75	-0.21	0.15
HF	0.16	-0.87	4.22	-0.46	2.53	-0.36	0.84	-0.39	1.97	-0.44	0.50
SVWN	1.79	0.48	9.59	0.22	5.86	0.47	2.77	1.02	9.88	1.84	0.81
BLYP	1.69	0.39	9.60	0.22	5.92	0.49	2.80	1.05	10.02	1.88	0.81
B3LYP	1.20	-0.01	8.12	0.03	5.13	0.29	2.23	0.64	7.17	1.06	0.73
CAMB3LYP	0.91	-0.25	7.17	-0.09	4.20	0.06	1.57	0.15	4.24	0.22	0.15
B971	1.18	-0.03	8.00	0.02	5.05	0.27	2.20	0.61	7.01	1.01	0.39
B972	1.12	-0.08	7.89	0.00	5.02	0.26	2.18	0.60	6.97	1.00	0.39
PBE	1.67	0.38	9.52	0.21	5.84	0.47	2.77	1.03	9.91	1.84	0.79
revPBE	1.62	0.34	9.49	0.21	5.83	0.47	2.77	1.02	9.92	1.85	0.78
PBE0	1.11	-0.09	7.79	-0.01	4.88	0.23	2.08	0.52	6.49	0.86	0.34
M06-L	1.29	0.06	8.27	0.05	5.56	0.40	2.62	0.91	9.22	1.65	0.61
M06	0.94	-0.22	7.49	-0.05	4.89	0.23	2.07	0.51	6.35	0.82	0.37
M06-2X	1.01	-0.16	7.20	-0.08	4.10	0.03	1.53	0.12	4.18	0.20	0.12
M06-HF	0.83	-0.31	6.48	-0.18	3.19	-0.20	1.05	-0.23	2.56	-0.27	0.24

Replacing every other carbon in a polyacetylene chain with nitrogen gives polymethineimines, conjugated systems with interesting NLO properties. The second hyperpolarizability and relative errors for these chains are shown in Figure 4.7 and Table 4.3. Introducing a heteroatom to the chain increases the relative error for almost all the methods, especially with larger molecules. Both CCSD and HF consistently underestimate γ values for all chains, with errors diverging as the chain lengthens. The effect of correlation for these systems is the same as for polyyne chains: $\gamma_{CCSD(T)}/\gamma_{HF}$ increases with the number of units, starting from a 3-unit chain. LDA and pure GGA functionals overestimate the second hyperpolarizability with errors increasing with chain length. Hybrid functionals benefits from including HF exchange and partially correct the error of pure functionals. However, the error still diverges with chain length, but not as fast as in pure functionals. Both CAMB3LYP and M06-2X show a different behaviour for the error and are very close to CCSD. As before, the value of the T1 diagnostic (T1 = 0.012 to 0.017 for the one- to five-unit chains) suggest that the CCSD and CCSD(T) values are trustworthy.

Adding electron donating and withdrawing groups on the opposite sides of a polyacetylene chain gives donor acceptor π-conjugated systems, the so-called push-pull molecules. As shown in Table 4.4, there is a significant increase in the error for these systems compared to the non-substituted polyacetylene chains, confirming that systems with strong electron delocalization are challenging for DFT. Unlike the previous conjugated systems, there is a consistent and significant underestimation of γ by all DFT

methods, without a systematic increase in the error in the extending chains, which makes the reference method questionable. These systems have a T1 diagnostic of 0.019, slightly under the acceptable threshold of 0.02, indicating a strong possibility of dealing with a system with multi-reference character. The ratio $\gamma_{CCSD(T)}/\gamma_{HF}$ consistently increases with chain length, indicating that extending the chain enhances the effect of electron correlation for these systems.

Table 4.4: Finite field γ values (in atomic units), relative errors, and average absolute relative errors for amino nitro polyacetylene units NH_2-$(CH=CH)_m$-NO_2, calculated by different methods using cc-pVTZ basis set. The relative error of a method is calculated by the expression $error = \frac{\gamma_{method}}{\gamma_{CCSD(T)}} - 1$.

	m=1		m=2		m=3		avg. error
	γ x10^4	error	γ x10^5	error	γ x10^5	error	
CCSD(T)	2.58		2.06		8.96		
CCSD	2.11	-0.18	1.72	-0.17	7.65	-0.15	0.16
HF	1.03	-0.60	0.64	-0.69	2.74	-0.69	0.66
SVWN	0.46	-0.82	0.13	-0.94	0.88	-0.90	0.89
BLYP	0.61	-0.76	0.17	-0.92	1.07	-0.88	0.85
B3LYP	0.60	-0.77	0.38	-0.82	2.16	-0.76	0.78
CAMB3LYP	0.81	-0.68	0.66	-0.68	3.47	-0.61	0.66
B971	0.60	-0.77	0.39	-0.81	2.18	-0.76	0.78
B972	0.58	-0.77	0.39	-0.81	2.19	-0.76	0.78
PBE	0.59	-0.77	0.17	-0.92	1.06	-0.88	0.86
revPBE	0.63	-0.76	0.19	-0.91	1.11	-0.88	0.85
PBE0	0.62	-0.76	0.42	-0.79	2.36	-0.74	0.76
M06-L	0.50	-0.81	0.22	-0.89	1.35	-0.85	0.85
M06	0.64	-0.75	0.44	-0.79	2.49	-0.72	0.75
M06-2X	0.90	-0.65	0.69	-0.66	3.61	-0.60	0.64
M06-HF	1.39	-0.46	0.97	-0.53	4.43	-0.51	0.50

4.4.2 Aromatic molecules

For aromatic molecules, as shown in Table 4.5, we observe underestimation of the second hyperpolarizability by all the methods except LDA and pure GGA functionals for benzene and phenol. It is surprising that pure density functionals give the lowest errors for these molecules, and that hybrid and long-range separated functionals don't benefit from including HF exchange. This seems to be because the underestimation by HF is much higher than the overestimation of DFT exchange for these molecules, so the usual compensation of errors does not occur. (A hybrid functional with a small fraction of exact exchange, like TPSSh, might work better for these aromatic molecules.) These are the only systems in this study where B3LYP outperformed CAMB3LYP.

There is a significant increase in the errors for all DFT functionals when a triple bond is introduced by replacing an OH group with a CN, changing phenol to benzonitrile. The Minnesota family functionals generally does worse than the rest of the functionals, with errors consistently increasing with the percentage of HF exchange. Using CCSD as a reference, hybrid functionals performs better than pure ones, and better than CAMB3LYP. In these molecules the value of the T1 diagnostic ranges from 0.010 to 0.012.

Table 4.5: Finite field γ values (in atomic units), relative errors, and average absolute relative errors for a set of aromatic molecules calculated by different methods using cc-pVTZ basis set. The relative error of a method is calculated by the expression $error = \frac{\gamma_{method}}{\gamma_{CCSD(T)}} - 1$.

	benzene		phenol		benzonitrile		avg. error
	γ	error	γ	error	γ	error	
CCSD(T)	6128		9419		40526		
CCSD	5664	-0.08	8417	-0.11	37004	-0.09	0.09
HF	3901	-0.36	4973	-0.47	29178	-0.28	0.37
SVWN	6856	0.12	10115	0.07	23482	-0.42	0.20
BLYP	6795	0.11	10063	0.07	23546	-0.42	0.20
B3LYP	5747	-0.06	8363	-0.11	20832	-0.49	0.22
CAMB3LYP	5038	-0.18	7272	-0.23	18286	-0.55	0.32
B971	5676	-0.07	8202	-0.13	20537	-0.49	0.23
B972	5542	-0.10	8009	-0.15	20424	-0.50	0.25
PBE	6696	0.09	9907	0.05	23359	-0.42	0.19
revPBE	6605	0.08	9783	0.04	23285	-0.43	0.18
PBE0	5466	-0.11	7941	-0.16	20092	-0.50	0.26
M06-L	5495	-0.10	8158	-0.13	21070	-0.48	0.24
M06	5221	-0.15	7710	-0.18	20215	-0.50	0.28
M06-2X	5030	-0.18	7189	-0.24	18097	-0.55	0.32
M06-HF	3842	-0.37	6038	-0.36	15529	-0.62	0.45

4.4.3 Small molecules

Table 4.6 shows that both HF and CCSD consistently underestimate γ values for a set of small molecules. HF has an average error of 39%, and the absence of perturbative triples correlations gives an average error of 10% for CCSD. This indicates the importance of including correlation when calculating γ for these simple systems.

LDA, pure GGA, and hybrid functionals consistently overestimate γ for the small molecules we considered. The pure GGA functionals, BLYP, PBE, and revPBE, and the local density approximation, SVWN, gave the worst results, with relative errors close to or higher than 100%. Introducing HF exchange improves the results significantly. We observe a consistent decrease in the error from BLYP to B3LYP to CAMB3LYP, with the later functional outperforming all other methods, including CCSD, and thus performing significantly better than B3LYP for these small molecules. These results show the inadequacy of conventional DFT functionals for calculating the second hyperpolarizability of small molecules.

For the M06 family, the behaviour of the error is systematic, except for ethanol. The calculated γ decreases as the amount of HF exchange in the functional is increased from 0% (M06-L), to 27% (M06), to 54% (M06-2X), to 100% (M06-HF). The meta-GGA M06-L is better than the pure functionals BLYP and PBE.

Table 4.6: Finite field γ values (in atomic units), relative errors, and average absolute relative errors for a set of molecules calculated by different methods using cc-pVTZ basis set. The relative error of a method is calculated by the expression $error = \frac{\gamma_{method}}{\gamma_{CCSD(T)}} - 1$.

	CH_3OH		C_2H_5OH		$C_2H_5NH_2$		C_3H_7CHO		avg. error
	γ	error	γ	error	γ	error	γ	error	
CCSD(T)	1083		3028		6857		7326		
CCSD	1038	-0.04	2800	-0.08	5564	-0.19	6579	-0.10	0.10
HF	654	-0.40	2169	-0.28	3458	-0.50	4555	-0.38	0.39
SVWN	1512	0.40	5708	0.88	15210	1.22	14383	0.96	0.87
BLYP	1534	0.42	5656	0.87	15609	1.28	13945	0.90	0.87
B3LYP	1211	0.12	4263	0.41	10064	0.47	10105	0.38	0.34
CAMB3LYP	1021	-0.06	3405	0.12	6756	-0.01	7660	0.05	0.06
B971	1174	0.08	4097	0.35	9532	0.39	9907	0.35	0.29
B972	1130	0.04	3945	0.30	8874	0.29	9605	0.31	0.24
PBE	1482	0.37	5461	0.80	14594	1.13	13841	0.89	0.80
revPBE	1462	0.35	5347	0.77	14119	1.06	13573	0.85	0.76
PBE0	1117	0.03	3889	0.28	8643	0.26	9392	0.28	0.21
M06-L	1204	0.11	3275	0.08	9062	0.32	10922	0.49	0.25
M06	1072	-0.01	3896	0.29	7972	0.16	9526	0.30	0.19
M06-2X	944	-0.13	4167	0.38	6169	-0.10	7865	0.07	0.17
M06-HF	753	-0.31	2673	-0.12	4244	-0.38	5886	-0.20	0.25

Table 4.7 shows a significant jump in the errors as π-bonds are introduced. We notice huge errors for calculating γ of CO by M06-L, M06, and M06-HF, with both M06-L and M06 giving the wrong sign for γ.

Table 4.7: Finite field γ values (in atomic units), relative errors, and average absolute relative errors for a set of small molecules calculated by different methods using cc-pVTZ basis set. The relative error of a method is calculated by the expression $error = \frac{\gamma_{method}}{\gamma_{CCSD(T)}} - 1$.

	NH3		H2O		CO		CO2		HCN		avg. error
	γ	error	γ	error	γ	error	γ	error	γ	error	
CCSD(T)	503		241		75		-297		699		
CCSD	489	-0.03	237	-0.02	65	-0.14	-345	0.16	646	-0.08	0.08
HF	464	-0.08	242	0.00	98	0.30	-55	-0.81	262	-0.63	0.36
SVWN	648	0.29	295	0.22	81	0.08	-106	-0.64	941	0.35	0.32
BLYP	672	0.34	305	0.26	87	0.16	-99	-0.67	994	0.42	0.37
B3LYP	598	0.19	282	0.17	87	0.16	-103	-0.65	675	-0.03	0.24
CAMB3LYP	548	0.09	269	0.12	80	0.07	-118	-0.60	526	-0.25	0.22
B971	584	0.16	275	0.14	95	0.27	-96	-0.68	656	-0.06	0.26
B972	561	0.11	270	0.12	103	0.38	-88	-0.70	665	-0.05	0.27
PBE	646	0.28	298	0.24	106	0.41	-85	-0.71	1012	0.45	0.42
revPBE	638	0.27	299	0.24	117	0.55	-77	-0.74	1033	0.48	0.46
PBE0	561	0.12	270	0.12	104	0.38	-91	-0.69	643	-0.08	0.28
M06-L	476	-0.05	207	-0.14	-194	-3.59	-262	-0.12	502	-0.28	0.84
M06	494	-0.02	236	-0.02	-19	-1.26	-208	-0.30	556	-0.21	0.36
M06-2X	492	-0.02	238	-0.01	79	0.05	-114	-0.62	480	-0.31	0.20
M06-HF	410	-0.18	285	0.18	189	1.51	-83	-0.72	539	-0.23	0.56

4.5 Conclusions

We performed a benchmark study to assess the errors of several DFT functionals, relative to CCSD(T), for calculating the static longitudinal second hyperpolarizabilities for 30 molecules. The performance of these functionals depends on the system under consideration.

Hybrid functionals generally perform better than pure ones, probably due to a partial correction of the self-interaction error, which leads the exchange-correlation potential to be too shortsighted. The error for both pure and hybrid functionals increases with the size of the molecule in conjugated systems, leading to disastrous results for longer chains, and indicating the inadequacy of conventional DFT functions for calculating the second hyperpolarizabilities for these systems. This behaviour is eliminated to a large degree in the range-separated CAMB3LYP functional and in functionals with more than 50% HF exchange: M06-2X and M06-HF. Conventional GGA functionals have high errors for small molecules as well. For aromatic molecules, pure GGA functionals have slightly smaller errors than global hybrid and long-range corrected functionals.

Overall, the CAMB3LYP functional has the best performance, followed by M06-2X, which has 54% HF exchange. CAMB3LYP is a long-range corrected functional that benefits from using more exact HF change at longer distances to correct the erroneous asymptotic decay of exchange-correlation potential, and represents a significant improvement over the B3LYP functional for π-conjugated chains and small molecules.

These two functionals, CAMB3LYP and M06-2X, are recommended for all systems except aromatic molecules, in which pure functionals have the best performance.

The effect of correlation on the second hyperpolarizability can be assessed by comparing results from Hartree-Fock and coupled cluster calculations. Including correlation leads to higher γ values, and Hartree-Fock consistently underestimation γ. The ratio $\gamma_{CCSD(T)}/\gamma_{HF}$ increases with chain length for all conjugated systems investigated here except for polyacetylene chains, it consistently decreases. We also observe a significant divergence between CCSD and CCSD(T) that increases as the length of conjugated chains increases. These results indicate the need for more accurate methods to assess the suitability of CCSD(T) as a benchmarking method for NLO properties of conjugated systems.

4.6 References

1. J. C. Chien, Polyacetylene: *Chemistry, Physics and Material Science* (Academic, Orlando, 1984).
2. H.-J. Werner, W. Meyer, Phys. Rev. A **13**, 13 (1975).
3. E.-A. Reinsch, W. Meyer, Phys. Rev. A **14**, 915 (1976).
4. H. Kahlert, O. Leitner, G. Leising, Synth. Met. **17**, 467 (1987).
5. B. J. Coe, J. A. Harris, L. A. Jones, B. S. Brunschwig, K. Song, K. Clays, J. Garin, J. Orduna, S. J. Coles, M. B. Hursthouse, J. Am. Chem. Soc. **127**, 4845 (2005).
6. F. Mançois, L. Sanguinet, J.-L. Pozzo, M. Guillaume, B. Champagne, V. Rodriguez, F. Adamietz, L. Ducasse, F. Castet, J. Phys. Chem. B **111**, 9795 (2007).
7. S. Salustro, L. Maschio, B. Kirtman, M. Rérat, .R. Dovesi, J. Phys. Chem. C **120**, 6756 (2016).
8. P. A. Limacher, K. V. Mikkelsen, H. P. Lüthi, J. Chem. Phys. **130**, 194114 (2009).
9. S. Borini, P. A. Limacher, H. P. Lüthi, J. Chem. Phys. **131**, 1241050 (2009).
10. R. Kanis, M. A. Ratner, T. J. Marks, Chem. Rev. **94**, 195 (1994)
11. B. Kirtman, in *Theoretical and Computational Modeling of NLO and Electronic Materials*, edited by S. P. Karna, A. T. Yeates (ACS, Washington DC, 1996), ACS Series Vol. 628, p. 58.
12. B. Champagne, B. Kirtman, in *Handbook of Advanced Electronic and Photonic Materials and Devices*, Nonlinear Optical Materials Vol. 9, Edited by H. S. Nalwa (Academic, San Diego, 2001), p. 63.
13. K. Y. Suponitsky, T. V. Timofeeva, M. Y. Antipin, Russ. Chem. Rev. **75**, 457 (2006).

14. J. B. Robinson, P. J. Knowles, J. Chem. Phys. **137**, 054301 (2012).

15. L. M. Abreu, T. L. Fonseca, M. A. Castro, J. Chem. Phys. **136**, 234311 (2012).

16. M. de Wergifosse, F. Wautelet, B. Champagne, R. Kishi, K. Fukuda, H. Matsui, M. Nakano, J. Phys. Chem. A **117**, 4709 (2013).

17. M. de Wergifosse, J. Phys. Chem. A **120**, 2727 (2016).

18. H. Matsui, K. Fukuda, S. Ito, T. Nagami, M. Nakano, J. Phys. Chem. A **120**, 948 (2016).

19. S. Wouters, V. Van Speybroeck, D. Van Neck, J. Chem. Phys. **145**, 054120 (2016).

20. M. de Wergifosse, B. Champagne. J. Chem. Phys. **134**, 074113 (2011)

21. A. A. K. Mohammed, P. A. Limacher, B. Champagne, J. Comput. Chem. **34**, 1497 (2013).

22. T. Wu, Y. N. Kalugina, A. J. Thakkar, Chem. Phys. Lett. **635**, 257 (2015).

23. A. A. K. Mohammed, P. A. Limacher, P. W. Ayers Chem. Phys. Lett. **682**, 160 (2017).

24. T. Wu, A. J. Thakkar, J. Chem. Phys. **143**, 144302 (2015).

25. J. M. Luis, M. Torrent-Sucarrat, O. Christiansen, B. Kirtman, J. Chem. Phys. **127**, 084118 (2007)

26. B. Kirtman, J. M. Luis, J. Chem. Phys. **128**, 114101 (2008).

27. J. Quertinmont, B. Champagne, F. Castet, M. H. Cardenuto, J. Phys. Chem. A **119**, 5496 (2015).

28. R. J. Bartlett, G. D. Purvis, Phys. Rev. A **20**, 1313 (1979).

29. B. M. Pierce, J. Chem. Phys. **91**, 791 (1989).

30. H. Sekino, R.J. Bartlett, J. Chem. Phys. **94** 3665 (1991).

31. D. Jacquemin, J. M. André, E. A. Perpète, J. Chem. Phys. **121**, 4389 (2004).

32. P. A. Limacher, Q. Li, H. P. Lüthi, J. Chem. Phys. **135**, 014111 (2011).

33. B. Champagne, E. A. Perpète, S. J. A. van Gisbergen, E.-J. Baerends, J. G. Snijders, C. Soubra-Ghaoui, K. A. Robins, B. Kirtman, J. Chem. Phys. **109**, 10489 (1998).

34. S. F. Sousa, P. A. Fernandes, M. J. Ramos, J. Phys. Chem. A **111**, 10439 (2007).

35. L. Goerigk, S. Grimme, J. Chem. Theory Comp. **6**, 107 (2010).

36. L. Goerigk, S. Grimme, J. Chem. Theory Comp. **7**, 291 (2011).

37. L. Goerigk, S. Grimme, PCCP **13**, 6670 (2011).

38. A. J. Cohen, P. Mori-Sanchez, W. T. Yang, Chem. Rev. **112**, 289 (2012).

39. C.-W. Tsai, Y.-C. Su, G.-D. Li, J.-D. Chai, PCCP **15**, 8352 (2013).

40. I. Y. Zhang, X. Xu, J. Phys. Chem. Lett. **4**, 1669 (2013).

41. N. Mardirossian, M. Head-Gordon, PCCP **16**, 9904 (2014).

42. H. Sun, J. Autschbach, J. Chem. Theory Comp. **10**, 1035 (2014).

43. N. Mardirossian, M. Head-Gordon, J. Chem. Phys. **140**, (2014).

44. T. Tsuneda, K.Hirao, WIREs Comput. Mol. Sci. **4**, 375 (2014).

45. J. Autschbach, M. Srebro, Acc. Chem. Res. **47**, 2592 (2014).

46. N. Mardirossian, M. Head-Gordon, J. Chem. Phys. **144**, 214110 (2016).

47. N. Mardirossian, M. Head-Gordon, J. Chem. Phys. **145**, 186101 (2016).

48. B. Champagne, E. A. Perpète, D. Jacquemin, S. J. A. van Gisbergen, E.-J.Baerends, C. Soubra-Ghaoui, K. A. Robins, B. Kirtman, J. Phys. Chem. A **104**, 4755 (2000).

49. S. J. A. van Gisbergen, P. R. T. Schipper, O. V. Gritsenko, E. J. Baerends, J. G. Snijders, B. Champagne, B. Kirtman, Phys. Rev. Lett. **83**, 694 (1999).

50. B. Champagne, F. A. Bulat, W. Yang, S. Bonness, B. Kirtman, J. Chem. Phys. **125**, 194114 (2006).

51. A. Ruzsinszky, J. P. Perdew, G. I. Csonka, O. A. Vydrov, G. E. Scuseria, J. Chem. Phys. **125**, 194112 (2006).

52. A. Ruzsinszky, J. P. Perdew, G. I. Csonka, O. A. Vydrov, G. E. Scuseria, J. Chem. Phys. **126**, 104102 (2007).

53. P. Mori-Sanchez, A. J. Cohen, W. T. Yang, Phys. Rev. Lett. **100**, 146401 (2008).

54. P. Mori-Sanchez, A. J. Cohen, W. T. Yang, J. Chem. Phys. **125**, 201102 (2006).

55. A. J. Cohen, P. Mori-Sanchez, W. T. Yang, Phys. Rev. B **77**, 115123 (2008).

56. A. J. Cohen, P. Mori-Sanchez, W. T. Yang, Science **321**, 792 (2008).

57. R. Haunschild, T. M. Henderson, C. A. Jimenez-Hoyos, G. E. Scuseria, J. Chem. Phys. **133**, 134116 (2010).

58. M. Kamiya, H. Sekino, T. Tsuneda, K. Hirao, J. Chem. Phys. **122**, 234111 (2005).

59. H. Sekino, Y. Maeda, M. Kamiya, K. Hirao, J. Chem. Phys. **126**, 014107 (2007).

60. D. Jacquemin, E. A. Perpete, G. Scalmani, M. J. Frisch, R. Kobayashi, C. Adamo, J. Chem. Phys. **126**, 144105 (2007).

61. S. Nenon B. Champagne, M. I. Spassovab, Phys. Chem. Chem. Phys. **16**, 7083 (2014).

62. M. B. Oviedo, N. V. Ilawe, B. M. Wong, J. Chem. Theory Comput. **12**, 3593 (2016).

63. M. Zouaoui-Rabah, M. Sekkal-Rahal, F. Djilani-Kobibi, A. M. Elhorri, M. Springborg J. Phys. Chem. A **120**, 8843 (2016).

64. L. F. Richardson, J. A. Gaunt, Phil. Trans. R. Soc. Lond. A **226**, 299 (1927).

65. Gaussian 09, Revision C.01, M. J. Frisch, G. W. Trucks, H. B. Schlegel, G. E. Scuseria, M. A. Robb, J. R. Cheeseman, G. Scalmani, V. Barone, B. Mennucci, G. A. Petersson, H. Nakatsuji, M. Caricato, X. Li, H. P. Hratchian, A. F. Izmaylov, J. Bloino, G. Zheng, J. L. Sonnenberg, M. Hada, M. Ehara, K. Toyota,

R. Fukuda, J. Hasegawa, M. Ishida, T. Nakajima, Y. Honda, O. Kitao, H. Nakai, T. Vreven, J. A. Montgomery, Jr., J. E. Peralta, F. Ogliaro, M. Bearpark, J. J. Heyd, E. Brothers, K. N. Kudin, V. N. Staroverov, T. Keith, R. Kobayashi, J. Normand, K. Raghavachari, A. Rendell, J. C. Burant, S. S. Iyengar, J. Tomasi, M. Cossi, N. Rega, J. M. Millam, M. Klene, J. E. Knox, J. B. Cross, V. Bakken, C. Adamo, J. Jaramillo, R. Gomperts, R. E. Stratmann, O. Yazyev, A. J. Austin, R. Cammi, C. Pomelli, J. W. Ochterski, R. L. Martin, K. Morokuma, V. G. Zakrzewski, G. A. Voth, P. Salvador, J. J. Dannenberg, S. Dapprich, A. D. Daniels, O. Farkas, J. B. Foresman, J. V. Ortiz, J. Cioslowski, and D. J. Fox, Gaussian, Inc., Wallingford CT, 2009.

66. T. Yanai, D. P. Tew, N. C. Handy, Chem. Phys. Lett. **393**, 51 (2004).

67. A. D. Becke, Phys. Rev. A **38**, 3098 (1988).

68. C. Lee, W. Yang, R. G. Parr, Phys. Rev. B **37**, 785 (1988).

69. A. D. Becke, J. Chem. Phys. **98**, 5648 (1993).

70. T. Leininger, H. Stoll, H.-J. Werner, A. Savin, Chem. Phys. Lett. **275**, 151 (1997).

71. A. V. Krukau, G. E. Scuseria, J. P. Perdew, A. Savin, J. Chem. Phys. **129**, 124103 (2008).

72. M. J. G. Peach, E. I. Tellgren, P. Salek, T. Helgaker, D. J. Tozer, J. Phys. Chem. A **111**, 11930 (2007).

73. R. A. Kendall, T. H. Dunning Jr., R. J. Harrison, J. Chem. Phys. **96**, 6796 (1992).

74. G. J. B. Hurst, M. Dupuis, E. Clementi, J. Chem. Phys. **89**, 385(1988).

75. M. Torrent-Sucarrat, M. Sola, M. Duran, J. M. Luis, B. Kirtman, J. Chem. Phys. **118**, 711(2003).

76. MOLPRO, version 2010.1, a package of ab initio programs, H.-J.Werner, P. J. Knowles, G. Knizia, F. R. Manby, M. Sch¨utz, P. Celani, T. Korona, R. Lindh, A. Mitrushenkov, G. Rauhut, K. R. Shamasundar, T. B. Adler, R. D. Amos, A. Bernhardsson, A. Berning, D. L. Cooper, M. J. O. Deegan, A. J. Dobbyn, F.

Eckert, E. Goll, C. Hampel, A. Hesselmann, G. Hetzer, T. Hrenar, G. Jansen, C. Koppl, Y. Liu, A. W. Lloyd, R. A. Mata, A. J. May, S. J. McNicholas, W. Meyer, M. E. Mura, A. Nicklass, D. P. O'Neill, P. Palmieri, K. Pfl¨uger, R. Pitzer, M. Reiher, T. Shiozaki, H. Stoll, A. J. Stone, R. Tarroni, T. Thorsteinsson, M. Wang, and A. Wolf, see http://www.molpro.net.

77. DALTON, a molecular electronic structure program, Release 2.0 (2005), see http://www.kjemi.uio.no/software/dalton/dalton.html.

78. J. C. Slater, Phys. Rev. **81**, 385 (1951).

79. S. J. Vosko, L. Wilk, M. Nusair, Can. J. Phys. **58**, 1200 (1980).

80. J. P. Perdew, K. Burke, M. Ernzerhof, Phys. Rev. Lett. **77**, 3865 (1996).

81. Y. Zhang, W. Yang, Phys. Rev. Lett. **80**, 890 (1998).

82. F. A. Hamprecht, A. J. Cohen, D. J. Tozer, N. C. Handy, J. Chem. Phys. **109**, 6264 (1998).

83. P. J. Wilson, T. J. Bradley, D. J. Tozer, J. Chem. Phys. **115**, 9233 (2001).

84. C. Adamo, V. Barone, J. Chem. Phys. **111**, 6158 (1999).

85. A. Savin, in Recent Developments and Applications of Modern Density Functional Theory, edited by J. J. Seminario (Elsevier, Amsterdam, 1996).

86. H. Iikura, T. Tsuneda, T. Yanai, K. Hirao, J. Chem. Phys. **115**, 3540 (2001).

87. Y. Zhao, D. G. Truhlar, J. Chem. Phys. **125,** 194101 (2006).

88. Y. Zhao, D. G. Truhlar, Theoretical Chemistry Accounts **120,** 215 (2006).

89. Y. Zhao, D. G. Truhlar, J. Phys. Chem. A **110**, 13126 (2006).

90. T. J. Lee, P. R. Taylor, Int. J. Quantum Chem. **36**, 199 (1989).

91. T. Helgaker, W. Klopper, A. Halkier, K. L. Bak, P. Jørgensen, J. Olsen, 2001. Highly Accurate Ab Initio Computation of Thermochemical Data, in *Quantum Mechanical Prediction of Thermodynamic Data*, Cioslowski, J. Ed., Kluwer:Dordrecht, 1.

92. Q. Li, L. Chen, Q. Li, Z. Shuai, Chem. Phys. Lett. **457**, 276 (2008).

93. J.-W. Song, M. A. Watson, H. Sekino, K. Hirao, J. Chem. Phys. **129**, 024117 (2008).

94. B. Kirtman, S. Bonness, A. Ramirez-Solis, B. Champagne, H. Matsumoto, H. Sekino, J. Chem. Phys. **128**, 114108 (2008).

95. B. Champagne, B. Kirtman, Int. J. Quantum Chem. **109**, 3103 (2009).

96. S. Wouters, P. A. Limacher, D. Van Neck, P. W. Ayers, J. Chem. Phys. **136**, 134110 (2012).

97. M. Nakano, T. Minami, H. Fukui, R. Kishi, Y. Shigeta, B. Champagne, J. Chem. Phys. **136**, 024315 (2012).

Chapter 5

Finite Field Method for Nonlinear Optical Property Prediction Using Rational Function Approximants[‡]

5.1 Motivation

Chapters 2-4 are based on calculating response properties using a polynomial function to model the dependence of the energy of a molecule on the applied field. In this chapter, we present and explore a novel variant of the FF method, which uses a rational function to fit a molecule's energy with respect to the applied electric field. Rational functions are more general than the polynomial model, and thus are expected to capture physical behaviour that the latter can't. Similarly to previous chapters, factors crucial for the method's accuracy were tuned. These factors include: the number of terms in the function, the distribution of fields used to construct the approximation, and the initial

[‡] This chapter was originally published as A. H. G. Patel, A. A. K. Mohammed, P. A. Limacher, P. W. Ayers, J. Phys. Chem. A **121**, 5313 (2017)**.**

field in the approximation. An overall comparison of the behaviour of the two methods is presented which shows that the rational function is less sensitive to the chosen initial field and that, unlike the polynomial model, no subsequent refinement steps were needed to obtain reliable results.

5.2 Introduction

Since the discovery of nonlinear optical (NLO) phenomena[1] and their uses, determining response polarizabilities and hyperpolarizabilities for molecules and polymers has become increasingly relevant to many fields, including materials science and organic chemistry.[2] Consequently, the demand for cheap and accurate computational methods to predict these molecular properties has increased.[3,4] However, producing a method that achieves these goals is challenging, as the (hyper)polarizabilities are higher-order derivatives of a molecule's energy with respect to an external homogeneous electric field (F), as follows:

$$E\left(F\right)=E\left(0\right)+\left.\frac{\partial E}{\partial F}\right|_0 F+\frac{1}{2!}\left.\frac{\partial^2 E}{\partial F^2}\right|_0 F^2+\frac{1}{3!}\left.\frac{\partial^3 E}{\partial F^3}\right|_0 F^3+\frac{1}{4!}\left.\frac{\partial^4 E}{\partial F^4}\right|_0 F^4+\ldots \qquad (5.1)$$

The dipole moment (μ), the dipole polarizability (α), the first hyperpolarizability (β) and the second hyperpolarizability (γ) can be substituted in the expansion:

$$E\left(F\right)=E\left(0\right)-\mu F-\frac{1}{2}\alpha F^2-\frac{1}{6}\beta F^3-\frac{1}{24}\gamma F^4+\ldots \qquad (5.2)$$

Several approaches are available to compute these NLO properties, including: sum over states,[5] coupled-perturbed Hartree-Fock,[6–8] response theory,[9,10] and the finite field (FF) method.[11–15] Of these, the FF method remains one of the most computationally inexpensive, since unlike the other methods, no excited state information or analytical derivatives are required.[16] This also makes the FF method one of the most facile to implement; simply knowing the energy at several field strengths is sufficient to compute a desired optical property. For these reasons, the FF method is commonly used first when one wishes to assess the performance of new quantum chemistry methods for (hyper)polarizabilities.[17–29]

Though the FF method has many advantages, the accuracy of a FF calculation is highly sensitive to the fields used. This sensitivity originates from the errors caused by choosing field strengths that are too high or low. The numerical nature of the FF method implies that choosing field strengths that are too low will cause finite-precision artefacts. Conversely, fields that are too high make higher-order terms in Eq. (5.1) nonnegligible, leading to errors when the Taylor series is truncated. When there are low-lying excited states, using fields that are too high can lead to a field-induced state inversion, where an excited state at zero-field becomes lower in energy than the ground state.[30] This leads to properties being evaluated for the more favourable excited state rather than for the ground state, as desired. As a consequence of these effects, chosen field strengths must be optimized to ensure that computed (hyper)polarizabilities are accurate.

In previous work, it was found that three factors play a key role in the accuracy of a FF method: the total number of fields used, the distribution of the fields, and the initial field value around which the other fields are picked.[31] This previous study tuned these three factors for a Taylor expansion based FF method.[31] In particular, this previous method was based on taking finite differences, using a Taylor polynomial, to compute NLO properties. The optimized method, in conjunction with iterative error reduction using Richardson extrapolation, was found to provide accurate predictions for NLO properties. However, the accuracy of this method was found to be quite sensitive to the initial field used for the calculation. This sensitivity tends to reduce the overall reliability of the method, creating a significant barrier to its widespread adoption and use.

To mitigate the field sensitivity observed with the finite difference method, we propose using a rational function to fit the energy instead:

$$E\left(F\right)=\frac{a+bF+cF^{2}+dF^{3}+\ldots}{1+BF+CF^{2}+DF^{3}+\ldots} \tag{5.3}$$

where a, b, c, d,… and B, C, D,… are fitting coefficients. By setting all the denominator coefficients to zero, a polynomial is obtained, so this function is a generalized form of the Taylor expansion. However, rational functions are well-suited to approximate asymptotic functions and, recalling their use in Padé approximants, (approximately) account for higher-order terms in the Taylor series (5.1), as one must do especially for larger fields. We hypothesized that these properties of rational functions may allow for improvement

in the energy fitting procedure. Consequently, the overall error in a FF calculation might be reduced, which would increase the range of electric fields that produce an acceptable error. To test this hypothesis, in this work, a rational function based FF method is optimized and compared to the Taylor FF method.

As in our previous work on the Taylor, or polynomial, FF model,[31] three factors vital to the accuracy of the rational FF model will be optimized in this study. First, the ideal number of terms for the rational function approximant will be determined, which gives the number of fields used in the calculation. Then, different distributions of the chosen fields will be tested, in order to determine which distributions allow for the most accurate calculation of NLO properties. Finally, the error dependence on initial field strengths for various molecules is explored. If any trends are present, they will be used to produce an algorithm that can choose initial fields optimally. After the rational-function FF method is optimized, its accuracy and behaviour in calculating response properties shall be compared to the previous polynomial-based method.

5.3 Methods

5.3.1 Overview of the rational function approximation for the FF method

To produce enough data points for the FF approximation, the energy of a molecule must initially be solved for at various field strengths. Selecting the appropriate field

strengths begins with choosing an initial field strength (F_0), around which the other chosen field strengths (F) are distributed. For this variant of the FF method, the selected fields are distributed according to:

$$F_n = x^n F_0 \tag{5.4}$$

In this study, $x = 2^{\frac{p}{100}}$ and $F_0 = F_{min} \times 2^{\frac{j}{100}}$. Substituting these forms into Equation (5.4) produces:

$$F_n = \left(2^{\frac{p}{100}n}\right)\left(F_{min} \times 2^{\frac{j}{100}}\right) = F_{min} \times 2^{\frac{(j+pn)}{100}} \tag{5.5}$$

where j is any integer between 1-800, p is any integer between 1-100, and $F_{min} = 0.0005\ a.u.$ For N unknown coefficients in the rational function (Equation (5.3)), $\left\{n \in \mathbb{Z}^* | 0 \leq n \leq (\frac{N}{2} - 1)\right\}$ for even values of N, and $\left\{n \in \mathbb{Z}^* | 0 \leq n \leq (\frac{N-3}{2})\right\}$ for odd values of N. In addition, for both even and odd values of N, the energy at $F = 0$ is also determined, since this simplifies Equation (5.3) to:

$$E(0) = a \tag{5.6}$$

allowing for a to be determined directly. To determine the remaining coefficients, each F_n value is substituted into Equation (5.3). Since both $+F_n$ and $-F_n$ are used, each F_n value produces two equations. These substituted equations can be rearranged into the form:

$$\begin{aligned} E\left(F_0\right)+BF\left(E\left(F_0\right)\right) &= a+F_0b+F_0{}^2c \\ E\left(-F_0\right)-B\left(F_0\left(E\left(-F_0\right)\right)\right) &= a-F_0b+F_0{}^2c \\ E\left(xF_0\right)+BxF_0\left(E\left(xF_0\right)\right) &= a+xF_0b+x^2F_0{}^2c \\ E\left(-xF_0\right)-BxF_0\left(E\left(-xF_0\right)\right) &= a-xF_0b+x^2F_0{}^2c \\ &\vdots \end{aligned} \tag{5.7}$$

By substituting $E(0) = a$, and rearranging into the form $A\vec{x} = \vec{b}$:

$$\begin{bmatrix} -F\left(E\left(F\right)\right) & F & F^2 \\ F(E\left(-F\right) & -F & F^2 \\ -xF\left(E\left(xF\right)\right) & xF & x^2F^2 \\ xF\left(E\left(-xF\right)\right) & -xF & x^2F \end{bmatrix}\begin{bmatrix} B \\ b \\ c \end{bmatrix} = \begin{bmatrix} E\left(F\right)-E\left(0\right) \\ E\left(-F\right)-E\left(0\right) \\ E\left(xF\right)-E\left(0\right) \\ E\left(-xF\right)-E\left(0\right) \end{bmatrix} \tag{5.8}$$

Since both the positive and negative fields are used, for even values of N the system is overdetermined. This overdetermined system can be solved through least squares, or by discarding one of the equations. Both approaches are discussed further in Section 5.3.3.

Once the coefficients for Equation (5.3) are determined by solving the system of equations (5.8), the response properties can then be determined by taking the appropriate derivatives of Equation (5.3) at $F = 0$:

$$\begin{aligned} \mu &= -E'(0) \\ \alpha &= -E''(0) \\ \beta &= -E'''(0) \\ \gamma &= -E^{(4)}(0) \end{aligned} \tag{5.9}$$

5.3.2 Optimizing the rational function form and field distribution

Using the general method presented in Section 5.3.1, the energies of five randomly selected molecules were fit by rational functions with various numbers of numerator and denominator terms (Table 5.1). The molecules tested were: acetamide, 4-amino-4'-nitrobiphenyl (DPAN), 1-hexadecanol, hexa-1,3,5-triene (PA3), and 1-amino-10-nitro-deca-1,3,5,7,9-pentaene (PA5AN). For each molecule, plots comparing the error in computed properties (α, β, γ) over varying p and F_0 (Equations (5.4) and (5.5)) were generated for each approximant form (Figure 5.1 and Figure 5.2). For more information on benchmark values and error calculation, refer to Section 5.3.5.

These plots were used to fix the form of the rational function as model 2 for the remainder of the study. The form of model 2 is:

$$E\left(F\right)=\frac{a+bF+cF^2+dF^3}{1+BF+CF^2} \tag{5.10}$$

Since this model has four terms in the numerator and three terms in the denominator, each further FF calculation requires the molecular energy at five nonzero field values, along with the molecular energy at $F = 0$. This is not surprising, since for a fixed (but large) basis set, one expects the energy to diverge to minus infinity linearly with *F* in the high-field limit.

Having determined the optimal functional form for the rational function, the generated plots were also used to fix the value of $p = 50$ for Equation (5.5). This corresponds to a common ratio of $x = \sqrt{2}$ for the geometric progression used to distribute fields in Equation (5.4) and it is the same ratio that we found when investigating the polynomial form in ref. 31.

5.3.3 Testing the least squares solution

The form of the rational function given by model 2 (Equation (5.10)) contains six unknown coefficients, one of which can be determined directly using Equation (5.6). For the remaining five unknown coefficients, positive and negative fields are picked using Equation (5.5). Thus, six equations were generated for five unknowns in this case, leading to an overdetermined system. To ensure that solving the system using least squares provides a consistently accurate result relative to discarding one of the equations, the error in computed response properties over varying F_0 values was plotted for both approaches. An example plot for acetamide is given in Figure 5.3. Using these plots, it was determined that least squares provided an adequate solution to the overdetermined system. Thus, for the remainder of the study, the least squares solution to Equation (5.8) was used. To obtain solutions to both the overdetermined and truncated system of equations, the linear systems were solved using the numpy.linalg Python package.

5.3.4 Developing a protocol to find optimal values of F_0

For FF methods, picking the optimal F_0value is crucial in ensuring the computed response properties are accurate.[31] However, the optimal F_0 drastically varies for each NLO property calculation. Thus, we devised an automatic method to determine an adequate F_0 value. This F_0 picking method arises from the investigation conducted in Section 5.3.3, as it uses the property values calculated by either least squares or truncating the system of equations (Equation (5.8)). In particular, the difference between the truncated solutions from the least squares solution is used to produce an indicator, denoted as r:

$$r = \frac{(q_{max} - q_{min})}{q_{regression}} \tag{5.11}$$

where $q = \alpha, \beta, \gamma,$ and max and min are the maximum and minimum values of the properties calculated by removing one of six equations, respectively. Additionally, $regression$ refers to the value of the properties computed using least squares. The quantity r can be thought of as an error metric that is the ratio between (a) the difference between the maximum and minimum values of q obtained when the equations are solved using leave-one-out analysis and (b) the predicted property value obtained by least-squares solution on the complete dataset.

In total, this procedure requires seven points for each F_0 value to generate the corresponding r value. A representative plot comparing γ values calculated via the two

methods of solving Equation (5.8) is given in Figure 5.5a. Additionally, an example of the r value plotted with respect to F_0 is given in Figure 5.5b.

To pick an F_0 value that minimizes the error in a calculated property, the r value was observed as the F_0 value is increased. Starting from the low-field limit, the first F_0 value for which the r value increases or decreases for five consecutive F_0 values was taken as the F_0 used for the FF calculation. The F_0 chosen in this manner was used to calculate α and γ for a set of 120 molecules (Figure 5.6), and β for a set of 91 molecules (Figure 5.7).

5.3.5 Electronic structure calculations and reference values to determine errors

All energy calculations in this study were performed using DALTON 2.0.[32] The level of theory used was Hartree-Fock, with a 6-31G* basis set.[33] For the calculation of electric properties, the HF method was found to be superior to conventional DFT.[34,35] All molecular geometries were optimized with this level of theory and basis set prior to computing the energy. The reference values for the α, β and γ properties were calculated using response theory (RT).[9,10] These RT values were used to calculate the error (ε) in a given response property using the following formula:

$$\varepsilon_{\alpha,\beta,\gamma} = \left| \frac{\alpha,\beta,\gamma_{calc}}{\alpha,\beta,\gamma_{RT}} - 1 \right| \tag{5.12}$$

where $\alpha, \beta, \gamma_{calc}$ is the response property computed using the rational-function FF method, and $\alpha, \beta, \gamma_{RT}$ is the corresponding property computed using RT. To ensure that the reference values computed by RT were accurate enough to compare to the properties computed using the FF method, the convergence criteria for α_{RT} was 10 significant figures or greater, and for β_{RT} and γ_{RT}, nine and eight significant digits, respectively.

Since assessing the finite field method requires the comparison of many similar and small numbers, issues related to numerical precision can become quite significant. Thus, all wave functions and molecular energies were tightly converged. All the energies used in this study are exact to at least 2e-12 au. Since the smallest molecules in this study have absolute energies above 40 au, this leads to a relative precision of 1e-13 au for the energy, corresponding to 13 significant digits.

5.4 Results and Discussion

5.4.1 Determining the optimal form of the rational function to fit the energy

Observing the plots for computing γ for acetamide in Figure 5.1, the accuracy and overall behaviour of the truncated rational functions (Table 5.1) were compared. Models 1 and 4 can immediately be excluded from consideration, due to their relative lack of accuracy. Moreover, for model 3, the two blue bands signifying a double minima preclude it from being considered further; the presence of more than one minimum makes

it difficult to optimally choose both the initial field and field distribution. Finally, a comparison between models 2 and 5 reveals that the minimum of model 5 is not as well defined when compared to model 2. This is supported by the diffuse blue band observed in the model 5 plot, which contrasts with the better-defined blue band in the model 2 plot. Overall, model 2 was found to have the best accuracy, while retaining desirable error behaviour. A similar analysis was performed with the graphs generated for the remaining test molecules and NLO properties; the behaviour and accuracy of model 2 was generally found to hold for these as well. Thus, for the remainder of the study, the form of the rational function used was model 2 (Equation (5.10)).

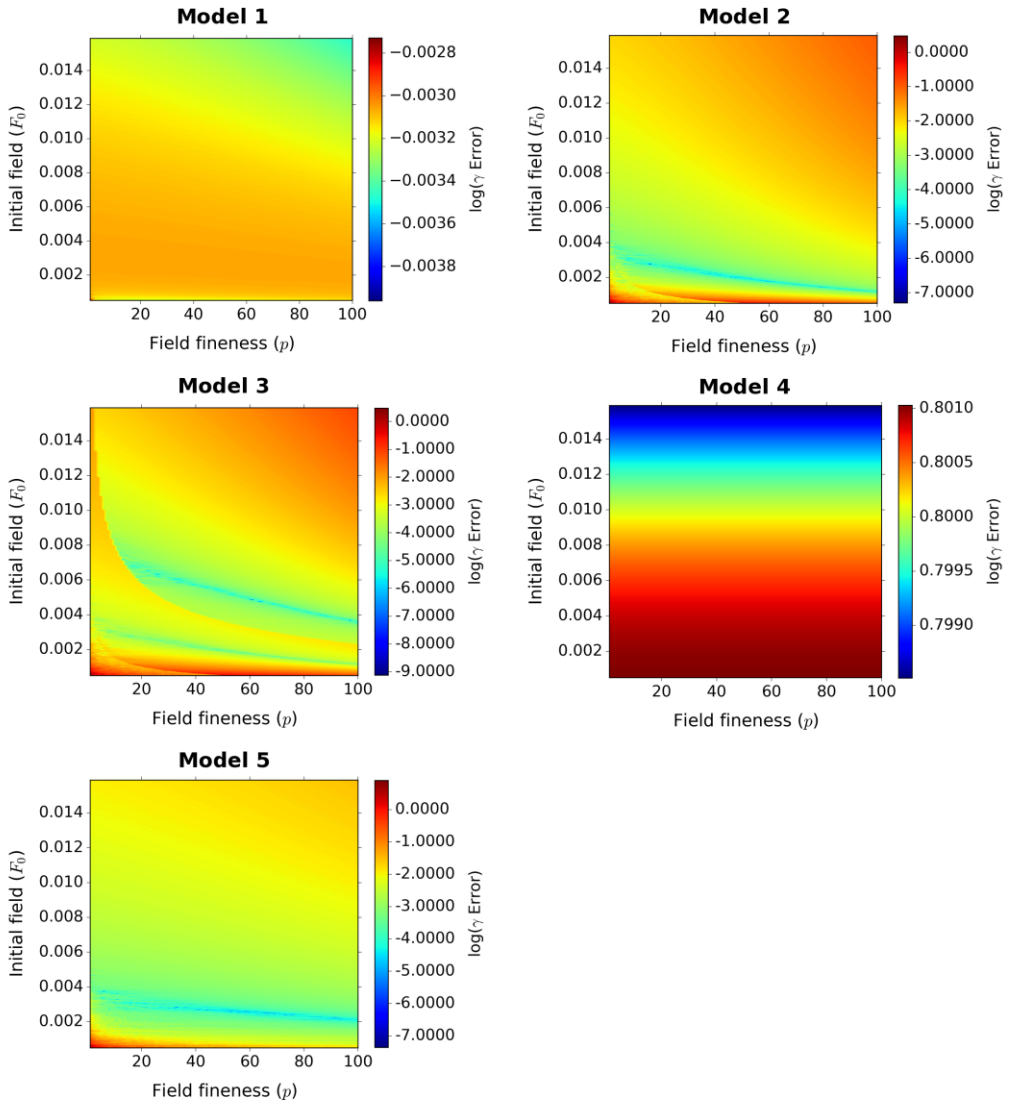

Figure 5.1. The behaviour of different rational function models in computing γ for acetamide. For each rational function form, the error relative to the reference value was determined as the initial field (F_0) and the field fineness (p) were changed. Model 2 was chosen as the best form of the rational function, since its plot contains a relatively tight and continuous blue band. This band indicates a desirable error distribution, along with low overall errors. The corresponding α and β plots for acetamide confirmed that model 2 should be used. The analysis was repeated with four additional molecules: 4,4-nitrophenyl aniline (DPAN), hexadecanol, 3-subunit polyacetylene (PA3), and 5-unit polyacetylene aminonitro (PA5AN). This confirmed the trends observed for acetamide.

Table 5.1. The forms of the rational function benchmarked for their accuracy in fitting molecular energies.

Model number	Numerator degree	Denominator degree
1	3	2
2	4	3
3	4	4
4	2	2
5	3	3

5.4.2 Optimizing the field distribution parameters

Once the form of the rational function was fixed to model 2, the following step is to optimize the field distribution for the FF calculations. For the previous polynomial based FF method,[31] the field distribution was found to be important for the accuracy of the method. In particular, using a geometric progression with a common ratio of $\sqrt{2}$ was found to produce the most accurate NLO property values. Thus, in this study, we also choose to distribute the fields according to a geometric progression (Equation (5.4)). The common ratio of this progression, denoted by x, is expanded as $x = 2^{\frac{p}{100}}$. Through

varying the value of p from 1-100, the interspacing between chosen fields can be tuned. The effect of varying the p value on the accuracy of the method was observed using plots such as those in Figure 5.2. Though only the plots for γ are shown for the five test molecules (Methods, Section 5.3.2), the plots for α and β were found to show the same trends as those observed for γ.

As predicted, the plots in Figure 5.2 demonstrate dependence between the accuracy in γ and the value of p picked for a calculation. However, since the bands corresponding to the minimal error span a large range of p values for the molecules, this implies that the value of p does not have to be picked precisely. For all five molecules, the minimal error band appears for values of p between 20-60. Though any value between these will work equally well, the remainder of the study fixed $p = 50$, producing a common ratio of $x = \sqrt{2}$. This optimal common ratio was found to be the same as that observed for the polynomial based FF method.[31]

5.4.3 Testing the least squares solution

For the rational function form given in Equation (5.10), there are six equations in five unknowns, i.e. the system is overdetermined. This system was solved by either least squares or truncating the system through removing one equation. Figure 5.3, where errors in γ are computed for acetamide, gives a representative example of a plot used to assess the accuracy of both methods.

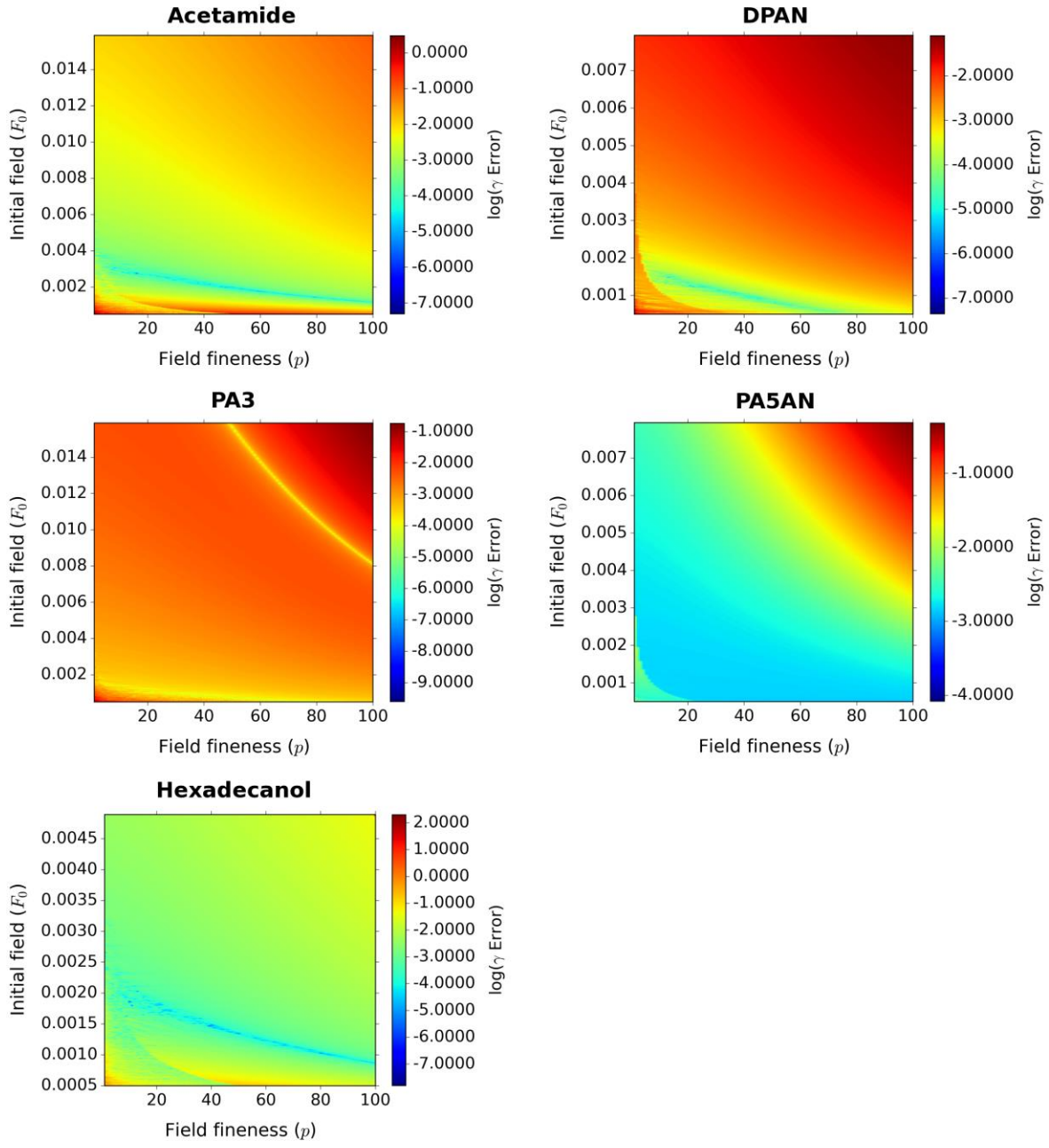

Figure 5.2. Contour plots of the error in γ for five test molecules to determine the optimal field fineness (*p*) value. The bands corresponding to minimal error are bright blue, except for PA3, where it is yellow. These error bands are present for every molecule from *p* = 20-60. The error within these bands is stable, indicating that any choice of *p* between 20-60 will be equally valid. Thus, the value of *p* was fixed to 50 for the remainder of the study.

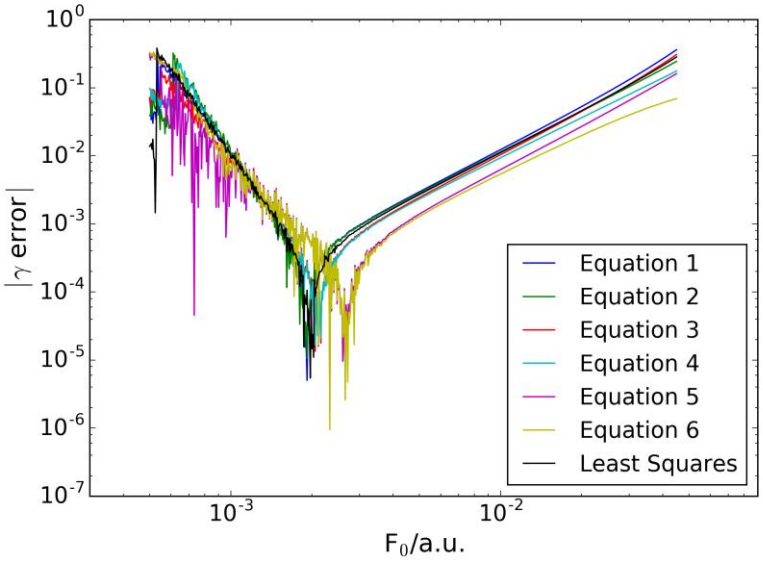

Figure 5.3. Example of a plot used to assess the performance of the least squares solution compared to solving a truncated system of equations. Here, the errors in computing γ for acetamide using model 2 are shown. No consistent trends between the least squares and truncated solutions could be found between molecules and properties. Thus, the least squares solution was used for the remainder of the study.

At lower fields, the accuracy of the least squares solution and the solutions obtained through leaving an equation out are similar. Depending on which equation was removed, the F_0 at which the error is minimized varies, with no discernable pattern. At higher fields, all solutions show similar behaviour, but have varying errors. One observed trend is that the solution obtained by removing the first equation from the system given in Equation (5.8) is generally very similar in behaviour and accuracy to the least squares solution. This suggests that the equations constructed with low field strengths contain less information than those using higher fields.

Though the solution obtained through removing the first equation showed predictable behaviour relative to the least squares solution, this did not hold true for the rest of the equations. By leaving an equation out of the system of equations (5.8), the error could increase or decrease, with no clear trends indicating which equations would lower the error when removed. Thus, as the least squares solution performed most predictably with regards to accuracy and behaviour, it was used for the remainder of the study.

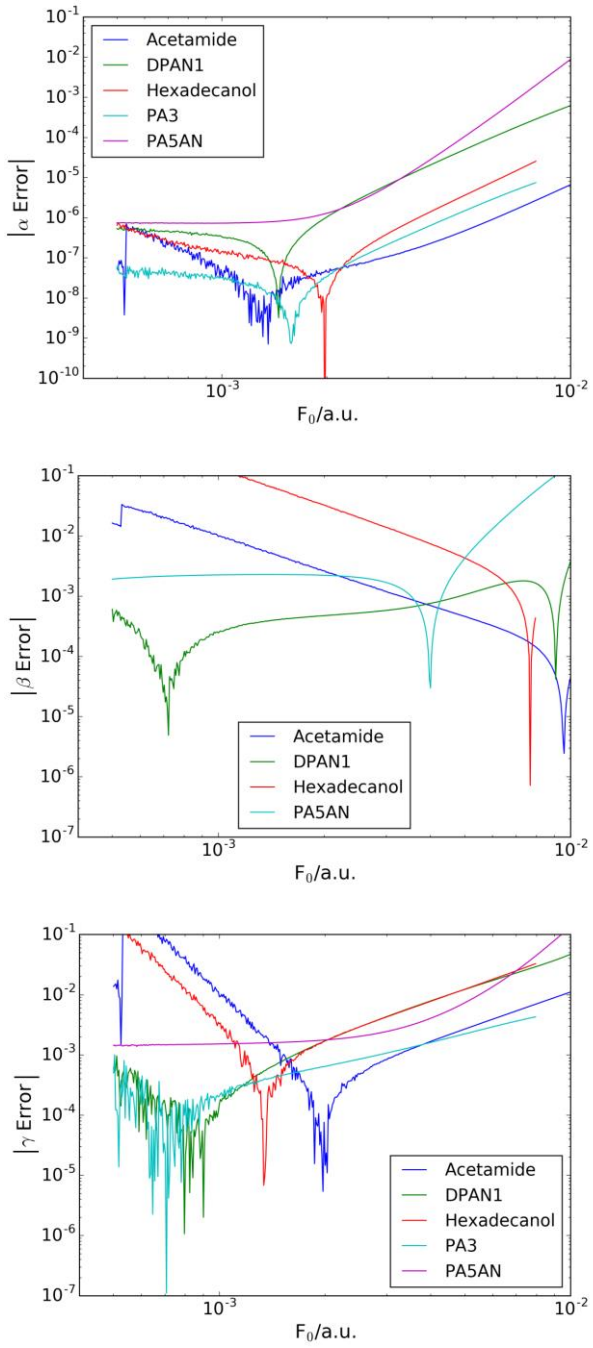

Figure 5.4. The optimal initial field value (F_0) that minimizes the error strongly depends on the molecule and NLO property for which the calculation is run.

5.4.4 Determining optimal initial fields for FF calculations

Unlike the p value or rational function form, the optimal F_0 value varies with the molecule and NLO property for which the FF calculation is performed. The strong dependence of the optimal F_0 on the molecule and property can be observed in Figure 5.4. This figure illustrates that F_0 must be picked precisely to minimize the error; using an F_0 that is not optimal leads to unusable results. Thus, a method to consistently choose the correct F_0 value is needed. As reference values are not available in practice, only the calculated response property value can be used for choosing F_0. Additionally, the response property cannot be computed for too many F_0 values, since this negates the cost advantage of the FF method.

To develop this method, plots similar to those generated for the least squares analysis (Section 5.3.3) were first used. However, instead of plotting the errors against F_0, the raw values of each computed property were plotted. An example of these plots, where γ is computed for acetamide, is given in Figure 5.5a. It can be observed that deviation from the least squares solution is minimized near the optimal field value, which is represented by the vertical red line. This deviation is quantified by the r value, calculated by Equation (5.11). Plotting the r value (Figure 5.5b) shows that it reaches a minimum at the optimal field, corresponding to the point at which the curves (Figure 5.5a) begin to follow the least squares solution. Thus, starting from the low-field limit and moving toward the high-field limit, the initial field is picked as the field after

which the r value consecutively increases or decreases for five F_0 values. The field chosen using these criteria, represented by the purple vertical line in Figure 5.5b, is not exactly at the optimal F_0. This is due to the roughness of r value curve at the minima, which makes it difficult to choose the F_0 value exactly corresponding to the minimum. Overall, this algorithm was used to compute the optimal F_0 for a set of 120 molecules (Figure 5.6). These F_0 values were used to compute α and γ for each molecule in the 120-molecule set. Similarly, β was computed using the F_0 chosen for a set of 91 non-centrosymmetric molecules (Figure 5.7). Overall, this field-picking method, along with the optimized common ratio and rational-function model allow for the computation of NLO properties in a quick and reasonably accurate manner.

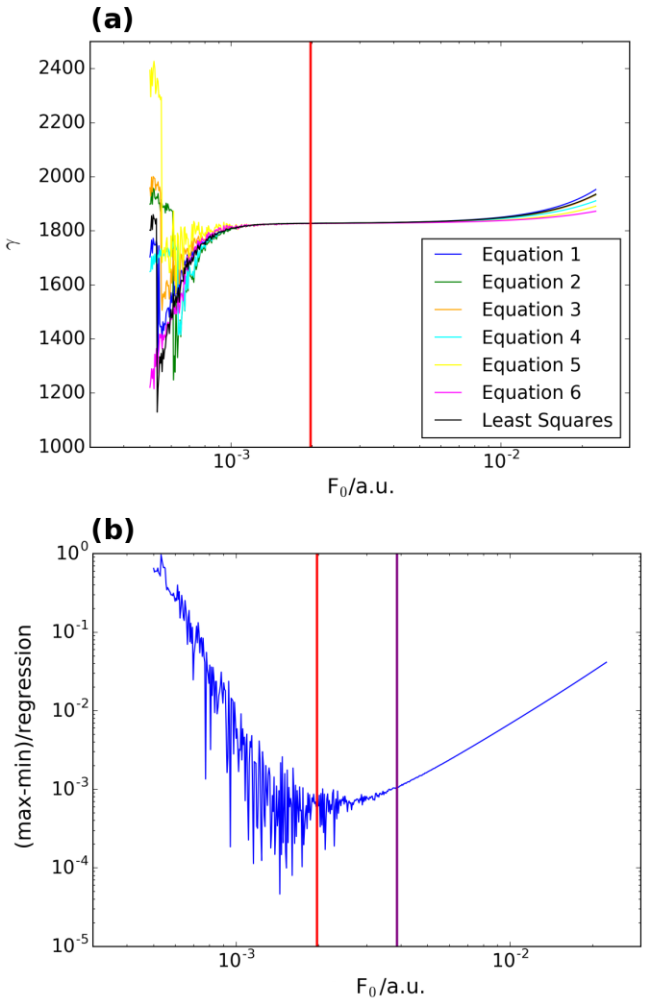

Figure 5.5. Determining a criterion for choosing an optimal initial field for the FF calculation. Both graphs shown are for the computed value of γ for acetamide. The vertical red lines represent the optimal field value. In (a), the deviation of the other solutions from the least squares result decreases as the optimal field value is approached. To determine the deviation from the least squares result, the maximum value of a calculated property can be subtracted from the minimum, and divided by the least squares regression result. A plot of this value is shown in (b). As the deviation decreases in plot (a), the curve in plot (b) reaches a minimum. The vertical purple line in plot (b) is the field chosen by the field-picking algorithm.

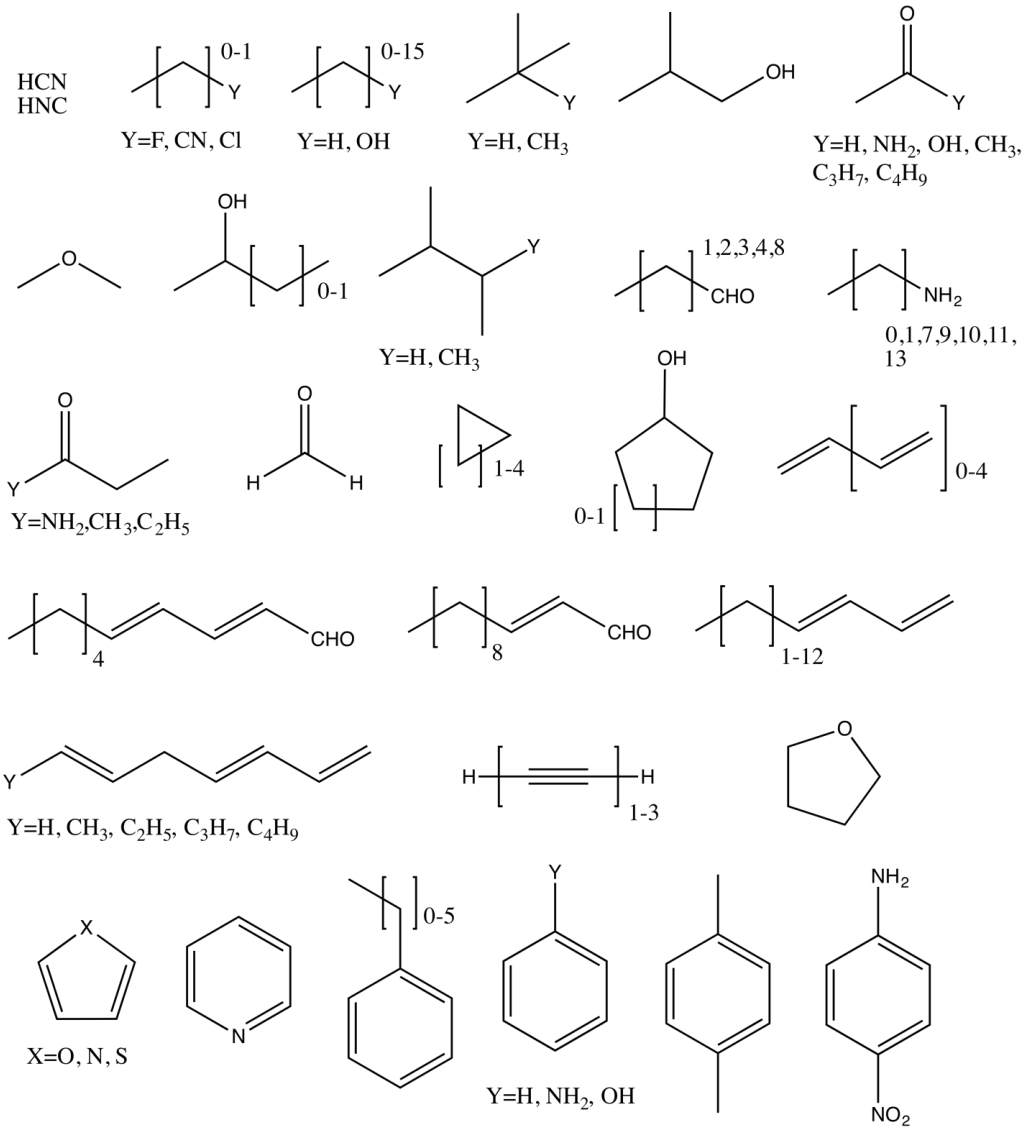

Figure 5.6.The 120 molecules for which α and γ were calculated using the rational-function based FF method.

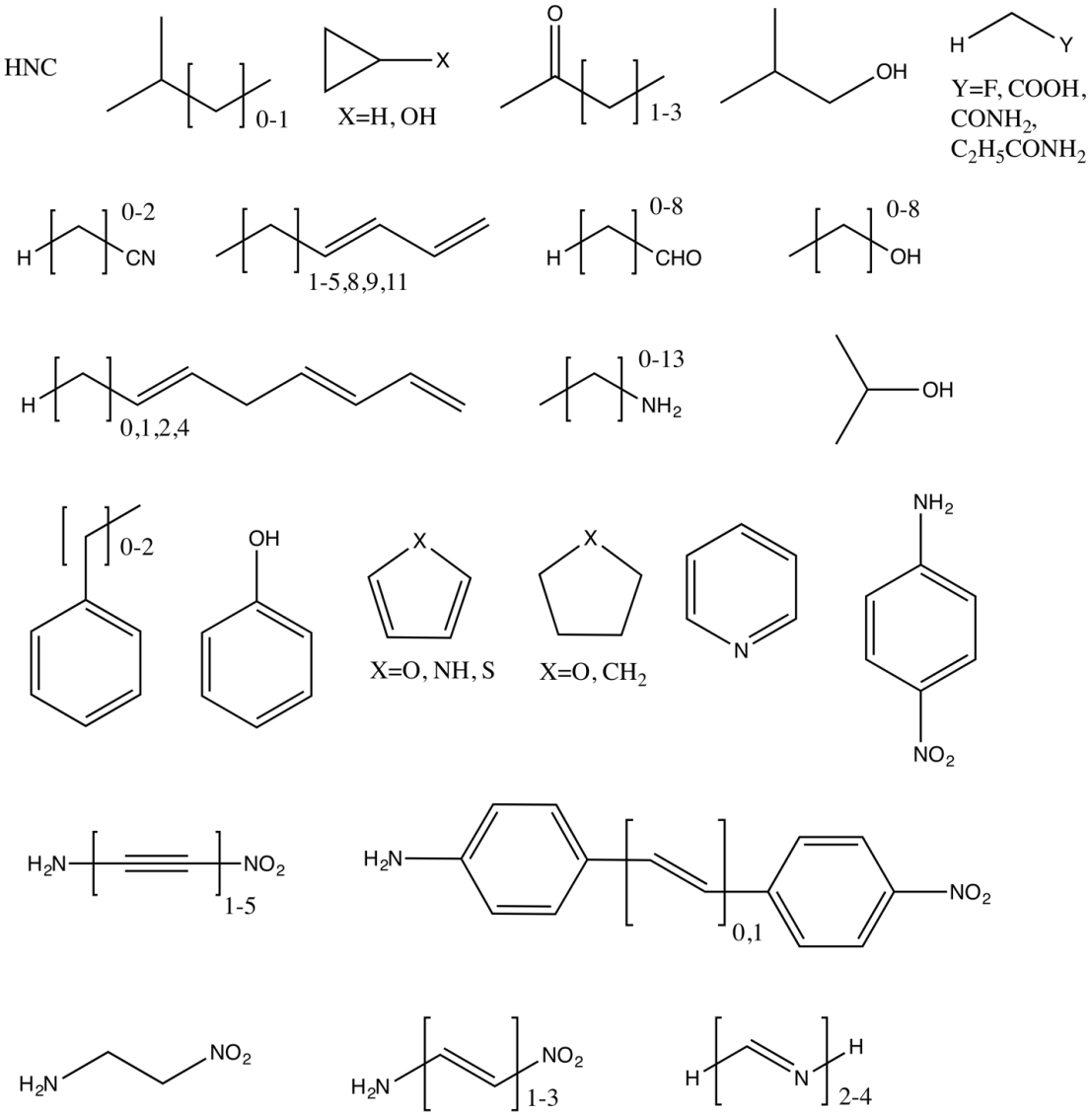

Figure 5.7. The 91 non-centrosymmetric molecules for which β was calculated using the rational-function based FF method.

5.4.5 Comparison of single-molecule error behaviour to the polynomial model

After having optimized the new FF method, its accuracy and behaviour is compared to the previous polynomial model.[31] To start, a single molecule comparison, using acetamide, is done. In general, the trends described for acetamide are representative of those observed for the entire dataset of molecules (Figure 5.6 and Figure 5.7). Errors in α, β, and γ as F_0 is varied were plotted for the rational-function and polynomial models, and are given in Figure 5.8. For the polynomial model, each iterative Richardson extrapolation used to refine the error is denoted as m = 0,1,2,3. For α and γ, the error in the ration-function model is comparable to the m = 2 polynomial refinement. For β, the error in the rational-function model is comparable to m = 1 for the polynomial model. For each property, the error curve for the rational function fit is smoother than the comparable polynomial curve. This smoothness likely reduces the need for error refinement steps. Additionally, the lack of a need for error refinement steps for the rational function model provides advantages in the form of lower computational cost and a simpler implementation.

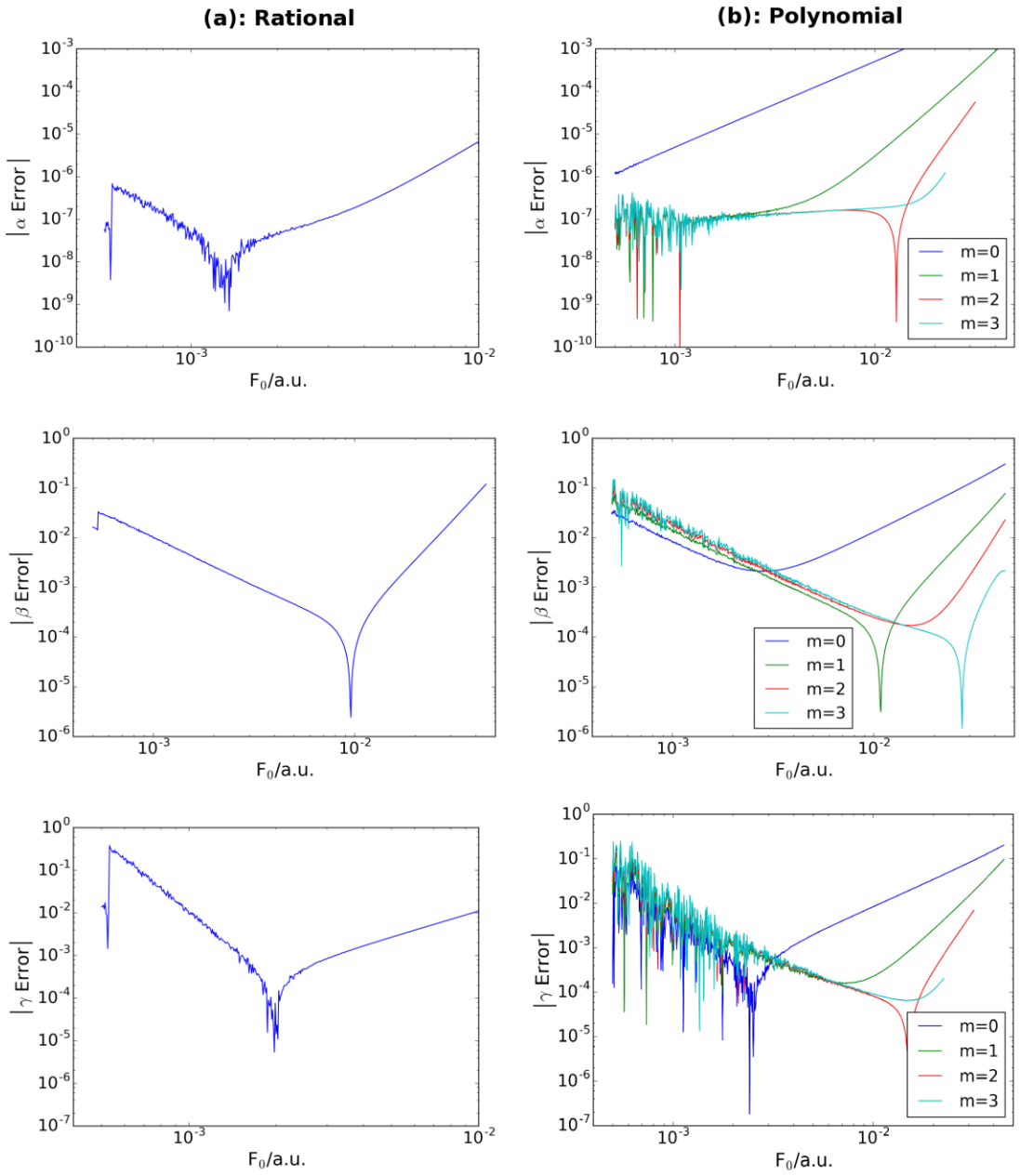

Figure 5.8. The α, β, and γ error behaviour for acetamide is compared between the rational-function (a) and polynomial (b) FF methods. For the polynomial method, the behaviour with iterative refinement via Richardson extrapolation is shown, denoted as m = 0,1,2,3.

5.4.6 Overall comparison of the rational-function and polynomial models

To compare the accuracy and robustness of the rational function model versus the polynomial model,[31] plots of the average α, β, and γ errors over χ for the entire dataset were created (Figure 5.9). Here, $\chi = \frac{F_0}{F_{0\,(optimized)}}$, where F_0 is the initial field, and $F_{0\,(optimized)}$ is the optimal initial field chosen by the protocol presented in Section 5.3.4. This normalization allows the average behaviour of the entire dataset to be compared around $F_{0\,(optimized)}$, where χ = 1. Though as many molecules as possible from the dataset were included, the energies of some molecules could not be calculated at enough F_0 values to span the full range of the graph. We found that at the χ values where the data for these molecules ended, large discontinuities in the graph would occur. Thus, these molecules were not included in the graphs. The two major errors in the FF method, truncation and round-off error,[36] can be observed in these graphs. Truncation error increases with increasing F_0 values, and round-off error increases with decreasing F_0 values.

For α, the accuracy at χ = 1 of the rational-function and polynomial models are quite similar, with minimum errors of approximately 10^{-7} for both. However, the rational function model is approximately half an order of magnitude less accurate than the polynomial model. Comparing the behaviour of both models, the rational function model remains at a lower overall error for a large range of fields compared to the polynomial

model. This means that the results are robust with respect to moderate errors in choosing the optimal F_0.

The errors at $\chi = 1$ for β are approximately 10^{-3}, with the rational-function model being half an order of magnitude less accurate than the polynomial model. Similar to α, the rational function model is more robust to changes in initial field strength. In general, errors are smaller than 10^{-2} for field strengths between χ values of 1-4. This is a greater range than that of the polynomial model, which remains in that range for 0.25-2.5 χ only. Thus, small errors in choosing the optimal F_0 are less detrimental to the accuracy of the rational-function model than the polynomial model.

At $\chi = 1$, the polynomial model[31] obtains average errors on the order of 10^{-4} for γ. The rational function model performs significantly worse, with an accuracy loss of approximately 1.5 orders of magnitude. However, the error for the rational function model remains lower over a larger range of fields, as observed for the α and β calculations. The rational function model consistently remains at an error of 10^{-1} or lower for $\chi = 0.1$-4, in contrast to the polynomial model, which achieves this for $\chi = 0.1$-2.0 only.

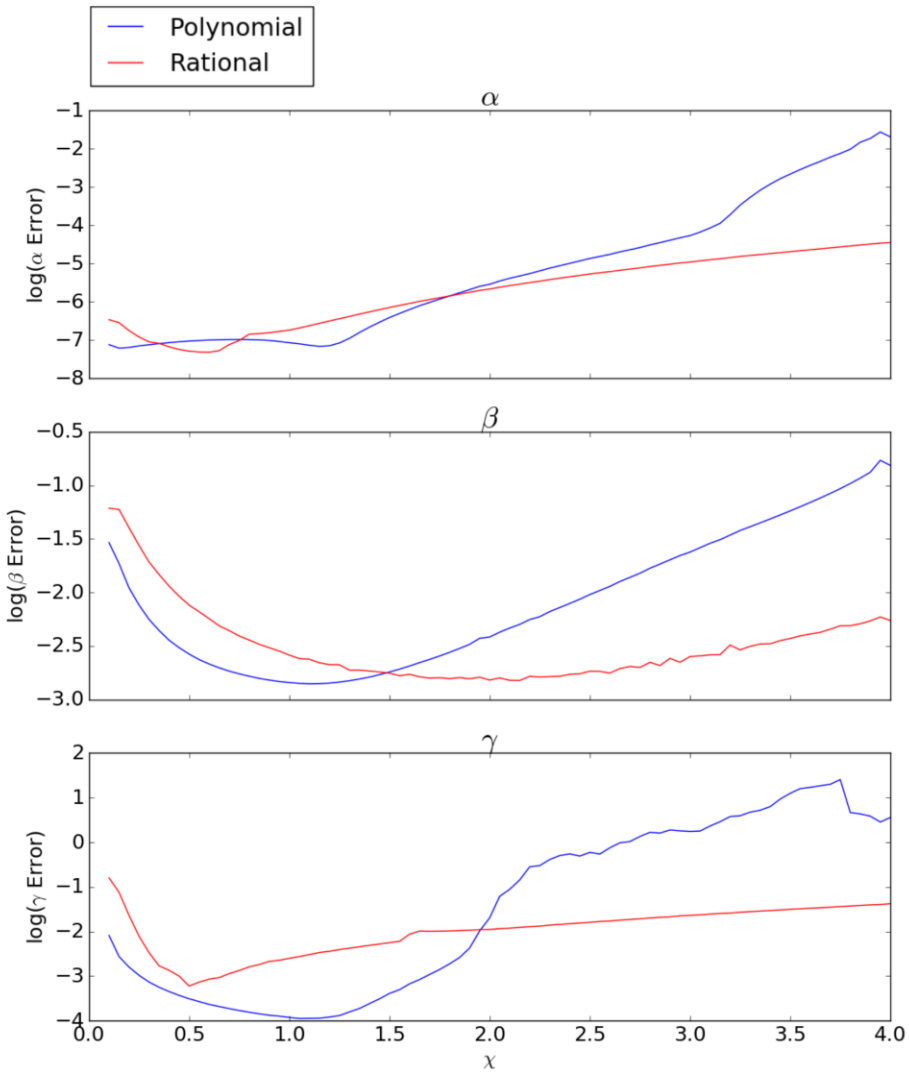

Figure 5.9. The average α, β, and γ error behaviour for the dataset of molecules is compared between the rational-function (red) and polynomial (blue) FF methods. The field values for each molecule are normalized using the optimal initial field value for each molecule. Thus, $\chi = \frac{F_0}{F_{0\,(optimized)}}$, where F_0 is the initial field used for the FF calculation, and $F_{0\,(optimized)}$ is the optimal initial field automatically chosen for the FF calculation. At $\chi = 1$, the overall error for the rational-function model is not as low as for the polynomial model. However, the rational model error remains lower over a larger range of χ, indicating that it is more robust to changes in F_i than the polynomial model. For the polynomial curves (blue), the Richardson refinement level is $m = 1$ for β, and $m = 2$ for α and γ.

Though the comparison above may lead to the conclusion that the rational function model is less accurate overall, this is not the case. Rather, the loss of accuracy is from not having the error minima centered on $\chi = 1$. For α and γ, the minimum error occurs at $\chi = 0.5$, while for β, the minimum error is at $\chi = 2$. This suggests that the protocol used to choose the optimal F_0 value overestimates this value for α and γ, and underestimates it for β. From Figure 5.5b, it can be observed that the r value becomes smooth only after the minimum is reached. For β, the r value becomes smooth before the minimum is reached. Thus, this over and underestimation of F_0 is expected, as the protocol only chooses the optimal F_0 value when the r value becomes smooth. Though different variations of the protocol were explored, none were able to yield any improvement. Thus, work will be continued on developing a more consistent method to find the minimum r value. However, despite issues with choosing F_0, the rational function model is more robust with regards to the initial field chosen; overestimation or underestimation of the optimal initial field will still yield reasonably accurate results. The robustness of the rational model is expected, as the rational function reduces the truncation error relative to a polynomial fit, which should increase the range of acceptable field strengths for a calculation. However, the round-off error remains similar for both models, but these errors are controlled by using very tight convergence criteria for the energies, and by selecting the minimum field appropriately. Overall, this robustness to the F_0 value used in the calculation is a key step in improving the overall user-friendliness and reliability of the FF method.

5.5 Conclusions

A variation of the FF method using a rational function was presented to calculate longitudinal polarizability and the first and second longitudinal hyperpolarizabilities of a wide range of molecules. To calculate NLO properties accurately, the functional form to best fit the energy was found, along with the optimal field distribution and a method of choosing F_0 reasonably well. The fitted rational function approximation has a polynomial of degree three in the numerator and a polynomial of degree two in the denominator. The field mesh used for this approximant was generated using a geometric progression with a common ratio of $\sqrt{2}$. To generate a good F_0 guess, it was found that the deviation from the least squares result could be used.

Comparison of the optimized rational-function FF method to the polynomial FF method from ref. 31 shows that both perform similarly with regards to error behaviour. Unlike the polynomial model, the rational function model does not need subsequent error refinement. This is advantageous in terms of computational cost, and for ease of implementation. Comparison of the two methods for the overall dataset reveals that the rational-function FF method loses approximately 0.5-1.5 orders of magnitude in accuracy relative to the polynomial method. However, the insensitivity of the rational-function FF method to F_0, along with not requiring refinement steps, makes this method a strong choice for new quantum chemistry codes that wish to implement a cheap and simple method for NLO property calculations.

5.6 References

(1) Franken, P. A.; Hill, A. E.; Peters, C. W.; Weinreich, G. Generation of Optical Harmonics. *Phys. Rev. Lett.* **1961**, *7*, 118–119.

(2) Nalwa, H. S.; Miyata, S. *Nonlinear Optics of Organic Molecules and Polymers*; CRC Press, 1997.

(3) Brédas, J. L.; Adant, C.; Tackx, P.; Persoons, A.; Pierce, B. M. Third-Order Nonlinear Optical Response in Organic Materials: Theoretical and Experimental Aspects. *Chem Rev* **1994**, *94*, 243–278.

(4) Luo, Y.; Ågren, H.; Jørgensen, P.; Mikkelsen, K. V. Response Theory and Calculations of Molecular Hyperpolarizabilities. *Adv. Quantum Chem.* **1995**, *26*, 165–237.

(5) Prasad, P. N.; Williams, D. J. *Introduction to Nonlinear Optical Effects in Molecules and Polymers*; Wiley, 1991.

(6) Caves, T. C.; Karplus, M. Perturbed Hartree–Fock Theory. I. Diagrammatic Double-Perturbation Analysis. *J. Chem. Phys.* **1969**, *50*, 3649–3661.

(7) Gerratt, J.; Mills, I. M. Force Constants and Dipole-Moment Derivatives of Molecules from Perturbed Hartree–Fock Calculations. II. Applications to Limited Basis-Set SCF–MO Wavefunctions. *J. Chem. Phys.* **1968**, *49*, 1730–1739.

(8) Stevens, R. M.; Pitzer, R. M.; Lipscomb, W. N. Perturbed Hartree—Fock Calculations. I. Magnetic Susceptibility and Shielding in the LiH Molecule. *J. Chem. Phys.* **1963**, *38*, 550–560.

(9) Jansik, B.; Sałek, P.; Jonsson, D.; Vahtras, O.; Ågren, H. Cubic Response Functions in Time-Dependent Density Functional Theory. *J. Chem. Phys.* **2005**, *122*, 54107.

(10) Helgaker, T.; Coriani, S.; Jørgensen, P.; Kristensen, K.; Olsen, J.; Ruud, K. Recent Advances in Wave Function-Based Methods of Molecular-Property Calculations. *Chem. Rev.* **2012**, *112*, 543–631.

(11) Cohen, H. D.; Roothaan, C. C. J. Electric Dipole Polarizability of Atoms by the

Hartree—Fock Method. I. Theory for Closed-Shell Systems. *J. Chem. Phys.* **1965**, *43*, S34–S39.

(12) Maroulis, G.; Bishop, D. M. On the Dipole and Higher Polarizabilities of Ne(1S). *Chem. Phys. Lett.* **1985**, *114*, 182–186.

(13) Maroulis, G.; Thakkar, A. J. Multipole Moments, Polarizabilities, and Hyperpolarizabilities for N_2 from Fourth-order Many-body Perturbation Theory Calculations. *J. Chem. Phys.* **1988**, *88*, 7623–7632.

(14) Bishop, D. M.; Pipin, J.; Lam, B. Field and Field-Gradient Polarizabilities of BeH, BH and CH^+. *Chem. Phys. Lett.* **1986**, *127*, 377–380.

(15) Bishop, D. M.; Pipin, J. Field and Field-Gradient Polarizabilities of H_2O. *Theor. Chim. Acta* **1987**, *71*, 247–253.

(16) Kurtz, H. A.; Stewart, J. J. P.; Dieter, K. M. Calculation of the Nonlinear Optical Properties of Molecules. *J. Comput. Chem.* **1990**, *11*, 82–87.

(17) Bartlett, R. J.; Purvis, G. D. Molecular Hyperpolarizabilities. I. Theoretical Calculations Including Correlation. *Phys. Rev. A* **1979**, *20*, 1313–1322.

(18) Bulat, F. A.; Toro-Labbé, A.; Champagne, B.; Kirtman, B.; Yang, W. Density-Functional Theory (Hyper)polarizabilities of Push-Pull π-Conjugated Systems: Treatment of Exact Exchange and Role of Correlation. *J. Chem. Phys.* **2005**, *123*, 14319.

(19) Wouters, S.; Limacher, P. A.; Van Neck, D.; Ayers, P. W. Longitudinal Static Optical Properties of Hydrogen Chains: Finite Field Extrapolations of Matrix Product State Calculations. *J. Chem. Phys.* **2012**, *136*, 134110.

(20) Nénon, S.; Champagne, B.; Spassova, M. I. Assessing Long-Range Corrected Functionals with Physically-Adjusted Range-Separated Parameters for Calculating the Polarizability and the Second Hyperpolarizability of Polydiacetylene and Polybutatriene Chains. *Phys. Chem. Chem. Phys.* **2014**, *16*, 7083.

(21) Matsui, H.; Nakano, M.; Champagne, B. Theoretical Study on the Spin State and Open-Shell Character Dependences of the Second Hyperpolarizability in Hydrogen Chain Models. *Phys. Rev. A* **2016**, *94*, 42515.

(22) de Wergifosse, M.; Liégeois, V.; Champagne, B. Evaluation of the Molecular Static and Dynamic First Hyperpolarizabilities. *Int. J. Quantum Chem.* **2014**, *114*, 900–910.

(23) Medved', M.; Jacquemin, D. Tuning the NLO Properties of Polymethineimine Chains by Chemical Substitution. *Chem. Phys.* **2013**, *415*, 196–206.

(24) Sekino, H.; Maeda, Y.; Kamiya, M.; Hirao, K. Polarizability and Second Hyperpolarizability Evaluation of Long Molecules by the Density Functional Theory with Long-Range Correction. *J. Chem. Phys.* **2007**, *126*, 14107.

(25) Salustro, S.; Maschio, L.; Kirtman, B.; Rérat, M.; Dovesi, R. Third-Order Electric Field Response of Infinite Linear Chains Composed of Phenalenyl Radicals. *J. Phys. Chem. C* **2016**, *120*, 6756–6761.

(26) Jacquemin, D.; Perpète, E. A.; Medved', M.; Scalmani, G.; Frisch, M. J.; Kobayashi, R.; Adamo, C. First Hyperpolarizability of Polymethineimine with Long-Range Corrected Functionals. *J. Chem. Phys.* **2007**, *126*, 191108.

(27) de Wergifosse, M.; Wautelet, F.; Champagne, B.; Kishi, R.; Fukuda, K.; Matsui, H.; Nakano, M. Challenging Compounds for Calculating Hyperpolarizabilities: *P* -Quinodimethane Derivatives. *J. Phys. Chem. A* **2013**, *117*, 4709–4715.

(28) de Wergifosse, M. Approximate Spin-Projected Density-Based Romberg Differentiation Procedure to Evaluate the Second-Hyperpolarizability of *P* -Quinodimethane and Twisted Ethylene and Their Diradical Character Dependence. *J. Phys. Chem. A* **2016**, *120*, 2727–2736.

(29) Wouters, S.; Van Speybroeck, V.; Van Neck, D. DMRG-CASPT2 Study of the Longitudinal Static Second Hyperpolarizability of All-Trans Polyenes. *J. Chem. Phys.* **2016**, *145*, 54120.

(30) Bishop, D. M.; Solunac, S. A. Breakdown of the Born-Oppenheimer Approximation in the Calculation of Electric Hyperpolarizabilities. *Phys. Rev. Lett.* **1985**, *55*, 1986–1988.

(31) Mohammed, A. A. K.; Limacher, P. A.; Champagne, B. Finding Optimal Finite Field Strengths Allowing for a Maximum of Precision in the Calculation of Polarizabilities and Hyperpolarizabilities. *J. Comput. Chem.* **2013**, *34*, 1497–1507.

(32) Aidas, K.; Angeli, C.; Bak, K. L.; Bakken, V.; Bast, R.; Boman, L.; Christiansen, O.; Cimiraglia, R.; Coriani, S.; Dahle, P.; et al. The Dalton Quantum Chemistry Program System. *Wiley Interdiscip. Rev. Comput. Mol. Sci.* **2014**, *4*, 269–284.

(33) Rassolov, V. A.; Ratner, M. A.; Pople, J. A.; Redfern, P. C.; Curtiss, L. A. 6-31G* Basis Set for Third-Row Atoms. *J. Comput. Chem.* **2001**, *22*, 976–984.

(34) Champagne, B.; Perpète, E. a; Jacquemin, D.; van Gisbergen, S. J. a; Baerends, E. J.; Soubra-Ghaoui, C.; Robins, K. a; Kirtman, B. Assessment of Conventional Density Functional Schemes for Computing the Dipole Moment and (Hyper)polarizabilities of Push-Pull π-Conjugated Systems. *J. Phys. Chem. A* **2000**, *104*, 4755–4763.

(35) Limacher, P. A.; Li, Q.; Lüthi, H. P. On the Effect of Electron Correlation on the Static Second Hyperpolarizability of π Conjugated Oligomer Chains. *J. Chem. Phys.* **2011**, *135*, 14111.

(36) Ruden, T. A.; Taylor, P. R.; Helgaker, T. Automated Calculation of Fundamental Frequencies: Application to AlH_3 Using the Coupled-Cluster Singles-and-Doubles with Pertubative Triples Method. *J. Chem. Phys.* **2003**, *119*, 1951–1960.

Chapter 6

Summary and Future Work

6.1 Motivation

Molecular nonlinear optical (NLO) properties have a broad range of applications in optical devices, but experimental characterization of molecules with superior NLO properties is often challenging. Computational methods are useful not only because they allow one to compute NLO properties, but also because the calculations can provide insight into the physico-chemical phenomena that underlie the nonlinear responses and uncover the structure-property relationship. These insights, in turn, can guide the design of new molecules with desirable response properties for various types of optoelectronic devices.

Computational studies of NLO properties are also challenging, and developing new computational methods, and improving existing methods, is an active area of research in theoretical chemistry. Existing methods for computing the NLO properties of atoms and

molecules have several drawbacks: (1) some methods are computationally demanding and can be applied only to small-to-medium-sized molecules; (2) some methods requiring analytical derivatives and information about excited states of the systems; (3) some methods are difficult to implement into computational quantum chemistry software, and are therefore not widely available for some types of quantum chemistry methods. The focus of this thesis is the finite field (FF) method, which is straightforward, computationally affordable, and easy-to-implement. The FF method is one of the best candidates for studying large molecules and using state-of-the-art electronic structure methods for modelling NLO properties.

However, the finite field method is not without problems. One of these main problems is the dependence of a calculated NLO property on the choice of the electric field strength(s) one uses in the calculation. Choosing a field that is too high or too small leads to nonsensical results. The second problem comes from the difficulty of disentangling the response property of interest from the effects of higher-order responses. Although the finite field method is widely used for calculating NLO properties, these problems persist. To our knowledge, no systematic way to mitigate these issues has been presented in the literature. The goal of my Ph.D. thesis is to overcome these obstacles to the routine and systematic application of FF calculations for predicting NLO properties. In particular, I have performed systematic studies of the finite field method and used the results of those studies to provide computational protocols that are suitable for routine calculations.

6.2 Summary

Chapter two presents a comprehensive study of the finite field methods for calculating the dipole polarizability and hyperpolarizabilities of molecules and oligomers. The dependence of the error on the initial field strength is explored and schemes to obtain the most precise results for response properties were proposed. The HOMO-LUMO gap and information about excited states were helpful in determining the critical field for calculating reliable response properties. We showed that using a common ratio $x < 2$ for generating the geometric progression for field strengths and two steps of Richardson extrapolation for refinement give the most precise results for γ. The study also shows that Richardson extrapolation is superior to polynomial fitting for calculating NLO properties.

Chapter three presents a protocol for predicting the optimal field strength for calculating NLO properties of molecules; this avoids the computationally demanding search for an appropriate field strength, which was the slowest part of the computations in chapter 2. The second hyperpolarizability γ showed the best correlation with the maximum internuclear distance within a molecule in the direction of the applied field. Based on these findings we designed, and successfully used, a protocol to estimate the optimal field strength for γ. The optimal field for calculating β doesn't depend on molecular size and depends, instead, on the structure of the molecule. Functional groups were the best way to estimate the optimal field for calculating β.

These two studies, presented in chapters 2 and 3, showed the optimal choices for the initial field, common ratio, and the number of refinement steps to produce the most accurate response properties. They helped in avoiding additional computational cost, guaranteed obtaining meaningful results, and paved the way toward automated calculations of NLO properties.

Chapter four is an investigation of the performance of different DFT functionals compared to the CCSD(T) method for calculating the second hyperpolarizability for a benchmark of 30 organic molecules and oligomers. The limitations of DFT methods for calculating NLO properties are shown in this study. The relative performance of DFT functionals depends on the system under consideration: different types of functionals are needed for different types of molecules. Conventional DFT functionals generally overestimate the second hyperpolarizability of medium-sized and large molecules with errors increasing linearly with the size of the molecule. The long-range corrected hybrid functionals perform significantly better than conventional hybrid functionals and pure functionals. The study also reveals the significant role of correlation in calculating the second hyperpolarizability γ. The reliability of the CCSD(T) as a benchmarking method for conjugated systems is examined. CCSD was shown to diverge rapidly from CCSD(T) as the π-conjugated chain lengthens.

Chapter five uses a rational function model to calculate NLO properties of molecules, instead of the commonly used Taylor expansion. The optimal function form

was determined and the optimal conditions for calculating response properties were outlined. Rational functions have the advantage of being less dependent on the initial field of calculation and not needing further refinements. Moreover, higher order derivatives can be approximated directly, without requiring additional energy evaluations. Rational function approximation methods have lower computational cost, are easier to implement, and are less sensitive to the field strength. However, the results from the rational function model seem slightly less accurate.

6.3 Future Work

6.3.1 Extending the benchmark study

For many applications, DFT methods represent the best compromise between accuracy and computational cost. Consequently, DFT is the method of choice for modelling large molecules and complex systems. This motivated the work in Chapter 4 on benchmarking DFT calculations (which are applicable to large systems) against coupled cluster results. This study should be extended to include more functionals (especially recently-developed DFT functionals that are not yet widely available in commercial quantum chemistry software) and additional molecules.

We observed that different DFT functionals perform better for different types of molecules. More aromatic molecules should be added to the dataset to test the surprising conclusion that pure functionals are better than hybrid and long-range corrected ones for

this type of systems. π-conjugated systems possess strong NLO properties and are under active investigation by those who design NLO devices. The response properties of these molecules increase as the chain lengthens and it is important to use DFT methods that show the correct dependence of NLO properties on molecule size. Longer conjugated molecules should be added to the dataset so that the size-dependence of DFT-predicted NLO properties is clearer.

Finally, in Chapter 4 we focussed on the second hyperpolarizability. A similar study for the polarizability and the first hyperpolarizability should be performed.

6.3.2 Method and basis set dependence of optimal field strength

Choosing the right field strengths for evaluating dipole polarizability and hyperpolarizabilities is crucial for obtaining meaningful results. The protocol for predicting the optimal field strengths for calculating the second hyperpolarizability γ is limited to the method and basis set used in the study. In general, as shown in chapter 2, the feasible field region starts at lower field for larger basis sets. Therefore, optimal field strengths are expected to decrease as the size of the basis set increases. Nonetheless, the qualitative behaviour of the error is the same for all basis sets. The protocol for finding optimal field strengths for γ that was developed in chapter 3 for HF/6-31G(d) level of theory can be extended in a straightforward manner to other methods and basis sets.

In Chapter 3 we observed that more accurate estimations of optimal field strengths are obtained when molecules with similar structures are considered. For example, more accurate predictions of the second hyperpolarizability of polyacetylene chains can be obtained by using a protocol specifically selected for those systems. The procedure that was used in chapter 3 to find protocols for optimal field strengths could be applied to families of molecules.

More ambitiously, it would be helpful to design a fully automated protocol, perhaps by selecting a sensible initial field, and then either reducing or increasing that field until reliable results are obtained. For this purpose the rational model in Chapter 5 may be preferable, since it is less sensitive to the choice of field.

6.3.3 Optimal field strengths for the first hyperpolarizability β

The first hyperpolarizability β, an odd-derivative of energy, was shown to have different behaviour from even-order energy derivatives, namely the dipole polarizability, α, and the second hyperpolarizability, γ. Because β is a lower energy derivative than γ, we expect computing γ to be trickier. Surprisingly, we observed that FF calculations of β are less numerically stable and have higher relative errors. Moreover, the optimal field for calculating β didn't show good correlations with any of the molecular descriptors we tested. In order to increase the precisions of calculations for β, we need to perform a systematic study of the relationship between β and molecular structure and design protocols to predict the optimal field strength for calculating β.

6.3.4 Hypergeometric functions

Traditionally, the finite field methods used for calculating NLO properties are based on using a Taylor expansion to describe the energy of the system. In chapter 5, we showed that a rational function, which is more general than a Taylor expansion and thus can capture more physical behaviour, can be used to calculate response properties. The success of rational function models motivated us to think about even more general functions to describe the dependence of the energy of a molecule on the applied field. It can be shown that the perturbative expansion of the electronic energy in powers of the applied field is an asymptotic series, and the functional form associated with this series is a hypergeometric function. Hypergeometric functions could potentially describe the energy of a molecule in a finite field better than both polynomial and rational functions.

One form of hypergeometric function that can be used is

$$ {}_k F_l \left(\begin{matrix} a_1,...,a_k \\ b_1,...,b_l \\ c \end{matrix} \right) = \sum_{n=0}^{\infty} \frac{(a_1)_n ... (a_k)_n}{(b_1)_n ... (b_l)_n} (cx)^n \qquad (6.1) $$

$$ (a)_n = \frac{\Gamma(a+n)}{\Gamma(n)} $$

The energy expression that one fits to the finite-field data is then

$$ E(F) \approx E(0) \left[{}_k F_l \left(\begin{matrix} a_1,...,a_k \\ b_1,...,b_l \\ cF \end{matrix} \right) \right] \qquad (6.2) $$

Writing Eq. (6.2) for several different fields gives a system of nonlinear equations to solve for the parameters in the hypergeometric function. The (hyper)polarizabilities can then be determined by evaluating coefficients in the Taylor series, (6.1).

6.3.5 Anisotropic properties

The work in this thesis was focused on the accurate calculation of the longitudinal polarizability and hyperpolarizabilities. The longitudinal properties are the most important one for linear molecules. However, the other components of the (hyper)polarizability tensors of response properties are often important. The methods developed in this thesis can be extended to calculate other tensor elements of response properties in a straightforward manner.

Applying a small static electric field F to a molecule with an energy $E(0)$ induces a perturbation that could be written as a Taylor expansion as

$$E\left(F\right)=E\left(0\right)-\sum_{i}\mu_{i}F_{i}-\sum_{ij}\frac{1}{2}\alpha_{ij}F_{i}F_{j}-\frac{1}{6}\sum_{ijk}\beta_{ijk}F_{i}F_{j}F_{k}-\frac{1}{24}\sum_{ijkl}\gamma_{ijkl}F_{i}F_{j}F_{k}F_{l}+\ldots$$

(6.3)

Here $i,j,k\ldots$ denote the Cartesian components of the applied field vector, $\mathbf{F}=\left[F_{x},F_{y},F_{z}\right]^{T}$ and the associated molecular responses. Most experimental measurements yield rotationally averaged response properties,

$$\langle \alpha \rangle = \frac{1}{3}\left(\alpha_{xx} + \alpha_{yy} + \alpha_{zz}\right) \tag{6.4}$$

Higher-order derivatives, β and γ, can be obtained from the relevant expressions (cf. Eqs. (1.6) and (1.7)). The methods and optimal conditions for calculating accurate NLO properties developed in this thesis should be extended to (hyper)polarizability tensors also.

6.3.6 Testing new theoretical approaches

One of the main advantages of the finite field methods is their ease of implementation. Specifically finite-field methods can easily be implemented within existing software and applied to new electronic structure methods because all that is required is to add an electric field term to the Hamiltonian (modifying the one-electron integrals) and then calculate the electronic energy.

Over the past years, several new quantum chemistry methods have been explored by the Ayers group and its collaborators for describing the electronic structures of molecules. These methods include geminals methods, matrix product states, and various types of advanced configuration interaction approaches. The schemes developed in this thesis can be used to test the performance of these new approaches for calculating NLO properties. As stressed in the introduction, NLO properties are much more sensitive to errors in the description of electron correlation than most other ground-state molecular

properties, and therefore provide a useful and stringent test for new electronic structure methods.

The finite field method can also be applied using new software for accurate electronic structure methods. These programs are often faster and more efficient than the long-established commercial programs, which enables doing highly accurate calculations of larger systems. However, the numerical algorithms that make these new programs so efficient also make it difficult, or even impossible, to implement analytical gradients (e.g., multipole moments); linear and higher-order responses are even more difficult to compute. By using the finite field method, these programs can be used to accurately calculate the NLO properties of extended π-conjugated systems, providing accurate computational benchmarks for this important class of molecules.

6.3.7 Automated response calculations

The finite field method depends on the choice of the initial field and thus requires human intervention. In chapters 2 and 3, we used a large dataset to determine the optimal conditions (choice of initial field, number of refinement steps, and common ratio for the progression of field strengths) for calculating response properties. These findings can be implemented in computational codes to automatically calculate NLO properties. The optimal field strength for the dipole polarizability and the second polarizability can be obtained from the maximum internuclear distance within the molecule, which is available *a priori*. Two steps of Richardson refinement and a common ratio of $\sqrt{2}$ give the most

precise results. This scheme will be implemented in the HORTON package, an quantum chemistry code developed jointly by researchers at McMaster University (Canada) and Ghent University (Belgium).

Appendix: List of Abbreviations

CI	Configuration Interaction
CC	Coupled Cluster
CPHF	Coupled-Perturbed Hartree-Fock
CPKS	Coupled-Perturbed Kohn-Sham
DFWM	Degenerate Four Wave Mixing
DFT	Density Functional Theory
DP	Dielectric Permittivity
D–A	Donor–Acceptor
EMS	Electron-Molecule Scattering
FF	Finite Field
GGA	Generalized Gradient Approximation
HF	Hartree-Fock
HOMO	Highest Occupied Molecular Orbital
ICT	Intramolecular Charge Transfer

LDA	Local Density Approximation
LUMO	Lowest Unoccupied Molecular Orbital
MWI	Matter-Wave Interferometry
MBD	Molecular Beam Deflection
MO	Molecular Orbital
NLO	Nonlinear Optical
OEP	Optimized Effective Potential
PA	Polyacetylene
PY	Polyyne
PES	Potential Energy Surface
RI	Refractive Index
RT	Response Theory
SHG	Second-Harmonic Generation
SOS	Sum-Over-States
TPA	Two-Photon Absorption
XC	exchange-correlation